



UNIVERSIDADE FEDERAL DE UBERLÂNDIA  
INSTITUTO DE QUÍMICA  
PROGRAMA DE PÓS-GRADUAÇÃO EM QUÍMICA

IVO AMILDON RICARDO

POTENTIAL OF ORGANIC IRON COMPLEXES AND PEROXIDE SOURCES AS  
ALTERNATIVE DEGRADATION OF THE MIXTURE OF BENZOPHENONE-3,  
FIPRONIL AND PROPYLPARABEN IN TERTIARY WASTEWATER UNDER SOLAR  
RADIATION

UBERLÂNDIA – MG

2023

IVO AMILDON RICARDO

POTENTIAL OF ORGANIC IRON COMPLEXES AND PEROXIDE SOURCES AS  
ALTERNATIVE DEGRADATION OF THE MIXTURE OF BENZOPHENONE-3,  
FIPRONIL AND PROPYLPARABEN IN TERTIARY WASTEWATER UNDER SOLAR  
RADIATION

Ph.D. Thesis submitted to the Post-Graduate Program in Chemistry from the Universidade Federal de Uberlândia as partial fulfillment of the requirements for the Ph.D. degree in Chemistry.

Research area: Environmental Chemistry, Sustainability and Education in Chemistry.

Supervisor: Prof. Dr. Alam Gustavo Trovó

UBERLÂNDIA – MG

2023

Ficha Catalográfica Online do Sistema de Bibliotecas da UFU  
com dados informados pelo(a) próprio(a) autor(a).

R488 Ricardo, Ivo Amíldon, 1984-  
2023 POTENTIAL OF ORGANIC IRON COMPLEXES AND PEROXIDE  
SOURCES AS ALTERNATIVE DEGRADATION OF THE MIXTURE OF  
BENZOPHENONE-3, FIPRONIL AND PROPYL PARABEN IN TERTIARY  
WASTEWATER UNDER SOLAR RADIATION [recurso eletrônico] /  
Ivo Amíldon Ricardo. - 2023.

Orientador: Alam Gustavo Trovó.

Tese (Doutorado) - Universidade Federal de Uberlândia,  
Pós-graduação em Química.

Modo de acesso: Internet.

Disponível em: <http://doi.org/10.14393/ufu.te.2023.338>

Inclui bibliografia.

Inclui ilustrações.

1. Química. I. Trovó, Alam Gustavo, 1980-, (Orient.).

II. Universidade Federal de Uberlândia. Pós-graduação em  
Química. III. Título.

CDU: 54

Bibliotecários responsáveis pela estrutura de acordo com o AACR2:  
Gizele Cristine Nunes do Couto - CRB6/2091  
Nelson Marcos Ferreira - CRB6/3074



**UNIVERSIDADE FEDERAL DE UBERLÂNDIA**  
 Coordenação do Programa de Pós-Graduação em Química  
 Av. João Naves de Ávila, 2121, Bloco 5I - Bairro Santa Mônica, Uberlândia-MG, CEP 38400-902  
 Telefone: (34) 3239-4385 - www.cpgquimica.iq.ufu.br - cpgquimica@ufu.br



### ATA

Programa de Pós-Graduação em:	Química				
Defesa de:	Defesa de Doutorado Acadêmico, 138, PPGQUI				
Data:	Vinte e três de junho de dois mil e vinte e três	Hora de início:	8:00	Hora de encerramento:	12:20
Matrícula do Discente:	11923QMI013				
Nome do Discente:	Ivo Amildon Ricardo				
Título do Trabalho:	"Potential of organic iron complexes and peroxide sources as alternative degradation of the mixture of benzophenone-3, fipronil and propylparaben in tertiary wastewater under solar radiation"				
Área de concentração:	Química				
Linha de pesquisa:	Química Ambiental, Sustentabilidade e Educação em Química				
Projeto de Pesquisa de vinculação:	"Degradação de contaminantes de interesse emergente em efluentes e águas superficiais pelo processo foto-Fenton mediado por complexos orgânicos de ferro: avaliação química e toxicológica"				

Reuniu-se, por meio de *Webconferência*, pelo link <https://meet.google.com/eto-wtwz-xyk>, a Banca Examinadora, designada pelo Colegiado do Programa de Pós-graduação em Química, assim composta: Professores Doutores: Antônio Otávio de Toledo Patrocínio e Osmando Ferreira Lopes, da Universidade Federal de Uberlândia; Darliana Mello Souza, da Universidade Federal de Santa Maria; Amilcar Machulek Junior, da Universidade Federal do Mato Grosso do Sul; e Alam Gustavo Trovó, orientador do candidato.

Iniciando os trabalhos o presidente da mesa, Dr. Alam Gustavo Trovó, apresentou a Comissão Examinadora e o candidato, agradeceu a presença do público e concedeu ao Discente a palavra para exposição do seu trabalho. A duração da apresentação do Discente e o tempo de arguição e de resposta foram conforme as normas do Programa.

A seguir o senhor(a) presidente concedeu a palavra, pela ordem sucessivamente, aos(às) examinadores(as), que passaram a arguir o(a) candidato(a). Ultimada a arguição, que se desenvolveu dentro dos termos regimentais, a Banca, em sessão secreta, atribuiu o resultado final, considerando o(a) candidato(a):

Aprovado.

Esta defesa faz parte dos requisitos necessários à obtenção do título de Doutor.

O competente diploma será expedido após cumprimento dos demais requisitos, conforme as normas do Programa, a legislação pertinente e a regulamentação interna da UFU.



Documento assinado eletronicamente por **Alam Gustavo Trovo, Professor(a) do Magistério Superior**, em 23/06/2023, às 12:27, conforme horário oficial de Brasília, com fundamento no art. 6º, § 1º, do [Decreto nº 8.539, de 8 de outubro de 2015](#).

---



Documento assinado eletronicamente por **Osmando Ferreira Lopes, Professor(a) do Magistério Superior**, em 23/06/2023, às 12:27, conforme horário oficial de Brasília, com fundamento no art. 6º, § 1º, do [Decreto nº 8.539, de 8 de outubro de 2015](#).

---



Documento assinado eletronicamente por **Antonio Otavio de Toledo Patrocínio, Professor(a) do Magistério Superior**, em 23/06/2023, às 12:28, conforme horário oficial de Brasília, com fundamento no art. 6º, § 1º, do [Decreto nº 8.539, de 8 de outubro de 2015](#).

---



Documento assinado eletronicamente por **Darlina Mello Souza, Usuário Externo**, em 23/06/2023, às 12:37, conforme horário oficial de Brasília, com fundamento no art. 6º, § 1º, do [Decreto nº 8.539, de 8 de outubro de 2015](#).

---



Documento assinado eletronicamente por **Amilcar Machulek Junior, Usuário Externo**, em 26/06/2023, às 11:44, conforme horário oficial de Brasília, com fundamento no art. 6º, § 1º, do [Decreto nº 8.539, de 8 de outubro de 2015](#).

---



A autenticidade deste documento pode ser conferida no site [https://www.sei.ufu.br/sei/controlador\\_externo.php?acao=documento\\_conferir&id\\_orgao\\_acesso\\_externo=0](https://www.sei.ufu.br/sei/controlador_externo.php?acao=documento_conferir&id_orgao_acesso_externo=0), informando o código verificador **4449803** e o código CRC **572CE2D4**.

---

I dedicate this work to GOD and to my family:  
EDNA ARGENTINA ALBERTO and JOSUÉ  
IVO RICARDO.

## ACKNOWLEDGEMENTS

Firstly, I am immensely grateful to God for the gift of life, protection, love and for the wisdom provided at every stage of my academic journey.

To my wife Edna Argentina Alberto, my son Josué Ivo Ricardo, my brothers Adérito José Ricardo and Ricardo Nelito, my sister Audência de Cádima Romão, my father-in-law and my mother-in-law, Narciso Alberto and Argentina Luís Alberto, respectively, and to all relatives, for the moral support for my academic formation. Special thanks to my wife and my son for their special love and affection.

To my supervisor Professor Alam Gustavo Trovó for his confidence in me, supervision, moral and material support for my trip and integration in Brazil, and for the opportunity to do my teaching internship.

To Professor Carlos Ueira-Vieira and Ph.D. student Serena Mares Malta for the noble collaboration in the bioassays performed at the Genetics Laboratory of the Universidade Federal de Uberlândia.

To Professor Miriam Maria de Resende and Ph.D. student Amanda Carmelo da Rocha for providing equipment for performing analysis of High Performance Liquid Chromatography (HPLC) in the laboratory of the Faculty of Chemical Engineering, Universidade Federal de Uberlândia.

To the members of the qualification examining board, Professors Rodrigo Alejandro Abarza Muñoz, Antonio Otavio de Toledo Patrocínio and João Flávio da Silveira Petrucí, for their readiness to contribute to this work.

To the members of the Examining Board, Professors Antônio Otávio de Toledo Patrocínio, Osmando Ferreira Lopes, Darliana Mello Souza and Amilcar Machulek Junior, for accepting the invitation to evaluate and contribute to the improvement of the quality of this work.

To the Postgraduate Programme in Chemistry of the Institute of Chemistry, Federal University of Uberlândia, for the opportunity to attend the academic Doctorate in Chemistry, as well as for the support offered, specifically, the Multipurpose Laboratory of the Institute of Chemistry for providing the High Performance Liquid Chromatograph with Diode Array Detection (HPLC-DAD).

To the Departamento Municipal de Água e Esgoto (DMAE) of Uberlândia-MG for supplying samples of treated sanitary effluent and respective results of the analyses of physicochemical characterization, used during the experiments.

To the University Save (Mozambique), my professional institution, for granting my full-time leave of absence in order to attend the academic doctorate at the Universidade Federal de Uberlândia.

To all the other Professors of the Institute of Chemistry, Universidade Federal de Uberlândia, for their valuable contribution to my academic training.

To Professors Ana Agüera and José Antonio Sánchez Pérez, both from the University of Almería (Spain) and Professor Maria Clara Vieira Martins Starling from Universidade Federal de Minas Gerais (Brazil), for their noble collaboration on the scientific papers discussed in this manuscript.

To Professors Elísio Machikane Tivane and Malaquias Zildo Antônio Tsambe, both from the Pedagogical University of Maputo (Mozambique), for their valuable contribution to my participation in the selective process that resulted in my admission to the Ph.D. course at the Universidade Federal de Uberlândia.

To my colleagues who are or have been members of the LaQAmb group: Bárbara Rezende Gonçalves, Bruna Andrade Silva, Edna Argentina Alberto, Gabriel Fernandes Vieira, Gabrielly Machado dos Santos, Moisés Joaquim Mbié, Oswaldo Gomes Júnior, Valdislaine Maria da Silva and Vinícius Alexandre Borges de Paiva, for the valuable suggestions, help in performing the experiments and for the pleasant experience during my training. Special thanks to Eduardo Oliveira Marson and Cleiseano Emanuel da Silva Paniagua for their support and partnership in the experiments.

I would like to personally thank Dr. Sarmento Júnior Mazivila (Universidade do Porto (Portugal)) and Professor Domingos Lusitâneo Pier Macuvel (Universidade Rovuma (Mozambique)), friends with whom I have enjoyed learning and working in different lines of research, as can be seen in our recent review papers (<https://doi.org/10.1016/j.teac.2019.e00072>; <https://doi.org/10.1016/j.cej.2021.130282>).

To my friend Afonso Filipe João and to all the Mozambican students at the Universidade Federal de Uberlândia, namely, Alegre de Nascimento Santana Cadeado, Anastácio Armando Boane, Assumane Joaquim Achuate, Carlos José Domingos Alface, Elina Afonso, Gonçalves Jotamo Marrenjo and Tássio Edno Atanásio Pitorro, for their moral and material support and for the pleasant coexistence.

This study was financed in part by the Coordenação de Aperfeiçoamento de Pessoal de Nível Superior – Brasil (CAPES) – Finance Code 001.

“The time is always right to do what is right.”

(Martin Luther King)

## ABSTRACT

This Ph.D. Thesis focuses on the use of Fe-citrate (FeCit) and Fe-nitrilotriacetic acid (FeNTA) complexes and different peroxide sources (hydrogen peroxide ( $\text{H}_2\text{O}_2$ ), persulfate ( $\text{S}_2\text{O}_8^{2-}$ ) and monopersulfate ( $\text{HSO}_5^-$ )) under solar radiation for the degradation of the mixture of benzophenone-3 (BP-3), fipronil (FIP) and propylparaben (PPB) ( $100 \mu\text{g L}^{-1}$  each, added in tertiary sanitary effluent at pH 7.4). In Chapter I, the theme was contextualised, followed by a conceptual approach to the key elements of this research. In Chapter II, a state-of-the-art review of advanced oxidation processes for the degradation of these compounds was carried out and the literature points to a satisfactory degradation, with formation of less toxic transformation products for BP-3 and PPB. However, the low degradation rates achieved in real matrices impose a challenge for full-scale application. Thus, in chapter III the performance of these complexes in the presence of  $\text{H}_2\text{O}_2$  on degradation of the mixture of the three micro-pollutants was evaluated. Degradation efficiencies were significantly improved by increasing the iron concentration (Fe/L (1:1)) from 12.5 to  $100 \mu\text{mol L}^{-1}$  for FeNTA, whereas degradation achieved with FeCit was limited to 30% due to the lower stability of the FeCit complex, and a higher Fe/Cit molar ratio (1:5) was required to maximise degradation efficiency. For the best Fe/L molar ratios, higher degradation rates were achieved using  $5.9 \text{ mmol L}^{-1}$  of  $\text{H}_2\text{O}_2$  for FeNTA and  $2.9 \text{ mmol L}^{-1}$  of  $\text{H}_2\text{O}_2$  for FeCit and a lower concentration of the oxidant was required in the FeCit system due to the *in situ* generation of  $\text{H}_2\text{O}_2$  at pH 7.4. In chapter IV, the performance of both complexes in the presence of  $\text{S}_2\text{O}_8^{2-}$  and  $\text{HSO}_5^-$  under the best experimental conditions determined for  $\text{H}_2\text{O}_2$  was evaluated. Degradation rates with  $\text{S}_2\text{O}_8^{2-}$  were limited to 30% for FeNTA and 55% for FeCit while the addition of  $5.9 \text{ mmol L}^{-1}$  of  $\text{HSO}_5^-$  resulted in acidic solutions and rates above 96%. Higher performance of  $\text{S}_2\text{O}_8^{2-}$  was obtained at acidic pH and after combined removal of chloride, bicarbonate and sulphate ions. The low degradation rates with  $\text{S}_2\text{O}_8^{2-}$  at pH 7.4 was also influenced by the structure of the target compounds. The acute toxicity to *D. Melanogaster* reduced significantly after treatment for both iron complexes with  $\text{H}_2\text{O}_2$ , indicating the formation of low-toxicity by-products. Although FeCit provided higher kinetics, its use inserts higher organic loading, resulting in higher cost-effectiveness ( $20 \text{ US\$ m}^{-3}$  versus  $13 \text{ US\$ m}^{-3}$  para FeNTA) and emphasizing the importance of evaluation and optimization of the operational parameters for each ligand and peroxide source.

**Keywords:** acute toxicity; advanced oxidation processes; aqueous matrices; *D. melanogaster*; micro-pollutants; peroxide sources; solar photo-Fenton.

## RESUMO

Esta Tese de Doutorado tem como foco o uso dos complexos Fe-citrato (FeCit) e Fe-ácido nitrilotriacético (FeNTA) e diferentes fontes de peróxido (peróxido de hidrogênio ( $\text{H}_2\text{O}_2$ ), íons persulfato ( $\text{S}_2\text{O}_8^{2-}$ ) e monopersulfato ( $\text{HSO}_5^-$ )) sob radiação solar para a degradação da mistura da benzofenona-3 (BP-3), fipronil (FIP) e propilparabeno (PPB) ( $100 \mu\text{g L}^{-1}$  cada, adicionados em efluente sanitário terciário a pH 7,4). No capítulo I, fez-se a contextualização sobre o tema, seguida da abordagem conceitual dos elementos-chave desta pesquisa. No Capítulo II, efetuou-se uma revisão referente ao estado-de-arte sobre os processos oxidativos avançados voltados à degradação desses compostos e a literatura aponta para uma degradação satisfatória, com formação de produtos de transformação menos tóxicos para BP-3 e PPB. Contudo, as baixas taxas de degradação alcançadas em matrizes reais impõem um desafio para aplicação à escala real. Assim, no capítulo III avaliou-se o desempenho desses complexos na presença de  $\text{H}_2\text{O}_2$  sobre degradação da mistura dos três micropoluentes. As eficiências de degradação melhoraram significativamente ao aumentar a concentração de ferro (Fe/L (1:1)) de 12,5 para  $100 \mu\text{mol L}^{-1}$  para FeNTA, enquanto que a degradação alcançada com FeCit foi limitada a 30% devido à menor estabilidade do complexo FeCit, sendo necessária uma razão molar Fe/Cit maior (1:5) para maximizar a eficiência de degradação. Para as melhores razões molares Fe/L, foram atingidas taxas de degradação mais elevadas utilizando  $5,9 \text{ mmol L}^{-1}$  de  $\text{H}_2\text{O}_2$  para FeNTA e  $2,9 \text{ mmol L}^{-1}$  de  $\text{H}_2\text{O}_2$  para FeCit e foi necessária uma menor concentração do oxidante no sistema FeCit devido à geração *in situ* do  $\text{H}_2\text{O}_2$  em pH 7,4. No capítulo IV, avaliou-se o desempenho de ambos complexos na presença de  $\text{S}_2\text{O}_8^{2-}$  e  $\text{HSO}_5^-$  sob as melhores condições experimentais determinadas para  $\text{H}_2\text{O}_2$ . As taxas de degradação com  $\text{S}_2\text{O}_8^{2-}$  foram limitadas a 30% para FeNTA e 55% para FeCit enquanto que a adição de  $5,9 \text{ mmol L}^{-1}$  de  $\text{HSO}_5^-$  resultou soluções ácidas e taxas acima de 96%. Maior desempenho de  $\text{S}_2\text{O}_8^{2-}$  foi obtido em meio ácido e após remoção combinada de íons cloreto, bicarbonato e sulfato. As baixa taxas de degradação com  $\text{S}_2\text{O}_8^{2-}$  em pH 7,4 também foi influenciada pela estrutura dos compostos-alvo. A toxicidade aguda para *D. Melanogaster* reduziu significativamente após tratamento para ambos complexos de ferro com  $\text{H}_2\text{O}_2$ , indicando a formação de subprodutos de baixa toxicidade. Embora FeCit tenha proporcionado maior cinética, seu uso insere maior carga orgânica, resultando em maior custo-benefício ( $20 \text{ US\$ m}^{-3}$  versus  $13 \text{ US\$ m}^{-3}$  para FeNTA) e enfatizando a importância de avaliação e otimização dos parâmetros operacionais para cada ligante e fonte de peróxido.

**Palavras-chave:** toxicidade aguda; processos oxidativos avançados; matrizes aquosas; *D. melanogaster*; micropoluentes; fontes de peróxido; foto-Fenton solar.

## LIST OF ILLUSTRATIONS

Figure 1.1 – Structural formula of NTA ( $C_6H_9NO_6$ – MM = 119.14 g mol <sup>-1</sup> ).....	27
Figure 1.2 – Molecular structure of sodium citrate ( $Na_3C_6H_5O_7$ – MM = 258.06 g mol <sup>-1</sup> ). ....	28
Figure 1.3 – UV - Vis absorption spectra of aqueous solutions of Fe(III)-Cit and Fe(III)-NTA complexes prepared in distilled water. Initial conditions: $[Fe^{3+}] = 100 \mu mol L^{-1}$ ; Fe/Ligand molar ratio: Fe/NTA = 1:1; Fe/Cit = 1:5. ....	30
Figure 1.4 – (a) $Na_2S_2O_8$ and (b) Oxone triple salt molecular structure (*potassium PMS ( $KHSO_5$ ) - active part of Oxone®). Reprinted from Waclawek et al. (2017).....	38
Figure 2.1 – Number of publications (a) per year and (b) per aqueous matrix in the last 10 years related to the application of AOPs for the degradation of BP-3, FIP and PPB. Reprinted from Ricardo et al. (2022). ....	42
Figure 2.2 – Number of publications per compound (■ Single; ● Target-Compound+other CEC; ▲ Real matrix; ▼ Synthetic matrix) related to the application of AOPs for the degradation of BP-3, FIP and PPB in the last 10 years. Reprinted from Ricardo et al. (2022).....	43
Figure 2.3 – Speciation diagrams of ferric complexes as a function of pH for a solution at T = 25 °C in the presence of $1.0 \times 10^{-5}$ M of Fe(III), $1.0 \times 10^{-5}$ M of EDTA (a), $1.0 \times 10^{-5}$ M of citrate (b), $1.0 \times 10^{-5}$ M of NTA (c), $3.0 \times 10^{-5}$ M of oxalate (d), $1.0 \times 10^{-5}$ M of tartrate (e), and $1.0 \times 10^{-5}$ M of EDDS (f). Reprinted from Clarizia et al. (2017). Copright 2017 Elsevier. ....	50
Figure 2.4 – Influence of molar iron/ligand ratio on fipronil (FIP) degradation by photo-Fenton at pH 6.0 using (a) FeCit and (b) FeOx in distilled water. Initial conditions: $[FIP] = 1000 \mu g L^{-1}$ ; $[H_2O_2] = 676 \mu mol L^{-1}$ ; $[iron] = 32 \mu mol L^{-1}$ . Reprinted from Gomes Júnior et al. (2020). Copright 2020 Elsevier.....	51
Figure 2.5 – Effect of pH on variation of (a) BP-3, (b) FIP and (c) PPB molecular ratio. Reprinted from Ricardo et al. (2022).....	57
Figure 2.6 – Proposed BP-3 transformation pathways via oxidation by (a) persulfate, (b) chlorination and UV/chlorination reactions. Adapted from (a) Pan et al. (2018) and (b) Lee et al. (2020). Copright 2017, 2020 Elsevier. ....	67
Figure 2.7 – Mechanism proposed for FIP degradation via FeCit/photo-Fenton process at pH 6 and main TPs. Reprinted from Gomes Júnior et al. (2020). Copyright 2020 Elsevier.....	69
Figure 2.8 – Proposed photocatalytic degradation pathways and mechanism of PPB in water. Reprinted from Fang et al. (2013). ....	71
Figure 3.1 – (a) Absorption spectra of the target compounds ( $1000 \mu g L^{-1}$ each, in deionised water at pH 7.0) and (b) Chromatogram for a solution containing FIP, PPB and BP-3 ( $100 \mu g$	

L <sup>-1</sup> ) in deionised water and near neutral pH (7.0), (c) tertiary sanitary effluent and (d) solution containing FIP, PPB and BP-3 (100 µg L <sup>-1</sup> each) in tertiary sanitary effluent (pH= 7.4 (natural effluent)) using the mobile phase 75% MeOH : 25% HAc (% v/v) for the wavelength (λ) of 279 nm. ....	83
Figure 3.2 – Analytical curves for quantification of (a) BP-3, (b) FIP and (c) PPB in MWWTP effluent at pH 7.4 (natural of the matrix). ....	84
Figure 3.3 – Influence of iron complex source and concentration (■ 12.5 µmol L <sup>-1</sup> , ● 25 µmol L <sup>-1</sup> , ▲ 50 µmol L <sup>-1</sup> and ▼ 100 µmol L <sup>-1</sup> ) on the degradation of the mixture of BP-3, FIP and PPB using the iron complexes (a) FeNTA and (b) FeCit and ((c) and (d)) on the concentration of total dissolved iron during the solar photo-Fenton. Initial conditions: [CEC] = 100 µg L <sup>-1</sup> (for each compound), [H <sub>2</sub> O <sub>2</sub> ] = 5.9 mmol L <sup>-1</sup> , Fe/L= 1:1; pH= 7.4 (natural of the MWWTP effluent). ....	87
Figure 3.4 – Influence of iron complex source and concentrations (■ 12.5 µmol L <sup>-1</sup> , ● 25 µmol L <sup>-1</sup> , ▲ 50 µmol L <sup>-1</sup> and ▼ 100 µmol L <sup>-1</sup> ) on H <sub>2</sub> O <sub>2</sub> consumption during the degradation of BP-3, FIP and PPB by solar photo-Fenton using the iron complexes (a) FeNTA and (b) FeCit. Initial conditions: [CEC] = 100 µg L <sup>-1</sup> (for each compound), [H <sub>2</sub> O <sub>2</sub> ] = 5.9 mmol L <sup>-1</sup> , Fe:L= 1:1; pH = 7.4 (natural of the MWWTP effluent). ....	88
Figure 3.5 – Influence of Fe/L molar ratio (■ 1:1, ● 1:2, ▲ 1:3, ▼ 1:4, ◆ 1:5 and ◀ 1: 6) in the degradation of the mixture of BP-3, FIP and PPB using the iron complexes (a) FeNTA and (b) FeCit, ((c) and (d)) dissolved iron concentration, and ((e) and (f)) H <sub>2</sub> O <sub>2</sub> consumption during the solar photo-Fenton process. Initial conditions: [CEC]= 100 µg L <sup>-1</sup> (for each compound), [H <sub>2</sub> O <sub>2</sub> ] = 5.9 mmol L <sup>-1</sup> , [Fe <sup>3+</sup> ] = 100 µmol L <sup>-1</sup> ; pH= 7.4 (natural of the MWWTP effluent). ....	90
Figure 3.6 – Influence of H <sub>2</sub> O <sub>2</sub> concentration (■ 0.74 mmol L <sup>-1</sup> , ● 1.5 mmol L <sup>-1</sup> , ▲ 2.9 mmol L <sup>-1</sup> , ▼ 5.9 mmol L <sup>-1</sup> , ► 11.8 mmol L <sup>-1</sup> ) on the degradation of the mixture of BP-3, FIP and PPB using the iron complexes (a) FeNTA and (b) FeCit. Initial conditions: [CEC]= 100 µg L <sup>-1</sup> (for each compound), Fe:L= 1:1 (FeNTA) and 1:5 (FeCit), [Fe <sup>3+</sup> ] = 100 µmol L <sup>-1</sup> ; pH= 7.4 (natural of the MWWTP effluent). ....	92
Figure 3.7 – Degradation efficiencies per compound (■ PPB, ● FIP, ▲ BP-3, ▼ Mixture) obtained during the degradation of the mixture of BP-3, FIP and PPB using the iron complexes (a) FeNTA and (b) FeCit. Initial conditions: [CEC]= 100 µg L <sup>-1</sup> (for each compound), Fe:L= 1:1 (FeNTA) and 1:5 (FeCit), [Fe <sup>3+</sup> ] = 100 µmol L <sup>-1</sup> ; [H <sub>2</sub> O <sub>2</sub> ] = 5.9 mmol L <sup>-1</sup> (for FeNTA) and 2.9 mmol L <sup>-1</sup> (for FeCit); pH= 7.4 (natural of the MWWTP effluent). ....	93

Figure 3.8 – <i>D. melanogaster</i> survival assay for MWWTP effluent samples enriched with the mixture of BP-3, FIP and PPB before and after solar/photo-Fenton treatment using different iron complexes: (a) FeNTA and (b) FeCit. Initial conditions: [CEC]= 100 $\mu\text{g L}^{-1}$ (for each compound), Fe/L= 1:1 (FeNTA) and 1:5 (FeCit), $[\text{Fe}^{3+}] = 100 \mu\text{mol L}^{-1}$ ; $[\text{H}_2\text{O}_2] = 5.9 \text{ mmol L}^{-1}$ (for FeNTA) and $2.9 \text{ mmol L}^{-1}$ (for FeCit). .....	94
Figure 3.9 – Results obtained during <i>D. melanogaster</i> survival assay for (a) control experiments; (b) individual solutions of the target compounds and ((c) and (d)) samples of MWWTP effluent in the absence of BP3, FIP and PPB but in the presence of iron complexes before and after solar photo-Fenton treatment. Initial conditions: [CEC] = 100 $\mu\text{g L}^{-1}$ (for each compound), Fe/L= 1:1 (FeNTA) and 1:5 (FeCit), $[\text{Fe}^{3+}] = 100 \mu\text{mol L}^{-1}$ ; $[\text{H}_2\text{O}_2] = 2.94 \text{ mmol L}^{-1}$ (for FeCit, $\text{Fe}^{3+}$ , $\text{H}_2\text{O}_2$ (in the dark) and $\text{H}_2\text{O}_2/\text{solar}$ ) and $5.9 \text{ mmol L}^{-1}$ (for FeNTA), pH = 7.4 (natural of the MWWTP effluent). .....	95
Figure 3.10 – Control experiments for the degradation of BP-3, FIP and PPB using the iron complexes FeNTA and FeCit. Initial conditions: [CEC]= 100 $\mu\text{g L}^{-1}$ (for each compound), Fe:L= 1:1 (FeNTA) and 1:5 (FeCit), $[\text{Fe}^{3+}] = 100 \mu\text{mol L}^{-1}$ ; $[\text{H}_2\text{O}_2] = 2.94 \text{ mmol L}^{-1}$ (for FeCit, $\text{Fe}^{3+}$ , $\text{H}_2\text{O}_2$ (in the dark) and $\text{H}_2\text{O}_2/\text{solar}$ ) and $5.9 \text{ mmol L}^{-1}$ (for FeNTA), pH= 7.4 (natural of the MWWTP effluent). .....	98
Figure 4.1 – Influence of $\text{HSO}_5^-$ concentration on the degradation of the mixture of BP-3, FIP and PPB using the iron complexes (a) FeNTA and (b) FeCit, ((c) and (d)) dissolved iron concentration, and ((e) and (f)) $\text{HSO}_5^-$ consumption. Initial conditions: [CEC]= 100 $\mu\text{g L}^{-1}$ (for each compound), Fe:L= 1:1 (FeNTA) and 1:5 (FeCit), $[\text{Fe}^{3+}] = 100 \mu\text{mol L}^{-1}$ ; pH= 7.4 (natural of the MWWTP effluent). .....	108
Figure 4.2 – Influence of $\text{S}_2\text{O}_8^{2-}$ concentration on the degradation of the mixture of BP-3, FIP and PPB using the iron complexes (a) FeNTA and (b) FeCit, ((c) and (d)) dissolved iron concentration, and ((e) and (f)) $\text{S}_2\text{O}_8^{2-}$ consumption. Initial conditions: [CEC]= 100 $\mu\text{g L}^{-1}$ (for each compound), Fe:L= 1:1 (FeNTA) and 1:5 (FeCit), $[\text{Fe}^{3+}] = 100 \mu\text{mol L}^{-1}$ ; pH= 7.4 (natural of the MWWTP effluent). .....	110
Figure 4.3 – Influence of $\text{S}_2\text{O}_8^{2-}$ and $\text{HSO}_5^-$ concentrations on the pH of the reaction medium during the degradation of the mixture of BP-3, FIP and PPB using FeNTA and FeCit complexes. Initial conditions: [CEC]= 100 $\mu\text{g L}^{-1}$ (for each compound), Fe:L= 1:1 (FeNTA) and 1:5 (FeCit), $[\text{Fe}^{3+}] = 100 \mu\text{mol L}^{-1}$ ; pH= 7.4 (natural of the MWWTP effluent). .....	112
Figure 4.4 – Influence of pH on the degradation efficiency of BP-3, FIP and PPB mixture by solar photo-Fenton using the (a) FeNTA and (b) FeCit complexes, ((c) and (d)) dissolved iron	

concentration, and ((e) and (f)) $S_2O_8^{2-}$ consumption. Initial conditions: $[CEC]= 100 \mu\text{g L}^{-1}$ (for each compound), $\text{Fe:L}= 1:1$ (FeNTA) and $1:5$ (FeCit), $[\text{Fe}^{3+}] = 100 \mu\text{mol L}^{-1}$ and $[S_2O_8^{2-}]=2.94 \text{ mmol L}^{-1}$ .....	114
Figure 4.5 – Effect of inorganic ion removal from tertiary wastewater on (a) degradation of BP-3, FIP and PPB mixture by solar photo-Fenton process using FeNTA and $S_2O_8^{2-}$ and (b) pH variation. Initial conditions: $[CEC]= 100 \mu\text{g L}^{-1}$ (for each compound), $\text{Fe(III):NTA}= 1:1$ , $[\text{Fe}^{3+}] = 100 \mu\text{mol L}^{-1}$ , $[S_2O_8^{2-}]= 5.9 \text{ mmol L}^{-1}$ and $\text{pH} = 7,4$ (natural da matriz). .....	119
Figure 4.6 – Degradation profile of NAP by solar photo-Fenton process using FeNTA complex in the presence of $S_2O_8^{2-}$ . Initial conditions: $[\text{NAP}]= 100 \mu\text{g L}^{-1}$ , $[\text{Fe}^{3+}]= 100 \mu\text{mol L}^{-1}$ , $\text{Fe:NTA} = 1:1$ and $\text{pH} = 7.4$ (natural of the matrix). .....	120
Figure 4.7 – Structural formula of NAP ( $C_{14}H_{14}O_3$ – Molar weight = $230.3 \text{ g mol}^{-1}$ ). .....	121

## LIST OF TABLES

Table 1.1 – Chemical structure and physicochemical properties of selected target compounds. ....	32
Table 2.1 – Summary of the application of Fenton reaction for the degradation of BP-3, FIP and PPB in aqueous matrices. ....	46
Table 2.2 – Experimental conditions applied in TiO <sub>2</sub> /UV-A, TiO <sub>2</sub> /H <sub>2</sub> O <sub>2</sub> /UV-A, TiO <sub>2</sub> /S <sub>2</sub> O <sub>8</sub> <sup>2-</sup> /UV, ZnO/S <sub>2</sub> O <sub>8</sub> <sup>2-</sup> /UV and UV-C/H <sub>2</sub> O <sub>2</sub> processes and efficiencies obtained for BP-3, FIP and PPB degradation in aqueous matrices. ....	59
Table 2.3 – Experimental conditions of SR-AOPs and efficiencies obtained for BP-3, FIP and PPB degradation in aqueous matrices. ....	64
Table 2.4 – Experimental conditions and efficiencies obtained during the degradation of BP-3, FIP and PPB in aqueous matrices by various AOPs. ....	71
Table 3.1 – Physicochemical characterization of MWWTP effluent sample. ....	81
Table 3.2 – Straight line equations of the analytical curves, linear ranges, linear correlation coefficient (R <sup>2</sup> ), limit of detection (LOD) and limit of quantification (LOQ) for the target compounds. ....	85
Table 3.3 – Reagents prices (iron, chelating agents and oxidant) for the photo-Fenton process, as according to Sigma-Aldrich®. ....	96
Table 3.4 – Pseudo-first kinetic constants and cost assessment for solar photo-Fenton using different iron complexes. ....	97
Table 4.1 – Influence of the ratio between the mobile phases (methanol and HAc) on the retention time of NAP and dead volume, in tertiary sanitary effluent. ....	106
Table 4.2 – Straight line equations of the analytical curves, linear ranges, linear correlation coefficient (R <sup>2</sup> ), limit of detection (LOD) and limit of quantification (LOQ) for the target compounds. ....	106
Tabela 4.3 – Variation of total carbon (TC), inorganic carbon (IC) and total organic carbon (TOC) of the tertiary sanitary effluent used in the experiments, as a function of pH. ....	116
Tabela 4.4 – Characterization of the matrix after isolated and simultaneous removal of HCO <sub>3</sub> <sup>-</sup> , Cl <sup>-</sup> and SO <sub>4</sub> <sup>2-</sup> . ....	116

## LIST OF ABBREVIATIONS AND ACRONYMS

AOPs	Advanced oxidation processes
BP-3	Benzophenone-3
CB	Conduction band
CEC	Contaminants of emerging concern
Cit	Citrate
COD	Chemical oxygen demand
CONAMA	Conselho Nacional do Meio Ambiente
DOC	Dissolved organic carbon
EDDS	Ethylenediamine-N,N'-disuccinic
EDTA	Ethylenediaminetetraacetic acid
Eq.	Equation
FIP	Fipronil
GC-QTOF/MS	Gas Chromatography Time-of-Flight mass Spectrometry
GC/MS	Gas Chromatography coupled to Mass Spectrometry
HPLC/MS	High Performance Liquid Chromatography coupled to Mass Spectrometry
IUPAC	International Union of Pure and Applied Chemistry
IR	Infra-Red
Kow	n-octanol/water partition coefficient
LC-MS/MS	Liquid chromatography–mass spectrometry
LC-QTOF/MS	Liquid Chromatography Quadrupole Time-of-Flight Mass Spectrometry
LOD	Limit of detection
LOQ	Limit of quantification
MPS	peroxymonosulphate
MWWTP	Municipal wastewater treatment plant
NTA	Nitrilotriacetic acid
Ox	Oxalate
PPB	Propylparaben
PPCPs	Pharmaceutical drugs and personal care products
PS	Persulfate
PZC	Point of zero charge
SR – AOPs	Sulfate radical-based advanced oxidation Processes

UASB	Upflow anaerobic sludge blanket
UV	Ultraviolet
VB	Valence band
Vis	Visible

## TABLE OF CONTENTS

<b>1</b>	<b>CHAPTER I – INTRODUCTION, BACKGROUND AND OBJECTIVES</b>	<b>24</b>
<b>1.1</b>	<b>Introduction and rationale</b>	<b>24</b>
<b>1.2</b>	<b>Selected organic ligands</b>	<b>27</b>
1.2.1	Nitrilotriacetic Acid (NTA)	27
1.2.2	Citrate (Cit)	28
<b>1.3</b>	<b>Selected micro-pollutants</b>	<b>30</b>
1.3.1	Benzophenone-3 (BP-3)	33
1.3.2	Fipronil (FIP)	33
1.3.3	Propylparaben (PPB)	34
<b>1.4</b>	<b>Advanced oxidation processes: An overview</b>	<b>35</b>
<b>1.5</b>	<b>Goals</b>	<b>39</b>
1.5.1	Research aim	39
1.5.2	Research objectives	39
<b>2</b>	<b>CHAPTER II – A CRITICAL REVIEW OF TRENDS IN ADVANCED OXIDATION PROCESSES FOR THE REMOVAL OF BENZOPHENONE-3, FIPRONIL, AND PROPYLPARABEN FROM AQUEOUS MATRICES: PATHWAYS AND TOXICITY CHANGES</b>	<b>40</b>
<b>2.1</b>	<b>Introduction</b>	<b>40</b>
<b>2.2</b>	<b>Advanced Oxidation Processes (AOPs)</b>	<b>45</b>
2.2.1	Fenton reactions	45
2.2.2	Heterogeneous photocatalysis	52
2.2.2.1	<i>Photocatalyst reusability and separation</i>	54
2.2.2.2	<i>pH effect on photocatalytic degradation of BP-3, FIP and PPB</i>	55
2.2.3	Photo-assisted peroxidation	57
2.2.4	Sulfate radical based AOPs (SR-AOPs)	62
2.2.5	Other AOPs	67
2.2.5.1	<i>Sonochemistry</i>	67
2.2.5.2	<i>Ozonation and electrochemical oxidation</i>	68
2.2.5.3	<i>Photolysis of monochloramine and hypochlorite ion</i>	69
<b>2.3</b>	<b>Degradation pathways, transformation products (TPs) and toxicity</b>	<b>66</b>
2.3.1	Benzophenone-3	66
2.3.2	Fipronil	67

2.3.3	Propylparaben .....	70
<b>2.4</b>	<b>Concluding remarks and future trends .....</b>	<b>71</b>
<b>2.5</b>	<b>Attachment .....</b>	<b>72</b>
<b>3</b>	<b>CHAPTER III: EFFECT OF IRON COMPLEX SOURCE ON MWWTP EFFLUENT TREATMENT BY SOLAR PHOTO-FENTON: MICROPOLLUTANT DEGRADATION, TOXICITY REMOVAL AND OPERATING COSTS.....</b>	<b>73</b>
<b>3.1</b>	<b>Introduction.....</b>	<b>73</b>
<b>3.2</b>	<b>Experimental.....</b>	<b>75</b>
3.2.1	Reagents.....	75
3.2.2	MWWTP effluent .....	75
<b>3.3</b>	<b>Photodegradation experiments.....</b>	<b>76</b>
<b>3.4</b>	<b>Chemical and bioassay analysis.....</b>	<b>77</b>
3.4.1	Target Compound .....	78
3.4.2	Hydrogen peroxide .....	78
3.4.3	Total iron dissolved ( $\text{Fe}^{3+}$ and $\text{Fe}^{2+}$ ) .....	79
3.4.4	Bioassays with <i>Drosophila melanogaster</i> .....	79
<b>3.5</b>	<b>Results and discussion .....</b>	<b>80</b>
3.5.1	Characterization of MWWTP effluent water.....	80
3.5.2	Analytical method by HPLC - DAD for determination of BP-3, FIP, PPB .....	82
3.5.3	Influence of the source and concentration of the iron on the degradation of BP-3, FIP and PPB .....	86
3.5.4	Influence of Fe/L molar ratio on the degradation of BP-3, FIP and PPB.....	89
3.5.5	Influence of $\text{H}_2\text{O}_2$ concentration on the degradation of BP-3, FIP and PPB.....	91
3.5.6	Acute toxicity assays: <i>Drosophila melanogaster</i> lifespan .....	93
3.5.7	Cost assessment .....	96
<b>3.6</b>	<b>Conclusions.....</b>	<b>99</b>
<b>3.7</b>	<b>Attachment .....</b>	<b>99</b>
<b>4</b>	<b>CHAPTER IV – PERSULFATE AND MONOPERSULFATE IONS AS PEROXIDE SOURCES IN SOLAR PHOTO-FENTON MODIFIED WITH ORGANIC IRON COMPLEXES FOR THE DEGRADATION OF MICRO-CONTAMINANTS IN A TERTIARY EFFLUENT FROM A MUNICIPAL WASTEWATER TREATMENT PLANT.....</b>	<b>100</b>
<b>4.1</b>	<b>Introduction.....</b>	<b>100</b>
<b>4.2</b>	<b>Experimental.....</b>	<b>101</b>

4.2.1	Reagents.....	101
4.2.2	MWWTP effluent .....	102
<b>4.3</b>	<b>Photodegradation experiments.....</b>	<b>102</b>
<b>4.4</b>	<b>Chemical analysis.....</b>	<b>104</b>
4.4.1	Persulfate and monopersulfate ions .....	104
<b>4.5</b>	<b>Results and discussion .....</b>	<b>105</b>
4.5.1	Analytical method by HPLC - DAD for determination of BP-3, FIP, PPB and NAP	105
4.5.2	Effect of $S_2O_8^{2-}$ and $HSO_5^-$ concentration on the degradation of BP-3, FIP and PPB	106
4.5.3	Effect of pH on the degradation of BP-3, FIP and PPB using $S_2O_8^{2-}$ .....	112
4.5.4	Influence of $Cl^-$ , $SO_4^{2-}$ and $HCO_3^-$ on the degradation of the mixture of BP-3, FIP and PPB	116
4.5.5	Comparison of the efficiency of degradation of the target compounds with NAP.....	120
<b>4.6</b>	<b>Conclusions.....</b>	<b>122</b>
<b>5</b>	<b>CHAPTER V: GENERAL CONCLUSIONS.....</b>	<b>123</b>
<b>6</b>	<b>CHAPTER VI: FUTURE RECOMMENDATIONS.....</b>	<b>124</b>
<b>7</b>	<b>REFERENCES.....</b>	<b>125</b>

## 1 CHAPTER I – INTRODUCTION, BACKGROUND AND OBJECTIVES

### 1.1 Introduction and rationale

The growth of the global economy combined with population growth has been pointed out as a precursor to the expansion of industrial activities and the increase in agricultural production. These activities are the main consumers of water resources and generate large amounts of waste, some of which have recalcitrant characteristics (SHUKLA et al., 2010). However, the improper disposal and treatment of these wastes generate environmental impacts on the biotic and abiotic environment (MONTAGNER; VIDAL; ACAYABA, 2017).

Different classes of compounds such as phthalates, surfactants, industrial additives, sunscreen/UV filters, perfluorinated compounds, disinfection by-products, pharmaceutical drugs and personal care products (PPCPs), hormones, pesticides, nanomaterials and microplastics, illicit drugs and degradation metabolites of these compounds have been detected in environmental monitoring studies (BÖGER et al., 2021; LÓPEZ-GARCÍA et al., 2021; MARSON et al., 2022a) and are part of the pollutants called contaminants of emerging concern (CEC). The term CEC has been used to refer to natural or synthetic substances that occur in different environmental compartments (groundwater, rain water, ocean water, drinking water, sediments and soil) with potential or real threat to human health and/or the environment.

CEC do not have legislation that establishes either potability standards or safe toxicity levels and/or are poorly regulated by Brazilian and international water quality standards (MARSON et al., 2022a; MONTAGNER; VIDAL; ACAYABA, 2017; STARLING; AMORIM; LEÃO, 2019). These contaminants occur at low concentrations ( $\mu\text{g L}^{-1}$  or  $\text{ng L}^{-1}$ ) in environmental matrices and these matrices contain several other components that make detection of these compounds difficult. Therefore, the occurrence or relevance of CEC in the environment was confirmed in the 1990s as a result of the development of advanced analytical methods such as High Performance Liquid Chromatography coupled to Mass Spectrometry (HPLC/MS) or Gas Chromatography coupled to Mass Spectrometry (GC/MS) for proper identification and quantification in aqueous matrices (MARSON et al., 2022a; MONTAGNER; VIDAL; ACAYABA, 2017; STARLING; AMORIM; LEÃO, 2019).

Even at low concentrations, the occurrence of CEC in aquatic compartments can contribute to the development of adverse effects on aquatic life and public health, such as bacterial resistance, endocrine disruption, toxicity, carcinogenicity, obesity and tumor development, respiratory diseases and diabetes in humans (MARSON et al., 2022a;

STARLING; AMORIM; LEÃO, 2019). In this regard, the continuous discharge of these pollutants into the environment and the establishment and implementation of legal norms to control such discharge has been one of the current concerns of the scientific and legislative communities in developed countries.

There are several sources (i.e. dumping of drug residues by pharmaceutical industries, disposal of expired or unused medicines and the use of cattle feces as soil fertilizer) of these contaminants for aquatic compartments (STARLING; AMORIM; LEÃO, 2019). However, considering that many municipal wastewater treatment plants (MWWTP) are not designed to remove organic compounds, such as pesticides, PPCPs, among others (KRZEMINSKI et al., 2019), which are mostly non-biodegradable, these facilities have been pointed out as the main sources of CEC for the environment. Thus, advanced oxidation processes (AOPs), based on the generation of highly reactive hydroxyl ( $\text{HO}^\bullet$ ) and sulfate ( $\text{SO}_4^{\bullet-}$ ) radicals (MAZIVILA et al., 2019; RAHIM POURAN; ABDUL AZIZ; WAN DAUD, 2015) have been evaluated as a complementary treatment step in MWWTP aiming at the degradation of these compounds (MAZIVILA et al., 2019).

Since natural water matrices generally have neutral pH, the evaluation of pH-independent AOPs is relevant for full-scale applications, avoiding the previous step of acidification followed by neutralization before the release of the treated effluent into the environment. The use of iron chelating agents is one of the strategies to circumvent the effects of pH on AOPs. These agents form stable iron complexes, keep iron soluble over a wide pH range, and increase light absorption efficiency (CLARIZIA et al., 2017), favoring the application of the photo-Fenton process in near-neutral conditions.

Organic iron ligands such as oxalate (Ox), citrate (Cit), nitrilotriacetic acid (NTA), ethylenediaminetetraacetic acid (EDTA) and ethylenediamine-N,N'-disuccinic (EDDS) have already been used in AOPs for the removal of CEC from aqueous matrices (DE LUCA; DANTAS; ESPLUGAS, 2014; SILVA et al., 2021; SORIANO-MOLINA et al., 2021). To the best of our knowledge, only one study evaluated the efficiency and operational costs associated with the use of different sources of iron (EDDS and NTA) in the degradation of a micropollutant in MWWTP effluent at neutral pH (SORIANO-MOLINA et al., 2021).

Considering that CEC occur in MWWTP effluents (FANG et al., 2019; SADARIA et al., 2019) and matrix components affect degradation efficiency and route, thus influencing the structure and concentration of transformation products (TPs) generated during degradation of organic matter from CEC, chelating agents and matrix itself (AMILDON RICARDO et al., 2018a; PANIAGUA et al., 2020), more studies using real effluents are needed. Besides, as

effluents vary in composition, toxicity must also be used as response variable for a comprehensive evaluation of the efficiency of each chelating agent in terms of environmental footprint (CLARIZIA et al., 2017).

In this context, this study focused on the effect of solar photo-Fenton applied in the presence of different chelating agents (Cit and NTA) for the degradation and toxicity removal of a mixture of CECs at neutral pH in MWWTP effluent and under solar irradiation. The personal care products (benzophenone-3 (BP-3) and propylparaben (PPB)) and the insecticide fipronil (FIP) were selected as model pollutants and were added to the matrix at an initial concentration of  $100 \mu\text{g L}^{-1}$  for each of them. These contaminants were selected because they have been detected in concentrations in the order of  $\mu\text{g L}^{-1}$  and  $\text{ng L}^{-1}$  in surface water (BASIN et al., 2016), raw wastewater (CANOSA et al., 2006; LEE; PEART; SVOBODA, 2005; LI et al., 2015a), treated effluent (HANEKAMP; BAST, 2014; HOPKINS; BLANEY, 2016; SADARIA et al., 2019), groundwater (SEMONES et al., 2017) and drinking water (MONTAGNER; VIDAL; ACAYABA, 2017) and associated to toxic effects (DA COSTA FILHO et al., 2016; SADARIA et al., 2019). In addition, studies evaluating the application of AOPs for the degradation of these three compounds are scarce and more than half were carried out in deionized water (RICARDO et al., 2022). Furthermore, considering that prior knowledge of the state-of-the-art of the target micro-pollutants, as well as the AOPs involved in their degradation in aqueous matrices, is an important "compass" for the development of the research, this Thesis also aimed to review the literature regarding the trends of AOPs (operational parameters, pathways and toxicity) for the removal of BP-3, FIP and PPB from aqueous matrices. In order to facilitate the reading and understanding of this manuscript, it was organized according to the following structure:

- Chapter I (this section): Introduction and background, state-of-the-art regarding the selected ligands and target micro-pollutants (occurrence and associated risk to the environment), overview on advanced oxidation processes (AOPs) and proposed objectives;
- Chapter II: Critical literature review on trends in advanced oxidation processes (number of publications per year and per aqueous matrix, operational parameters, mechanisms and toxicity evolution) applied for the degradation of target compounds;
- Chapter III: Evaluation of the use of NTA and Cit as iron sources for hydrogen peroxide ( $\text{H}_2\text{O}_2$ ) activation aiming at the degradation of the mixture of BP-3, FIP

and PPB at natural matrix pH with focus on the evaluation and optimization of operational parameters (iron concentration, iron/ligand molar ratio, H<sub>2</sub>O<sub>2</sub> concentration), evaluation of acute toxicity to the drosophila melanogaster fly and analysis of the costs associated with each iron complex.

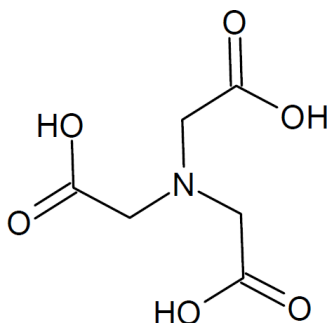
- Chapter IV: Evaluation of the influence of S<sub>2</sub>O<sub>8</sub><sup>2-</sup> and HSO<sub>5</sub><sup>-</sup> concentration on the degradation of BP-3, FIP and PPB mixture in the presence of both iron complexes (FeNTA and FeCit); effect of pH, matrix composition and structure of the target compounds on the performance of the photo-Fenton process involving S<sub>2</sub>O<sub>8</sub><sup>2-</sup>.
- Chapter V: Outlooks with regard to the data generated during this work.
- Chapter VI: Future recommendations.

## 1.2 Selected organic ligands

### 1.2.1 Nitriilotriacetic Acid (NTA)

Nitriilotriacetic acid (NTA) (Figure 1.1) is an aminopolycarboxylic acid distinguished by three carboxylate groups linked via carbon atoms to a nitrogen atom. Aminopolycarboxylic acids have the ability to form very stable water-soluble complexes with many di- or trivalent metal ions and are therefore used for domestic and industrial applications to control the solubility and precipitation of metal ions (DE LUCA; DANTAS; ESPLUGAS, 2015).

**Figure 1.1** – Structural formula of NTA (C<sub>6</sub>H<sub>9</sub>NO<sub>6</sub> – MM = 119.14 g mol<sup>-1</sup>).



**Source:** The Author.

The strong capacity of NTA as an iron chelator (pK<sub>a</sub> = 15.9 for FeNTA) makes it a reasonable candidate to be employed as an iron source in photo-Fenton process at near neutral

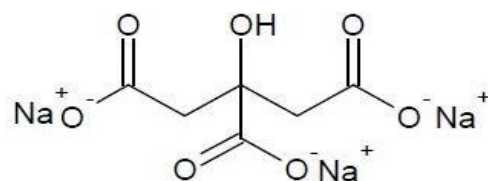
pH (DE LUCA; DANTAS; ESPLUGAS, 2015; HOWSAWKENG et al., 2001; SILVA et al., 2021). Furthermore, this chelator shows good stability under irradiation and higher biodegradability compared to other strong chelators (MEANS; KUCAK; CRERAR, 1980; SVENSON; KAJ; BJÖRNDAL, 1989). On the other hand, concerns about the toxicity of NTA have been belied, especially when considering the low concentration assumptions for its application (DE LUCA; DANTAS; ESPLUGAS, 2015). However, the toxicity and biodegradability of chelates are strongly dependent on the metal speciation (PIRKANNIEMI; SILLANPÄÄ; SOROKIN, 2003; SILLANPÄÄ; PIRKANNIEMI; DHONDUP, 2003) and on certain occasions the toxicity of the chelate may be even lower than that of the free chelator (DE LUCA; DANTAS; ESPLUGAS, 2015). Although an increase in acute toxicity is expected in case of heavy metal chelation, considering the higher value of the equilibrium constant of FeNTA, the exchange of iron for other heavy metals may be lower.

In the presence of 4-chlorophenol at pH 6.0, FeNTA shows a low value (0.16) of quantum yield of ferrous ion generation at 313 nm (ABIDA et al., 2006), which is a reflection of the low reactivity of NTA with hydroxyl radicals (HO•) and this justifies the higher stability of this chelate.

### 1.2.2 Citrate (Cit)

Citric acid is a ubiquitous molecule of biological relevance and one of the biological roles of its salt (citrate) is its ability to chelate metals and particularly iron. Sodium citrate (Figure 1.2) is commonly used as an organic iron ligand in the photo-Fenton. The ability of Cit to solubilize iron hydroxide has been exploited by both plants and microbes and, in bacteria, citric acid acts as an exogenous siderophore (SILVA et al., 2009).

**Figure 1.2** – Molecular structure of sodium citrate ( $\text{Na}_3\text{C}_6\text{H}_5\text{O}_7$  – MM = 258.06 g mol<sup>-1</sup>).

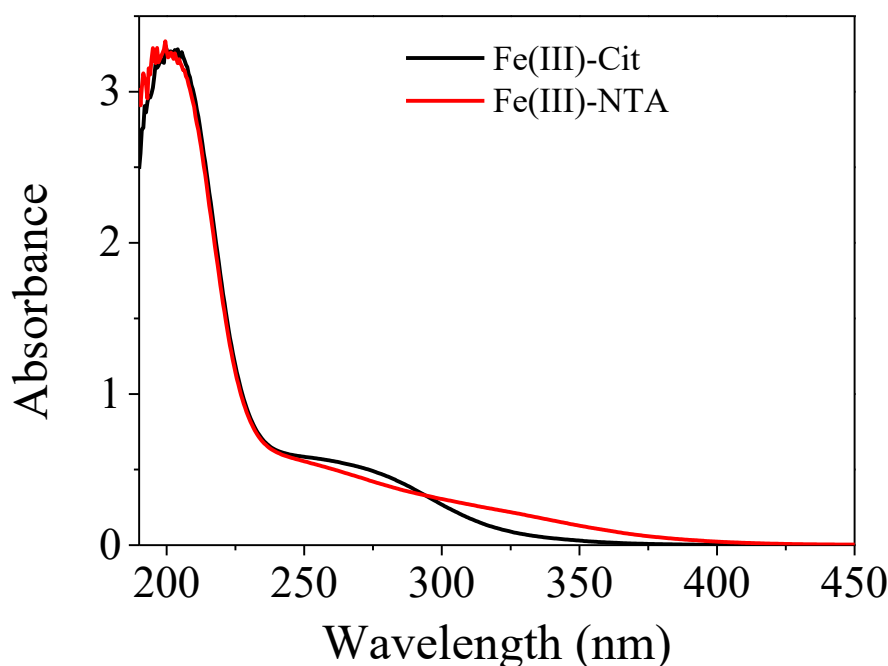


**Source:** The Author.

In humans, Fe(III) binding by citrate is of particular importance in conditions of iron overload (SILVA et al., 2009). However, the chemistry of ferric citrate is complex and a definitive description of its aqueous speciation at neutral pH remains unclear. The alcoholic function of citrate ( $\text{Cit}^{4-}$ ) is also involved in Fe(III) coordination and the deprotonation of this functional group occurs after complex formation (MATZAPETAKIS et al., 1998). The inability to include this deprotonation in the affinity constant calculations was the main source of divergence among several studies of FeCit affinity constants. However, the determination of the alcoholic pKa of citric acid ( $\text{H}_4\text{Cit}$ ) (SILVA; KONG; HIDER, 2009) made it possible to re-evaluate the ferric citrate system. Although thermodynamics predicts the precipitation of hydrated ferric ions above pH 7.0, this precipitation is slow, with homogeneous FeCit species predominating (CHEN et al., 2011). In this context, FeCit is the predominant species up to pH 4.0 and, above this pH, the formation of the species  $\text{FeOHCit}^-$  and  $\text{Fe}_2(\text{OH})_2(\text{Cit})_2^{2-}$  occurs, the first two being responsible for inducing the photochemical formation of  $\text{HO}^\bullet$  (CHEN et al., 2011).

Nevertheless, the FeCit complex is a viable alternative for iron solubility in the photo-Fenton process. Although its photolysis shows a lower quantum yield for  $\text{Fe}^{2+}$  generation compared to ferrioxalate, citrate is less toxic with higher cumulative stability constants ( $\log \beta = 14.29$ ), is readily available and can be used at higher pH values than oxalate (up to pH 9.0) (CLARIZIA et al., 2017; RUALES-LONFAT et al., 2016). Like NTA, iron availability by FeCit occurs up to near-neutral pH values (CLARIZIA et al., 2017). Furthermore, FeCit and FeNTA contribute to increasing light absorption efficiency, as they extend the absorption band to the UV-A (315-400 nm) region (Figure 1.3), allowing the use of solar radiation for the activation of these complexes. It is worth noting that the sun is a natural and renewable source of electromagnetic radiation and its use in AOPs minimizes the process costs associated with electricity consumption (MARCELINO; QUEIROZ; AMORIM, 2015; MARSON et al., 2022a). The photolytic mechanisms of these complexes for  $\text{Fe}^{2+}$  formation in the photo-Fenton process were described in detail in subsection 2.2.1 of this Ph.D. Thesis.

**Figure 1.3** – UV - Vis absorption spectra of aqueous solutions of Fe(III)-Cit and Fe(III)-NTA complexes prepared in distilled water. Initial conditions:  $[\text{Fe}^{3+}] = 100 \mu\text{mol L}^{-1}$ ; Fe/Ligand molar ratio: Fe/NTA = 1:1; Fe/Cit = 1:5.



Source: The Author, 2023.

### 1.3 Selected micro-pollutants

As described, BP-3 (PPCPs), FIP (Pesticide) and PPB (PPCPs) were selected due to their frequent detection in aqueous matrices and their adverse effects on public health and the environment. Furthermore, recent data regarding the occurrence of CEC in Brazilian aqueous matrices reveal that PPCPs are at the top, with 56.12% of the total classes of contaminants detected, followed by pesticides with 37.42% (MARSON et al., 2022a).

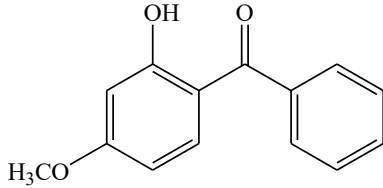
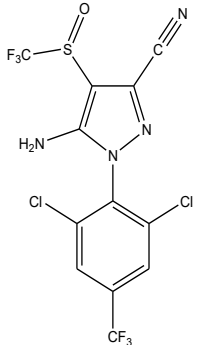
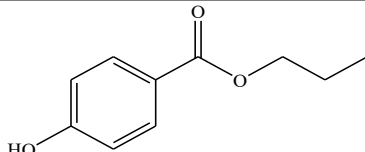
The physicochemical properties of the selected micro-pollutants (BP-3, FIP and PPB) are presented in Table 1. These compounds, except PPB, are poorly soluble in water (Table 1). The hydrophobicity of a compound can be measured using the  $\log k_{ow}$  (n-octanol/water partition coefficient) (BERNAL-ROMERO DEL HOMBRE BUENO; BOLUDA-BOTELLA; PRATS RICO, 2019) because compounds with  $\log k_{ow} \geq 2$  are considered hydrophobic (CONNELL, 2000). In this context, the micro-pollutants BP-3, FIP and PPB are hydrophobic

because  $\log k_{ow} \geq 2$  values were observed for each of these compounds (Table 1). This finding largely justifies the low solubility of these compounds in water.

For neutral substances, increased hydrophobicity has been related to greater adsorption (BERNAL-ROMERO DEL HOMBRE BUENO; BOLUDA-BOTELLA; PRATS RICO, 2019), implying that selected micro-pollutants, mainly BP-3 ( $\log k_{ow} = 4.0$ ) and FIP ( $\log k_{ow} = 4.1$ ), may also be susceptible to sedimentation.

A brief discussion regarding the risk assessment associated with residues of micro-pollutants BP-3, FIP and PPB to human health and the environment is also addressed in this section.

**Table 1.1** – Chemical structure and physicochemical properties of selected target compounds.

Compound	Class	Molecular formulae	Chemical structure	Molar weight (g mol <sup>-1</sup> )	Boiling point (°C)	Solubility in water 25 °C (mg L <sup>-1</sup> )	pKa at pH 7	Log kow
Benzophenone-3 (CAS: 131-57-7)	PPCPs	C <sub>14</sub> H <sub>12</sub> O <sub>3</sub>		228.2	370.3 <sup>a</sup>	57.05 <sup>b</sup>	9.65 <sup>c</sup>	4.0 <sup>a</sup>
Fipronil (CAS: 120068-37-3)	PPCPs	C <sub>12</sub> H <sub>4</sub> Cl <sub>2</sub> F <sub>6</sub> N <sub>4</sub> OS		437.2	510.1	1.9 <sup>d</sup>	-	4.01 <sup>e</sup>
Propylparaben (CAS: 94-13-3)	Insecticide	C <sub>10</sub> H <sub>12</sub> O <sub>3</sub>		180.2	294.0 <sup>1</sup>	500 <sup>1</sup>	8.24 <sup>f</sup>	3.04 <sup>1</sup>

Data from <sup>a</sup>Kim and Choi, (2014); <sup>b</sup>Daoud-Mahammed et al. (2010); <sup>c</sup>Li et al. (2016b); <sup>d</sup>Ying and Kookana (2001); <sup>e</sup>Tingle et al. (2003); <sup>1</sup>Bernal-Romero Del Hombro Bueno, Boluda-Botella and Prats Rico (2019); <sup>f</sup>Fang et al. (2013).

### 1.3.1 Benzophenone-3 (BP-3)

Benzophenone-3 (BP-3), chemically known as 2-hydroxy-4-methoxybenzophenone, is one of the most widely used UV filters in sunscreen formulations as it absorbs UV-B (280-315 nm) and UV-A (315-400 nm) light and enhances UV-B protection of other sunscreen agents (homosalate, octyl salicylate, octinoxate, among others). UV filters have already been detected in wastewater effluents at concentrations around 116 000 ng L<sup>-1</sup>, values higher than LC<sub>20</sub> (62 ng L<sup>-1</sup>) for coral genotoxicity (HOPKINS; BLANEY, 2016). These compounds can reach aquatic compartments through i) their removal from the skin during recreational activities such as swimming and bathing in water bodies and ii) discharges, via MWWTP, from laundry or showering processes (KIM; CHOI, 2014).

BP-3 is also an endocrine disruptor. Despite its sun protection capacity, this UV filter has been shown to penetrate the skin and cause photosensitivity. Therefore, BP-3 has been associated with some adverse human health effects, such as eczema and contact melanoma (DAOUD-MAHAMMED et al., 2010). BP-3 behaves similarly to the hormone estrogen, suggesting that it may cause breast cancer. This micropollutant is also harmful to aquatic organisms, and has been identified as a major factor in coral bleaching (DANOVARO et al., 2008) and abnormal sex hormone signaling in fish (GHAZIPURA et al., 2017; ZHANG et al., 2017) and benthic insects (CAMPOS et al., 2017, 2019).

As reported, BP-3 is poorly soluble in water (Table 1), which poses a serious concern for the development of efficient formulations. Thus, while the pharmaceutical industry seeks to develop cosmetic formulations that prevent the penetration of BP-3 into the skin, there is an urgent need for the scientific community to investigate and establish efficient methods for the removal of BP-3 from aqueous matrices.

### 1.3.2 Fipronil (FIP)

Fipronil (FIP), a pesticide whose IUPAC name is 5-amino-1-(2,6-dichloro- $\alpha,\alpha,\alpha$ -trifluoro-*p*-tolyl)-4-trifluoromethyl sulfinylpyrazole-3-carbonitrile is a soil insecticide that acts on receptors for  $\gamma$ -aminobutyric acid, the main nerve transmitter of insects, preventing the inhibition of this acid (GOMES JÚNIOR et al., 2020). Therefore, this insecticide is active against a wide range of soil and foliar insects such as rice locusts, vine weevils, termites and black ants in agricultural, forest and pastoral areas. In addition, biological studies have shown

that FIP interferes with the passage of chloride ions through the  $\gamma$ -aminobutyric acid-regulated chloride channel, disrupting central nervous system activity (YING; KOOKANA, 2001).

FIP is stable in acidic and neutral aqueous solutions (RICARDO et al., 2022) and has a low solubility in water (table 1.1), but a high solubility in organic solvents such as acetone and acetonitrile. This insecticide is not stable in aquatic habitats (FERREIRA et al., 2022) and can undergo degradation to its major metabolites (BHARDWAJ et al., 2012; FERREIRA et al., 2022) by reduction to FIP-sulfide, oxidation to FIP-sulfone, hydrolysis to FIP-amide and photolysis to FIP-desulfinyl (BHARDWAJ et al., 2012). Some of these metabolites are more toxic than the parent compound (FERREIRA et al., 2022). The metabolite FIP-desulfinyl is about 10 times more acutely toxic to mammals than FIP itself. The metabolites FIP-sulfone and FIP-sulfide are more toxic to freshwater invertebrates than FIP.

On the other hand, studies have demonstrated that FIP is recalcitrant to conventional wastewater treatment, being discharged into the environment through the recovery of treated wastewater and sewage sludge considered suitable for reuse in agriculture and detected at trace concentrations (SADARIA et al., 2019). FIP and its metabolites have already been detected in the USA at a combined concentration of 0.02 and 190.1 ng L<sup>-1</sup> (SADARIA et al., 2019). The unwanted toxicity of FIP and mainly that of its metabolites (FIP-amide, FIP-sulfide, FIP-sulfone and FIP-desulfinyl) for mammals, fish, aquatic invertebrates and beneficial terrestrial insects has attracted the attention of regulatory agencies worldwide (DA COSTA FILHO et al., 2016; SADARIA et al., 2019). In fact, FIP is included in the new water potability legislation, as set out in Decree GM/MS No. 888 of 4 May 2021.

### 1.3.3 Propylparaben (PPB)

Propylparaben (PPB) and other parabens are chemicals that contain alkyl esters of p-hydroxybenzoic acid, which give them antimicrobial, antifungal, and preservative properties. PPB is often used in cosmetics and personal care products as a preservative, antimicrobial, and mould and yeast inhibitor (GUO; KANNAN, 2013). There are numerous properties that make PPB ideal for use in personal care products: it is odourless, biodegradable, stable at varying pH levels and temperatures, and does not interfere with product colour or consistency. Furthermore, PPB is commonly used in food preservation because of its low toxicity (VANDENBERG; BUGOS, 2021).

Several toxicity studies on parabens in animals and humans have not shown any marked toxicity, as they are rapidly absorbed, metabolised and excreted from the body (SONI;

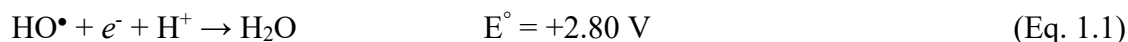
CARABIN; BURDOCK, 2005). However, recent reports have indicated that they could act as endocrine disruptors (BOBERG et al., 2010) with a moderate estrogenic activity which should lead to a possible undesirable reaction in human health (ABBAS et al., 2010; VANDENBERG; BUGOS, 2021). Because of its structural similarities to alkylphenols, PPB may exhibit estrogenic activity and may bind to oestrogen receptors (SIVARAMAN et al., 2018). In addition, parabens containing antiperspirants have been suspected of increasing the incidence of breast cancer (ABBAS et al., 2010).

PPB has already been detected in concentrations above 100 ng L<sup>-1</sup> in public water supply in Brazil (MONTAGNER; VIDAL; ACAYABA, 2017). In addition, traces of the same paraben in wastewater were also detected in the order of 1.95 ng L<sup>-1</sup> (LI et al., 2015a), 200–2430 ng L<sup>-1</sup> (LEE; PEART; SVOBODA, 2005) and 230–810 ng L<sup>-1</sup> (CANOSA et al., 2006) in China, Canada and Spain, respectively. The occurrence of parabens in different environmental samples is also justified by their easy dispersion and bioaccumulation in the environment (HAMAN; DAUCHY; ROSIN, 2014).

Although parabens are considered weak estrogens because of their low affinity for the estrogen receptor relative to estradiol, changes to hormone action, including "weak" estrogen receptor agonists, will always produce adverse effects to some sensitive organs or outcomes if exposures occur during vulnerable periods of development (HARVEY; EVERETT, 2004; VANDENBERG; BUGOS, 2021).

#### 1.4 Advanced oxidation processes: An overview

Advanced oxidation processes (AOPs) are proposed as a complementary step to conventional physicochemical and biological treatments, aiming at the degradation of persistent pollutants and fulfill the exigent limits fixed by various environmental regulations (DEWIL et al., 2017; MAZIVILA et al., 2019). Classically, AOPs are defined as aqueous phase oxidation technologies involving the *in-situ* generation of HO•, which are highly reactive due to their high value of standard reduction potential (+2.80 V) (Eq. 1.1) (AMILDON RICARDO et al., 2018b; GHANBARI; MORADI, 2017; RAHIM POURAN; ABDUL AZIZ; WAN DAUD, 2015). Therefore, these processes are mainly based on the non-selective character of the reaction of HO• with organic pollutants at high reaction rates (generally between 10<sup>8</sup> -10<sup>11</sup> L mol<sup>-1</sup> s<sup>-1</sup>) (BABUPONNUSAMI; MUTHUKUMAR, 2014; RAYAROTH et al., 2022).

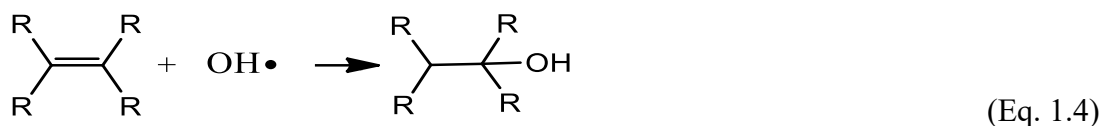


There are several possibilities of HO<sup>•</sup> production: *i*) combination of ultraviolet (UV) or visible (Vis) irradiation with strong oxidizing agents such as ozone (O<sub>3</sub>) and H<sub>2</sub>O<sub>2</sub>; presence of catalysts (semiconductors or metallic ions); *iii*) different possibilities of combinations from radiation and these oxidizing agents (CUERDA-CORREA; ALEXANDRE-FRANCO; FERNÁNDEZ-GONZÁLES, 2020). Depending on the molecular structure of the target compound, the HO<sup>•</sup> generated can react under different mechanisms: electrophilic addition, hydrogen atom abstraction and ring substitution (CUERDA-CORREA; ALEXANDRE-FRANCO; FERNÁNDEZ-GONZÁLES, 2020; NOGUEIRA et al., 2007).

The HO<sup>•</sup> formed can oxidise organic compounds by hydrogen abstraction, generating organic radicals (Eq. 1.2). Subsequently, molecular oxygen is added, forming peroxy radicals (Eq. 1.3), intermediates that initiate thermal chain reactions which, depending on the operational conditions, lead the degradation until mineralisation (CO<sub>2</sub>, H<sub>2</sub>O<sub>2</sub> and inorganic salts). The reaction by hydrogen abstraction generally occurs with aliphatic hydrocarbons (CUERDA-CORREA; ALEXANDRE-FRANCO; FERNÁNDEZ-GONZÁLES, 2020; MELO et al., 2009; NOGUEIRA et al., 2007).



Electrophilic addition of HO<sup>•</sup> to organic compounds containing π-bonds (Eq. 1.4) results in the formation of organic radicals, which usually occurs with unsaturated or aromatic hydrocarbons (CUERDA-CORREA; ALEXANDRE-FRANCO; FERNÁNDEZ-GONZÁLES, 2020; NOGUEIRA et al., 2007).



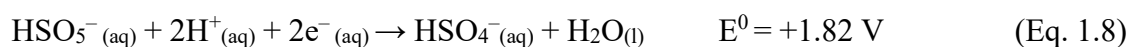
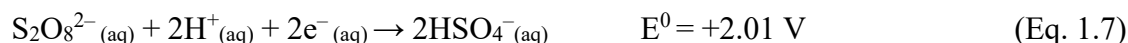
Electron transfer reactions (Eq. 1.5) occur when electrophilic addition and hydrogen abstraction are unfavoured, as in the case of chlorinated hydrocarbons (CUERDA-CORREA; ALEXANDRE-FRANCO; FERNÁNDEZ-GONZÁLES, 2020; MELO et al., 2009; NOGUEIRA et al., 2007).



The new perspectives of AOPs are characterized by the generation of sulfate radicals ( $\text{SO}_4^{\bullet-}$ ) (BOCZKAJ; FERNANDES, 2017; DEWIL et al., 2017; MAZIVILA et al., 2019). The  $\text{SO}_4^{\bullet-}$  is highly reactive ( $E^\circ = +2.5$  to  $+3.1$  V (GHANBARI; MORADI, 2017)) (Eq. 1.6), its production is pH-independent and it reacts more efficiently than the  $\text{HO}^\bullet$  with compounds having higher electron density sites (BABU et al., 2019; BOCZKAJ; FERNANDES, 2017; SILVA et al., 2021).

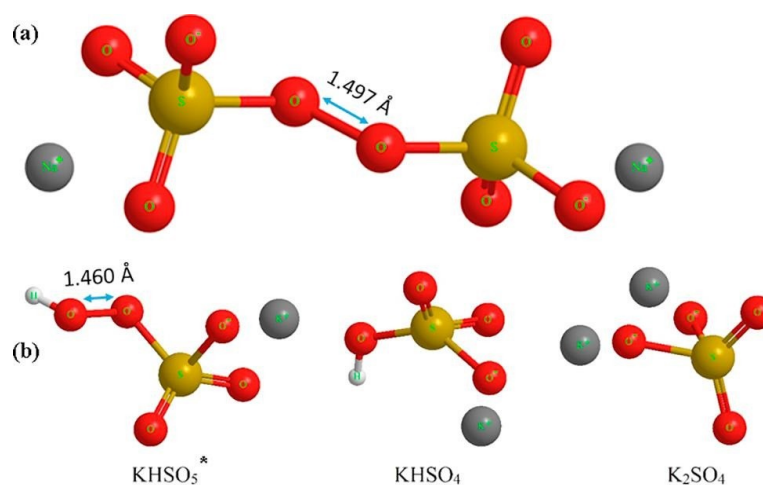


Persulfate – PS ( $\text{S}_2\text{O}_8^{2-}$ ) and peroxymonosulfate – MPS ( $\text{HSO}_5^-$ ) anions are among the strongest oxidising agents (Equations 1.7 (WACŁAWEK et al., 2017) and 1.8 (GHANBARI; MORADI, 2017)) and have been used for  $\text{SO}_4^{\bullet-}$  generation.



PS can be found in the form of three salts (sodium, potassium and ammonia) and, among them, sodium persulfate ( $\text{Na}_2\text{S}_2\text{O}_8$ ) is an excellent source of PS due to its high solubility in water ( $730 \text{ g L}^{-1}$  at  $25^\circ\text{C}$ ) and because it does not cause secondary contamination in the reaction system, as is the case with ammonia (BEHRMAN; DEAN, 1999; WACŁAWEK et al., 2017). As oxygen is easily reactive, PMS is usually found in a more stable form of a highly soluble triple white salt that has the trade name Oxone<sup>®</sup> ( $2\text{KHSO}_5\text{-KHSO}_4\text{-K}_2\text{SO}_4$ ) (GHANBARI; MORADI, 2017). Although PS and MPS are thermodynamically strong oxidants, their direct reactions with most pollutants are too slow, so activation is required (GHANBARI; MORADI, 2017).  $\text{SO}_4^{\bullet-}$  can be generated by peroxy-bond scission of PMS or PS during its activation. Unlike PS (Figure 1.4a), MPS (Figure 1.4b) is an asymmetric oxidant and requires more energy ( $377 \text{ kJ mol}^{-1}$  vs  $140 \text{ kJ mol}^{-1}$ ) for homolytic cleavage of the peroxy-bond, as it has a shorter bond length ( $1,460 \text{ \AA}$ ) (GHANBARI; MORADI, 2017; WACŁAWEK et al., 2017).

**Figure 1.4** – (a)  $\text{Na}_2\text{S}_2\text{O}_8$  and (b) Oxone triple salt molecular structure (\*potassium PMS ( $\text{KHSO}_5$ )) - active part of Oxone®. Reprinted from Waclawek et al. (2017).



PMS can automatically adjust the solution pH with producing protons, reducing the pH of the reaction medium. This reduction is attributed to the presence of acidic bisulfate ( $\text{HSO}_4^-$ ) in Oxone salt (Figure 1.4b). Moreover,  $\text{HO}^\bullet$  is another precious product of PMS activation (Eq. 1.9) (GHANBARI; MORADI, 2017; WANG; CHU, 2011).



Nowadays, sulfate radical-based AOPs (SR - AOPs) are attracting much attention due to some special features, which (including different oxidant activation methods) were discussed in detail in section 2.2.4 of this Ph.D. Thesis.

AOPs can be used as pre or post-treatment to biological processes. The application as pre-treatment contributes to increase the biodegradability of recalcitrant compounds, while its application as post-treatment aims at the degradation of compounds not removed by conventional processes. These combinations are an important driving force of AOPs because they prevent the occurrence of refractory species, consequently improving the performance of these processes (LUTTERBECK et al., 2015; MAZIVILA et al., 2019). Furthermore, this allows the effective degradation of CEC without generating a secondary waste stream, through synergistic hybrid technologies based on the combination of different AOPs (MAZIVILA et al., 2019). However, all AOPs are affected by different operational parameters and generate intermediates and degradation by-products with significant overlaps. Details on different types of AOPs and their specifics have been presented in chapter II of this manuscript.

## 1.5 Goals

### 1.5.1 Research aim

To compare the use and feasibility of different organic binders (Cit and NTA) and peroxide sources ( $\text{H}_2\text{O}_2$ ,  $\text{S}_2\text{O}_8^{2-}$ ,  $\text{HSO}_5^-$ ) in the solar photo-Fenton process for the simultaneous degradation of BP-3, FIP and PPB in tertiary sanitary effluent, as an alternative of a complementary treatment step in MWWTP.

### 1.5.2 Research objectives

- To review the literature regarding the state-of-the-art and trends (operational parameters, pathways and toxicity) of AOPs for the removal of BP-3, FIP and PPB from aqueous matrices;
- To evaluate the influence of the operational parameters (iron concentration, iron/ligand molar ratio and oxidant concentration) and optimize the experimental conditions for the photo-Fenton process in the presence of Cit and NTA ligands;
- To compare the performance of FeCit and FeNTA systems in the presence of different peroxide sources ( $\text{H}_2\text{O}_2$ ,  $\text{S}_2\text{O}_8^{2-}$ ,  $\text{HSO}_5^-$ );
- To evaluate the pH effect and matrix composition (inorganic ions) on the degradation efficiency of the mixture of BP-3, FIP and PPB in tertiary sanitary effluent by the FeNTA/ $\text{S}_2\text{O}_8^{2-}$ /UV system;
- To evaluate the evolution of toxicity to *D. melanogaster* before and after treatment, under optimized conditions;
- To estimate a comparative cost analysis between different ligands and oxidants, under the best experimental conditions.

## 2 CHAPTER II – A CRITICAL REVIEW OF TRENDS IN ADVANCED OXIDATION PROCESSES FOR THE REMOVAL OF BENZOPHENONE-3, FIPRONIL, AND PROPYLPARABEN FROM AQUEOUS MATRICES: PATHWAYS AND TOXICITY CHANGES

### 2.1 Introduction

In recent years, there has been serious environmental concern associated to the frequent detection of contaminants of emerging concern (CEC) in aqueous matrices, with emphasis on pharmaceuticals drugs and personal care products (PPCPs) and pesticides (STARLING; AMORIM; LEÃO, 2019). The detection of these CEC at trace-levels, specifically benzophenone-3 (BP-3), fipronil (FIP) and propylparaben (PPB) has also increased (CANOSA et al., 2006; LEE; PEART; SVOBODA, 2005; LI et al., 2015a; MONTAGNER; VIDAL; ACAYABA, 2017; SADARIA et al., 2019). BP-3 was detected in outdoor swimming pool water (MAO; HE; GIN, 2019; RAMOS et al., 2015) and surface water (CELEIRO et al., 2018) at concentration levels up to hundreds of  $\text{ng L}^{-1}$ . FIP was detected in concentrations that exceed established reference value to preserve aquatic life *c.a.* ( $11 \text{ ng L}^{-1}$ ) by 46% in California surface waters (BUDD et al., 2015), 70% in U.S. streams and rivers (STONE; GILLIOM; RYBERG, 2014), and by more than 20% in agricultural multi-use streams in the USA (STONE; GILLIOM; RYBERG, 2014). PPB has been recognized for its constant presence in water at concentrations levels ranging from  $\text{ng L}^{-1}$  to  $\mu\text{g L}^{-1}$  (CANOSA et al., 2006; DOROTA; GROMADZIŃSKA; WOJCIECH, 2014; LEE; PEART; SVOBODA, 2005; LI et al., 2015a), which are known to affect aquatic biota (BAZIN et al., 2010; PALHARIM; GRAÇA; TEIXEIRA, 2020).

There are several sources of these contaminants to aquatic compartments (STARLING; AMORIM; LEÃO, 2019), such as *i)* discharge of domestic and industrial effluents; *ii)* disposal of expired or unused pesticides and pharmaceutical products and *iii)* application of sludge from municipal wastewater treatment plants (MWWTP) in agricultural fields, with subsequent runoff to surface water. Disposal and inadequate treatment of waste containing BP-3, FIP and PPB impact biotic and abiotic components of ecosystems (BOBERG et al., 2010; GARCIA et al., 2011; WESTON; LYDY, 2014).

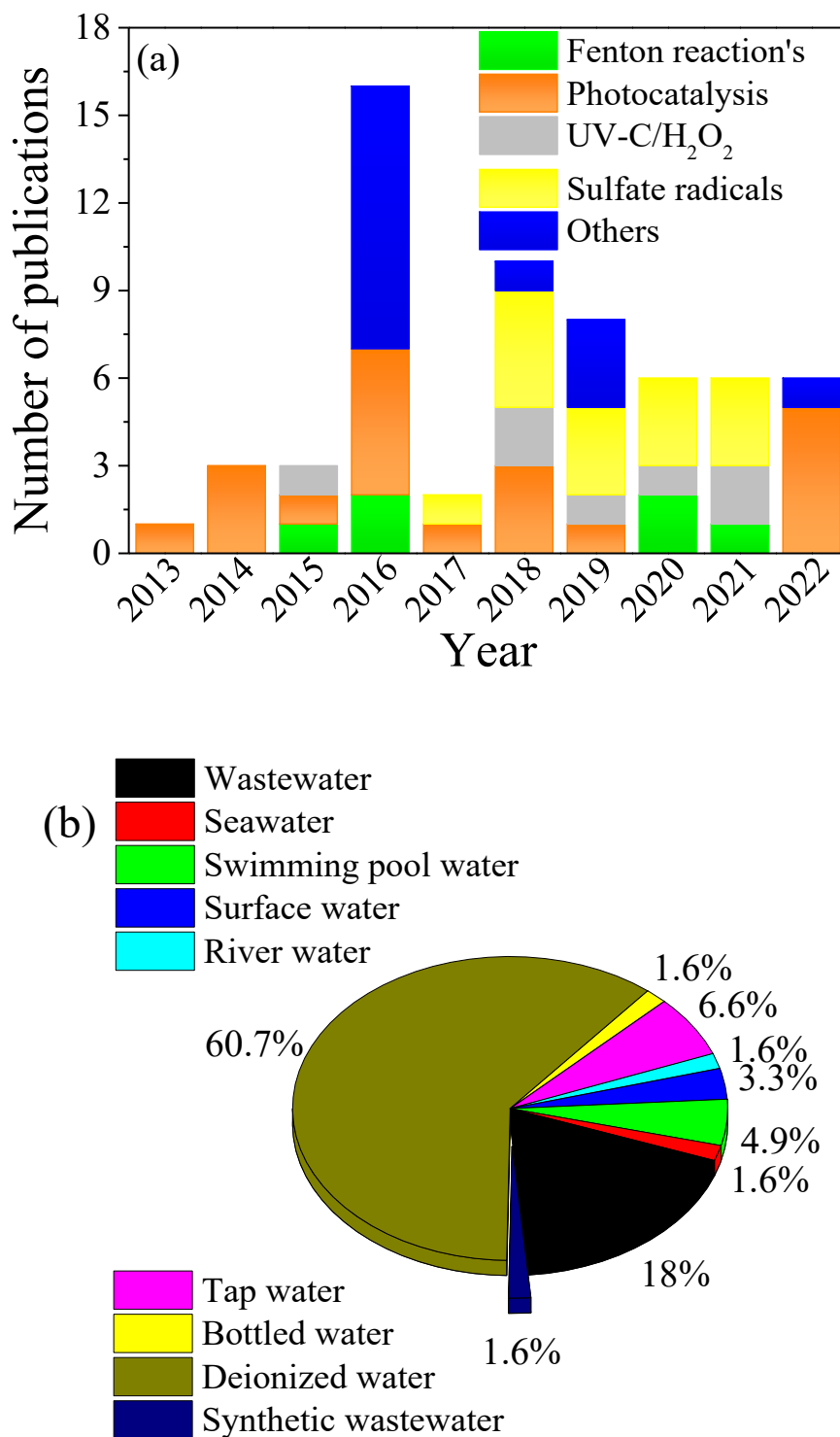
BP-3 is one of the most widely used UV filters and exposure to high levels of this compound during critical growth periods of the marine diatom *Chaetoceros gracilis* may cause

endocrine alterations to these species (TOVAR-SÁNCHEZ et al., 2013). Some harmful effects reported for BP-3 in aquatic organisms include: *a*) effects on reproduction and signaling of sex hormones, thus damaging egg production and incubation, and reducing testosterone and negative regulation of steroidogenic genes in fish (GHAZIPURA et al., 2017; ZHANG et al., 2017); *b*) inhibition of growth, development, and reproduction on the benthic insect *Chironomus riparius* (CAMPOS et al., 2017, 2019) and *c*) coral discoloration (DANOVARO et al., 2008).

FIP is used to control fleas and ticks in pets and its occurrence in MWWTP effluents discharged to the environment has been identified as a potential toxicity factor to aquatic invertebrates (WESTON; LYDY, 2014). PPB is widely applied in the formulation of personal care products, due to its preservative action, thus showing antimicrobial activity (ANDERSEN, 2008). This compound may affect human health due to its endocrine disrupting activity (BOBERG et al., 2010). Furthermore, long-term use of PPB has been associated with breast cancer (DARBRE et al., 2004; PALHARIM; GRAÇA; TEIXEIRA, 2020).

Studies evaluating alternatives for the treatment of aqueous matrices containing BP-3, FIP and PPB deserve special attention as these compounds are hazardous to ecosystem integrity. Advanced oxidation processes (AOPs), based on the generation of highly reactive hydroxyl (HO<sup>•</sup>) and sulfate (SO<sub>4</sub><sup>•-</sup>) radicals (MAZIVILA et al., 2019; RAHIM POURAN; ABDUL AZIZ; WAN DAUD, 2015) have been identified as effective technologies for the degradation of CEC in different aqueous matrices. In contrast, studies evaluating the application of these processes for the degradation of these three compounds are scarce (Figure 2.1a) and more than half were carried out in deionized water (Figure 1b). This strongly justifies the need for a structured review on the main findings from these few studies.

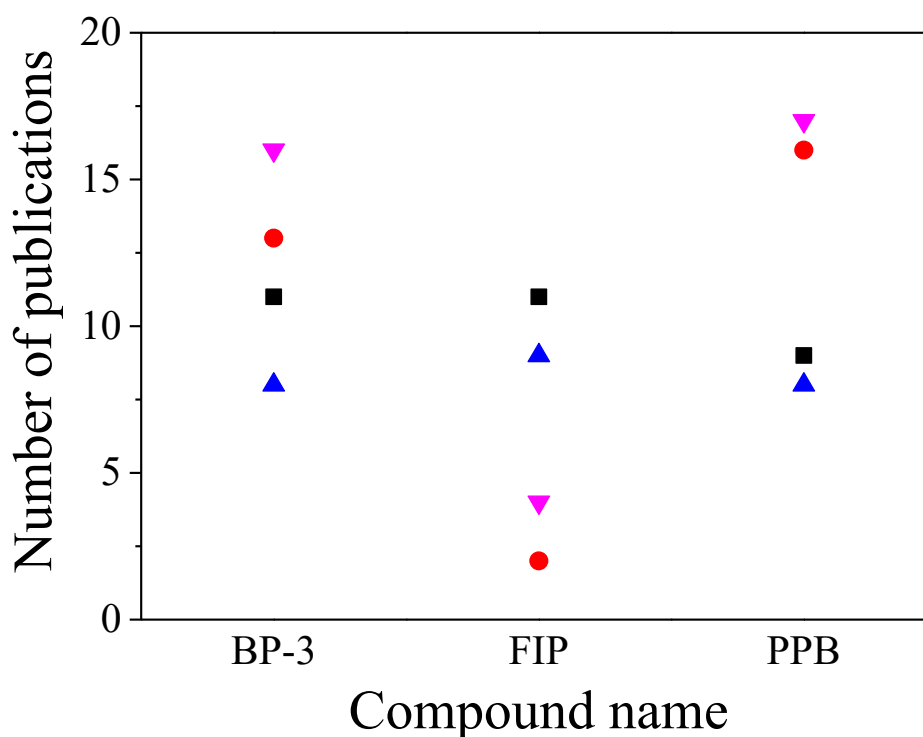
**Figure 2.1** – Number of publications (a) per year and (b) per aqueous matrix in the last 10 years related to the application of AOPs for the degradation of BP-3, FIP and PPB. Reprinted from Ricardo et al. (2022).



A search on scientific databases pointed out to a total of 62 scientific publications on AOPs applied either for individual or simultaneous degradation of BP-3, FIP, and PPB in

aqueous matrices (Figures 2.1a and 2.2). The lowest number of publications (13 publications) is associated to FIP (Figure 2.2). However, considering only the studies in real matrices, the number of publications for this compound is in the order of 36%, against 32% for the other two compounds (BP-3 and PPB) (Figure 2.2). Interestingly, to the best of our knowledge, there is no study reporting simultaneous degradation of all three target compounds or, at least, two of them. This gap reinforces the need for this critical review.

**Figure 2.2** – Number of publications per compound (■ Single; ● Target-Compound+other CEC; ▲ Real matrix; ▼ Synthetic matrix) related to the application of AOPs for the degradation of BP-3, FIP and PPB in the last 10 years. Reprinted from Ricardo et al. (2022).



Recent and relevant review papers have compiled results concerning the degradation of parabens (AJIBOYE; OYEWU; ONWUDIWE, 2021; NGUYEN et al., 2021; TAHIR et al., 2020) and FIP (SINGH et al., 2021) in aqueous matrices with a focus on photocatalysis aimed at the development of efficient photocatalytic semiconductor materials. Some authors have extended their review beyond photocatalysis (BOLUJOKO et al., 2021; NGIGI; NOMNGONGO; NGILA, 2021), and focused on the classical operating principles of these AOPs while compiling degradation results on paraben. However, to the best of our knowledge, no review papers including reports of AOPs for sunscreen (especially BP-3) degradation have been published yet. This is the first critical review of the current literature focusing exclusively

on AOPs reported either for single or simultaneous degradation of BP-3, FIP, and PPB in aqueous matrices (with emphasis on real matrices) while aiming at the evaluation of operational parameters, toxicity changes and degradation pathways which lead to the main transformation products (TPs). The main goal of this review is to highlight the advantages of innovative strategies arising from adaptation of operational parameters in each reviewed AOPs, in order to achieve satisfactory degradation efficiencies and reduced toxicity. Among these strategies, the following stand out: i) replacement of iron salts by organic iron complexes in the conventional photo-Fenton process aiming at handling the treatment at the natural pH of real aqueous matrices; ii) the effect of the relationship between light source and catalyst film thickness on photocatalytic properties; iii) integration of AOPs with biological processes, aiming at toxicity reduction and increased biodegradability; iv) use of apparently useless natural material or waste (in example: red mud) as alternative persulfate activators.

Furthermore, this review provides clarity for the choice of the most eco-friendly photocatalysts, as photocatalytic properties of TiO<sub>2</sub>-based and non-TiO<sub>2</sub>-based photocatalysts are compared as a function of required dosages and toxicity of TiO<sub>2</sub> and ZnO nanoparticles to aquatic ecosystems and human health. Overall, this critical review provides an in-depth discussion regarding the new development and use of AOPs, as well as their merits and limitations on the degradation of target CEC. Comparison and discussion of the intricacies of various AOPs and prediction of future areas for their application justify the relevance of this review. In terms of reviewed literature, the study focused on research published in the past ten years. However, older papers which had an important impact and contributions to the research progress were also included to the present review. The choice of BP-3, FIP and PPB as target compounds was based on their widespread use, occurrence in aquatic compartments at unsafe concentration levels for the environment, and scarcity of studies on their treatment and removal. Finally, this review also provides recommendations for future research on the application and improvement of AOPs. The review is organized according to the following structure:

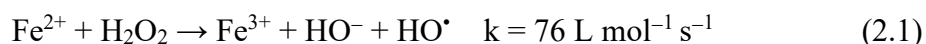
- Section 2.2: effects of operational parameters of each revised AOPs (Fenton reactions, heterogeneous photocatalysis, photo-assisted peroxidation, sulfate radicals-based AOPs, sonochemistry, ozonation, electrochemical oxidation, photolysis of monochloramine and hypochlorite ions) on the degradation of target compounds and main advances and outcomes related to each one.
- Section 2.3: degradation pathways and TPs for each target – CEC, as well as toxicity evolution in all treatment stages.

- Section 2.4: concluding remarks and outlooks which provide highlights on the current integration between innovative and conventional treatment strategies while aiming to circumvent negative effects of AOPs operational parameters and challenges associated to the removal of BP-3, FIP and PPB in real matrices.

## 2.2 Advanced Oxidation Processes (AOPs)

### 2.2.1 Fenton reactions

The Fenton process is characterized by the generation of HO• radicals through catalytic decomposition of H<sub>2</sub>O<sub>2</sub> in the presence of Fe<sup>2+</sup> ions at acid medium (Eq. 2.1) (Fenton 1894; Haber et al. 1934). The reaction between Fe<sup>3+</sup> and H<sub>2</sub>O<sub>2</sub> represents one of the main Fenton reaction mechanisms and occurs slowly in the dark ( $k = 9.1 \times 10^{-7} \text{ mol L}^{-1} \text{ s}^{-1}$ ). One of the alternatives to accelerate this reaction is through exposition to UV-Vis radiation, known as the photo-Fenton process (PLGNATELLO, 1992). Incidence of UV-Vis radiation on Fe(III) aquo-complexes (Eq. 2.2) promotes transfer of the ligand-metal charge, which implies on the reduction of Fe(III) to Fe(II) and oxidation of the ligand, thus generating HO• radical.



Fenton reaction reached satisfactory degradation of BP-3, FIP and PPB (DA COSTA FILHO et al., 2016; GOMES JÚNIOR et al., 2020; INTICHER et al., 2021; LUCAS; PERES, 2015; YE et al., 2019; ZÚÑIGA-BENÍTEZ; ARISTIZÁBAL-CIRO; PEÑUELA, 2016). Table 2.1 shows removal rates and percent reductions on dissolved organic carbon (DOC) and chemical oxygen demand (COD) obtained by this process in various water matrices.

**Table 2.1** – Summary of the application of Fenton reaction for the degradation of BP-3, FIP and PPB in aqueous matrices.

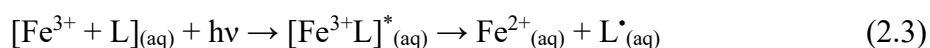
Process	CEC/Matrix	Experimental conditions	Degradation	Reference
Conventional photo-Fenton	BP-3/deionized water	Time= 60 min; [BP-3]= 1.0 mg L <sup>-1</sup> ; [Fe <sup>2+</sup> ]= 168 mg L <sup>-1</sup> ; [H <sub>2</sub> O <sub>2</sub> ]= 3449 mg L <sup>-1</sup> ; pH= 3.0; Xenon lamp (350 ± 10 W m <sup>-2</sup> ); 35 ± 2 °C.	100% BP-3 60% DOC	(ZÚÑIGA-BENÍTEZ; ARISTIZÁBAL-CIRO; PEÑUELA, 2016)
	FIP/industrial wastewater	Time= 60 min; [FIP]= 20.9 mg L <sup>-1</sup> ; pH= 2.9; [Fe <sup>2+</sup> ]= 60 mg L <sup>-1</sup> ; [H <sub>2</sub> O <sub>2</sub> ]= 6723 mg L <sup>-1</sup> ; 400 W high-pressure mercury vapor lamp (UV-A: 1100 W m <sup>-2</sup> ).	<LOQ (0.12 mg L <sup>-1</sup> ) FIP; 60% DOC; 74% COD	(DA COSTA FILHO et al., 2016)
	PPB/deionized water	Time= 180 min; [PPB]= 216 mg L <sup>-1</sup> ; [Fe <sup>2+</sup> ]= 22 mg L <sup>-1</sup> ; [H <sub>2</sub> O <sub>2</sub> ]= 197 mg L <sup>-1</sup> ; pH= 5.7; UV lamp = TNN 15/32; 20 ± 5 °C.	63% PPB	(LUCAS; PERES, 2015)
Photoelectro-Fenton	FIP/deionized water	Time= 15 min; [FIP]= 10 mg L <sup>-1</sup> ; [H <sub>2</sub> O <sub>2</sub> ]= 1000 mg L <sup>-1</sup> ; electric current: 0.7 A; flow rate: 0.6 L min <sup>-1</sup> ; pH= 5.83.	96.5% FIP	(INTICHER et al., 2021)
	BP-3/MWWTP effluent	Time= 20 min; [BP-3]= 5.48 mg L <sup>-1</sup> ; pH= 3.0; [Fe <sup>2+</sup> ]= 28 mg L <sup>-1</sup> ; BDD/air-diffusion cell: 33.3 mA cm <sup>-2</sup> ; 35 °C.	99.8% BP-3	(YE et al., 2019)

Photo-Fenton modified with organic ligands at near neutral pH	FIP/distilled water	Time = 60 min; [FIP]= 1000 $\mu\text{g L}^{-1}$ ; [Fe <sup>3+</sup> -Citrate]= 32 $\mu\text{mol L}^{-1}$ ; [H <sub>2</sub> O <sub>2</sub> ]= 22.3 $\text{mg L}^{-1}$ pH= 5.8; solar radiation.	98.3% FIP	(GOMES JÚNIOR et al., 2020)
	FIP/MWWTP effluent	Time= 60 min; [FIP]= 600 $\mu\text{g L}^{-1}$ ; pH 6.0; [Fe <sup>3+</sup> -Citrate]= 192 $\mu\text{mol L}^{-1}$ ; [H <sub>2</sub> O <sub>2</sub> ]= 23 $\text{mg L}^{-1}$ ; solar radiation.	83% FIP	(GOMES JÚNIOR et al., 2020)

DOC: Dissolved organic carbon; COD: Chemical Oxygen Demand; LOQ: Limit of quantification.

BP-3 was completely degraded by photo-Fenton in deionized water (ZÚÑIGA-BENÍTEZ; ARISTIZÁBAL-CIRO; PEÑUELA, 2016) and by photoelectro-Fenton in MWWTP effluent (YE et al., 2019). Mineralization levels above 60% in water were reached after 300 min of photo-Fenton at pH 3 (ZÚÑIGA-BENÍTEZ; ARISTIZÁBAL-CIRO; PEÑUELA, 2016). Despite incomplete mineralization of BP-3 in deionized water (ZÚÑIGA-BENÍTEZ; ARISTIZÁBAL-CIRO; PEÑUELA, 2016), organic content remained in the matrix, thus indicating the formation of highly stable TPs.

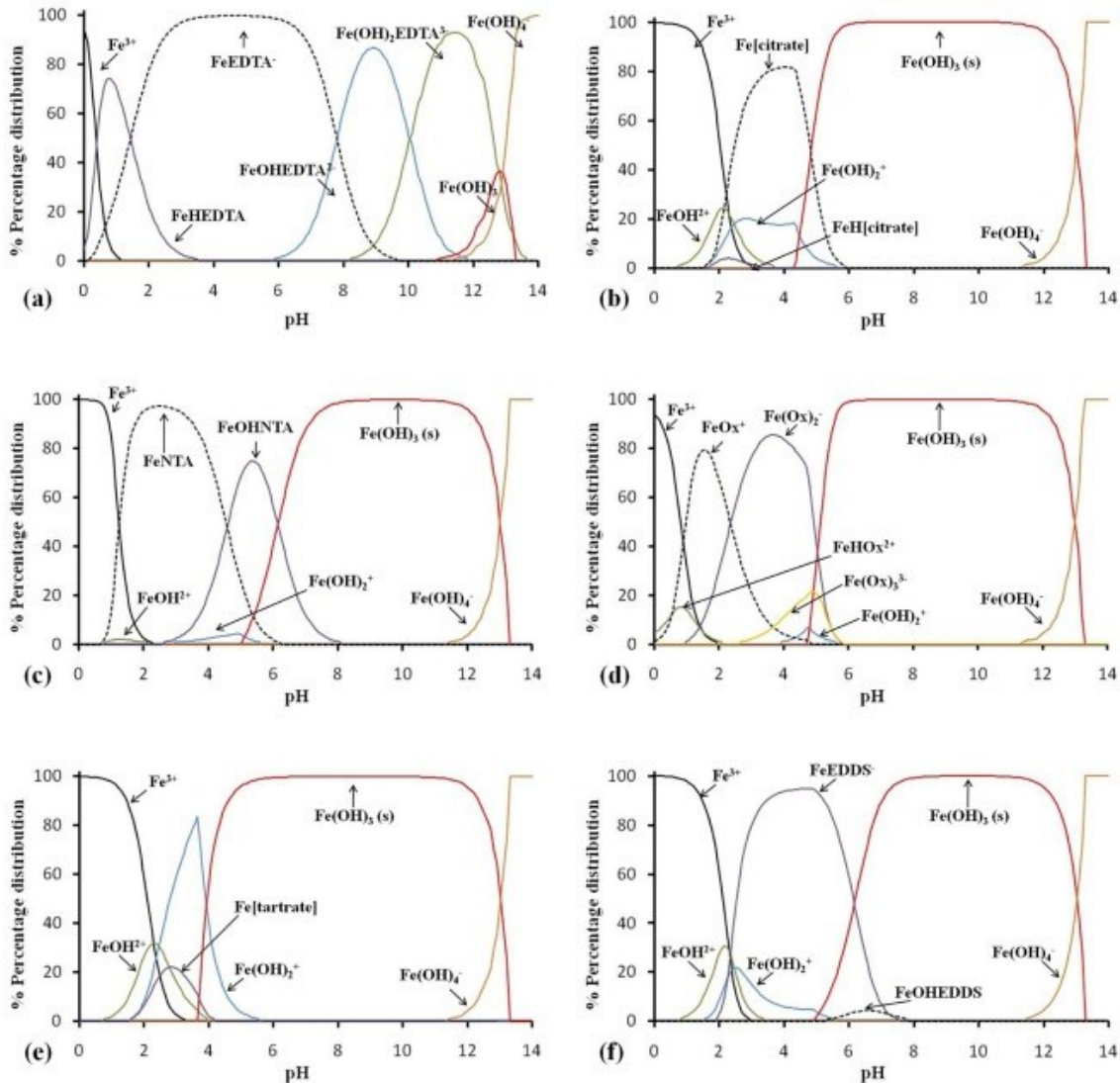
A similar behavior was observed during the degradation of FIP in industrial wastewater via photo-Fenton at pH 2.9, reaching 60% and 75% removals of DOC and COD, respectively (DA COSTA FILHO et al., 2016). Treatment of industrial water (a much more complex matrix than previously mentioned studies) containing high levels of FIP required the integration of coagulation/flocculation/settling processes that allowed for toxicity reduction and increased biodegradability. In contrast, 63% degradation of PPB was obtained after a longer treatment time (180 min) in deionized water and at pH 5.7 (LUCAS; PERES, 2015). Limited degradation rate (< 70%) is justified by iron precipitation in the form of insoluble hydroxides at pH>3.0, thus drastically decreasing its interaction with H<sub>2</sub>O<sub>2</sub> and, consequently, reducing the production of HO• radicals. Considering that the natural pH of environmental aqueous matrices is close to neutrality (AMILDON RICARDO et al., 2018b; GOMES JÚNIOR et al., 2020), acidification and neutralization are required, respectively, before and after treatment, thus increasing treatment cost and time and making the application of photo-Fenton at acidic pH unlikely in real aqueous matrices. Photo-Fenton process at neutral pH is enabled by the introduction of organic iron complexes that allow for dissolved iron availability over a broad pH range (CLARIZIA et al., 2017). Furthermore, iron complexes contribute to increasing light absorption efficiency, as they extend the absorption band to the visible region (MACHULEK et al., 2012; MIRALLES-CUEVAS et al., 2014). Photolysis of these iron complexes leads to the formation of Fe<sup>2+</sup> (Eq. 2.3), thus improving the efficiency of the photo-Fenton process (AMILDON RICARDO et al., 2018a; CLARIZIA et al., 2017).



Different organic iron ligands (oxalate-Ox, citrate-Cit, nitrilotriacetic acid-NTA, ethylene diaminetetraacetic acid-EDTA and ethylenediamine-N,N'-succinic-EDDS), have been reported as efficient for the treatment of various aqueous matrices containing CECs (AMILDON RICARDO et al., 2018a, 2018b; DE LUCA; DANTAS; ESPLUGAS, 2014;

MANENTI et al., 2015; MANIAKOVA et al., 2020; MIRALLES-CUEVAS et al., 2019; RASTOGI; AL-ABED; DIONYSIOU, 2009; SILVA et al., 2021). When Fe(III) is dissolved in aqueous solutions in the presence of one of the aforementioned ligands, soluble compounds containing Fe(III) are formed at  $\text{pH} > 3.0$  (CLARIZIA et al., 2017). Understanding the speciation of organic iron complexes as a function of pH is extremely important for choosing the complex to be used in the degradation process for each matrix. For instance, EDTA forms soluble complexes without Fe(III) precipitation up to basic pH values (Figure 2.3a) while Cit, NTA, Ox and EDDS make Fe(III) available until almost neutral pH by forming soluble complexes (Figures 2.3b-d and 2.3f).

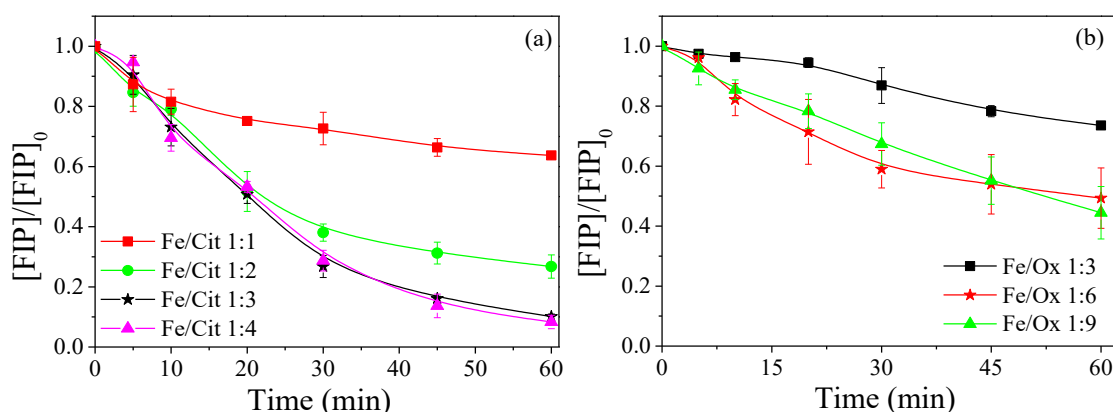
**Figure 2.3** – Speciation diagrams of ferric complexes as a function of pH for a solution at  $T = 25\text{ }^{\circ}\text{C}$  in the presence of  $1.0 \times 10^{-5}\text{ M}$  of Fe(III),  $1.0 \times 10^{-5}\text{ M}$  of EDTA (a),  $1.0 \times 10^{-5}\text{ M}$  of citrate (b),  $1.0 \times 10^{-5}\text{ M}$  of NTA (c),  $3.0 \times 10^{-5}\text{ M}$  of oxalate (d),  $1.0 \times 10^{-5}\text{ M}$  of tartrate (e), and  $1.0 \times 10^{-5}\text{ M}$  of EDDS (f). Reprinted from Clarizia et al. (2017). Copyright 2017 Elsevier.



Solar photo-Fenton conducted at pH 6.0 led to 83% FIP degradation in MWWTP effluent in the presence of Fe/Cit complex at 1:3 molar ratio (GOMES JÚNIOR et al., 2020). In this context, a previous study evaluated the performance of FeCit and FeOx species for FIP degradation in distilled water (Figure 2.4). Best results were obtained with FeCit compared to FeOx (Figure 2.4) due to higher solubility of iron-citrate complexes compared to iron-oxalate complexes, which agrees with speciation diagrams shown in Figures 4b and 4d. These results show that the adaptation of the photo-Fenton process by using FeCit complex may be a viable alternative to prevent the precipitation of iron in natural water matrices during FIP degradation.

In addition, an improvement in FIP degradation occurred when Fe/Cit molar ratios increased from 1:1 to 1:3 (Figure 2.4a) and FeOx from 1:3 to 1:6 (Figure 2.4b), yet this was not observed for higher molar ratios. These results demonstrate the importance of optimizing iron:ligand molar ratios for each complex and matrix to avoid simultaneous iron precipitation and competition of the ligand for hydroxyl radicals, thus maximizing the degradation efficiency (Figure 2.4). The use of FeCit complexes is also interesting considering that effluents from some production processes may be used as alternative sources of Cit, thus increasing processes sustainability (DELGADO-VARGAS et al., 2021).

**Figure 2.4** – Influence of molar iron/ligand ratio on fipronil (FIP) degradation by photo-Fenton at pH 6.0 using (a) FeCit and (b) FeOx in distilled water. Initial conditions:  $[FIP] = 1000 \mu\text{g L}^{-1}$ ;  $[H_2O_2] = 676 \mu\text{mol L}^{-1}$ ;  $[\text{iron}] = 32 \mu\text{mol L}^{-1}$ . Reprinted from Gomes Júnior et al. (2020). Copyright 2020 Elsevier.



Although maximum FIP degradation ( $< \text{LOQ} = 17 \mu\text{g L}^{-1}$ ) was obtained in distilled water (GOMES JÚNIOR et al., 2020), this result is associated to the absence of inorganic ions and natural organic matter in this matrix. The competitive action of some inorganic ions (chloride, sulfate, phosphate, carbonate and bicarbonate) present in real environmental matrices constitutes one of the main limitations for the application of AOPs in real matrices, since they act as scavengers of  $\text{HO}^\bullet$  radicals and/or absorb or scatter light (GOGATE; PANDIT, 2004), thus reducing removal efficiency.

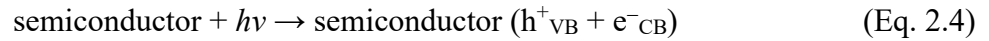
The Fenton reaction has also been adapted to electrochemical AOPs (i.e., photoelectron-Fenton process), which are characterized by continuous *in situ* generation of  $\text{H}_2\text{O}_2$  by electrochemical reduction of  $\text{O}_2$  in the cathode, and continuous supply of Fe(II), which allows for the formation of  $\text{HO}^\bullet$  radicals. Photoelectron-Fenton has been highlighted as an emerging

technology in the context of AOPs (IGHALO et al., 2021; MAZIVILA et al., 2019). The merits of the photoelectron-Fenton process also include the involvement of other processes, such as adsorption, anodic oxidation, and flocculation (IGHALO et al., 2021). BP-3 was completely degraded in MWWTP effluent after 20 min of treatment by photoelectron-Fenton (YE et al., 2019).

According to outcomes highlighted in this section, different adaptations to the Fenton reaction have been successfully applied for the degradation of BP-3, FIP and PPB. Effective treatment in real applications is still a challenge due to pH limitations and natural matrix constituents. Therefore, strategies aimed at increasing treatment effectiveness at circumneutral pH (natural pH for most industrial and MWWTP effluents), such as the use of organic iron complexes, should be encouraged. Furthermore, the use of solar radiation (GOMES JÚNIOR et al., 2020) and the search for innovative and selective oxidants are crucial to reduce energy costs and to circumvent the competitive action of inorganic ions present in the matrix.

### 2.2.2 *Heterogeneous photocatalysis*

Heterogeneous photocatalysis is based on the electronic excitation of a semiconductor oxide in the presence of artificial or solar radiation to generate hydroxyl radicals capable of oxidizing natural organic matter (NEZAR; LAOUFI, 2018), and also CEC present in water matrices. Several semiconductors have been used in heterogeneous photocatalysis, such as: Fe<sub>2</sub>O<sub>3</sub>, ZnO, ZnS, CdS and TiO<sub>2</sub> (IBHADON; FITZPATRICK, 2013). When a semiconductor is bombarded with photons, electrons in the valence band (VB) are transferred to the conduction band (CB) leaving positive holes (h<sup>+</sup>) (Eq. 2.4) (NOSAKA; NOSAKA, 2017) which react with water or hydroxyl groups adsorbed on the semiconductor surface, and finally generating HO<sup>•</sup> radicals (Equations 2.5 and 2.6). Besides, the h<sup>+</sup> has a high standard reduction potential (+2.0 to +3.5 V) and can also oxidize target contaminants (KHAKI et al., 2017; ZHONG; HAGHIGHAT; LEE, 2013). The photon energy needed to generate an electron/gap pair must be equal to or greater than that of the gap (NOSAKA; NOSAKA, 2017). Electrons present in the CB, freely or trapped on its surface, reduce the adsorbed O<sub>2</sub> forming the superoxide anion radical (O<sub>2</sub><sup>•-</sup>) (Eq. 2.7) and reducing the probability of recombination of the electron-gap pair (PANIAGUA et al., 2020). The superoxide radical is highly oxidizing and generates new radical forms (ZHONG; HAGHIGHAT; LEE, 2013) leading to mineralization of organic pollutants adsorbed on the semiconductor surface (LLORENTE-GARCÍA et al., 2020).



Furthermore, photocatalytic degradation efficiency is influenced by total irradiated energy absorbed by the suspended catalyst. Absorbed energy depends on the optical properties of each photocatalyst (scattering and absorption coefficients).

Photocatalytic oxidation of FIP in drinking water was performed using ZnO and TiO<sub>2</sub> as catalysts under solar and artificial irradiation (FENOLL et al., 2014). The addition of Na<sub>2</sub>S<sub>2</sub>O<sub>8</sub> (section 2.2.4) was relevant to improve FIP degradation efficiency (FENOLL et al., 2014). Catalyst concentrations required to reach the same rate of energy absorption during the process were equivalent to 200 mg L<sup>-1</sup> for ZnO and 53 mg L<sup>-1</sup> for TiO<sub>2</sub> (FENOLL et al., 2014). However, toxic effects including alteration of intracellular Ca<sup>2+</sup> flux, generation of reactive oxygen species, membrane damage and mitochondrial dysfunction were detected in the presence of ZnO nanoparticles (VANDEBRIEL; DE JONG, 2012). Besides, TiO<sub>2</sub> and ZnO nanoparticles were harmful to Gram-positive *Bacillus subtilis* and Gram-negative *Escherichia coli* organisms and antibacterial activity was higher for ZnO compared to TiO<sub>2</sub> (ADAMS; LYON; ALVAREZ, 2006). Despite high degradation efficiencies using any of the tested oxides (ZnO = 99.2%; TiO<sub>2</sub> = 98.5%) (Table 2), a lower concentration of TiO<sub>2</sub> is required (53 mg L<sup>-1</sup>) when compared to ZnO (200 mg L<sup>-1</sup>). Thus, TiO<sub>2</sub> represents lower environmental impact. This underlines, from an environmental point view, the relevance of a deep understanding regarding optical properties of photocatalysts. Still, toxicity associated to TiO<sub>2</sub> nanoparticles and other catalysts must be further investigated (RASHID; TAVČER; BRIGITA, 2021).

Still concerning heterogeneous photocatalysis, it is important to highlight the merit of monolithic cellulose acetate structures coated with commercial films of catalyst nanoparticles. These structures can be arranged in different geometries to obtain a larger area of illuminated catalyst per reactor volume. In addition, they contain a large number of walls in which photocatalyst nanoparticles are deposited, thus providing a high area/volume ratio (CELEIRO et al., 2018). Evidently, high BP-3 degradation efficiencies (>95%) were achieved using supported catalyst (monolithic structures coated with P25) (CELEIRO et al., 2018). Besides, an increase in the number of thin layers of immobilized TiO<sub>2</sub>-P25 on the outer walls of the monolithic cellulose acetate structure from 1 to 3 led to a decrease in half-life time (t<sub>1/2</sub>) required

for BP-3 degradation (from 13 to 6 min) and resulted in maximum degradation efficiency equivalent to 91% within 30 min of irradiation (CELEIRO et al., 2018). This result was obtained by the frontal lighting mechanism, during which an increase in the thickness of the catalyst film increases the generation of charge carriers to the point where the light is completely absorbed by the catalyst layer (CHEN; LI; RAY, 2001). The addition of 20 mg L<sup>-1</sup> H<sub>2</sub>O<sub>2</sub> to the TiO<sub>2</sub>-P25/UV-A system treating real swimming pool water reached BP-3 concentration below the limit of detection (LOD < 0.20 µg L<sup>-1</sup>) within 6 min of irradiation, with a consumption of 22% of the initial H<sub>2</sub>O<sub>2</sub> concentration (CELEIRO et al., 2018). This synergistic effect was also observed for PPB degradation (CUERDA-CORREA et al., 2016b). The addition of H<sub>2</sub>O<sub>2</sub> to the photocatalytic system prevents electron-hole recombination by accepting photogenerated electrons from the CB and allows for the production of additional HO<sup>•</sup>. The work also evaluated the effect of water matrix composition upon PPB degradation, and treatment efficiency decreased in the presence of higher concentrations of organic matter, as follows: ultrapure water > reservoir water > river water > wastewater. This fact was justified by the competition between natural organic matter and target pollutant for HO<sup>•</sup> and also by the scavenging action of PO<sub>4</sub><sup>3-</sup> and HCO<sub>3</sub><sup>-</sup> species (CUERDA-CORREA et al., 2016b).

#### 2.2.2.1 Photocatalyst reusability and separation

Although photocatalyst suspensions are efficient for secondary wastewater quality improvement, separation of catalyst from solution after treatment and its reusability are some of the main drawbacks associated the application of photocatalysis in real scale. Catalyst recovery may be enhanced through charge neutralization and coagulation with electrolytes (FERNÁNDEZ-IBÁÑEZ et al., 2003; KAGAYA et al., 1999; SURYAMAN; HASEGAWA, 2010). Regarding TiO<sub>2</sub>, its isoelectric point or point of zero charge (pH<sub>PZC</sub>) (6.4–6.6 (XI; GEISSEN, 2001)) is close to pH 7 (FERNÁNDEZ-IBÁÑEZ et al., 2003). At this pH value, TiO<sub>2</sub> particle surface is mainly occupied by neutral groups (TiOH), and a small amount of charged species (TiO<sup>-</sup> > TiOH<sub>2</sub><sup>+</sup>), thus reducing electrostatic repulsion between TiO<sub>2</sub> particles (SURYAMAN; HASEGAWA, 2010). Electrolytes present in the aqueous matrix neutralize charged species and reduce the thickness of the electrochemical double layer of the particles, thus resulting in lower repulsion between particles and promoting coagulation (O'SHEA; PERNAS; SAIERS, 1999; SURYAMAN; HASEGAWA, 2010). Therefore, sedimentation rates and the hydrodynamic diameter of TiO<sub>2</sub> particles are maximum at the isoelectric point (pH of natural water matrices) (FERNÁNDEZ-IBÁÑEZ et al., 2003) which can be adequate for

full-scale application. Besides, metal-free photocatalysts may be adapted for recycling and reuse. A recent progress consisted in the preparation of graphitic carbon nitride hydrogel microspheres with cross-linking reactions between sodium alginate and calcium ions. This material is separation-free from the liquid phase for reuse (HAO et al., 2021). The potential of calcium alginate lies in its hydroxyl that allows for increased adsorption of organic pollutants, as well as increased transfer and separation of photogenerated charge carriers (HAO et al., 2021). However, studies on real wastewater are still needed to consolidate progress on the separation and reuse of metal-free photocatalysts.

#### 2.2.2.2 pH effect on photocatalytic degradation of BP-3, FIP and PPB

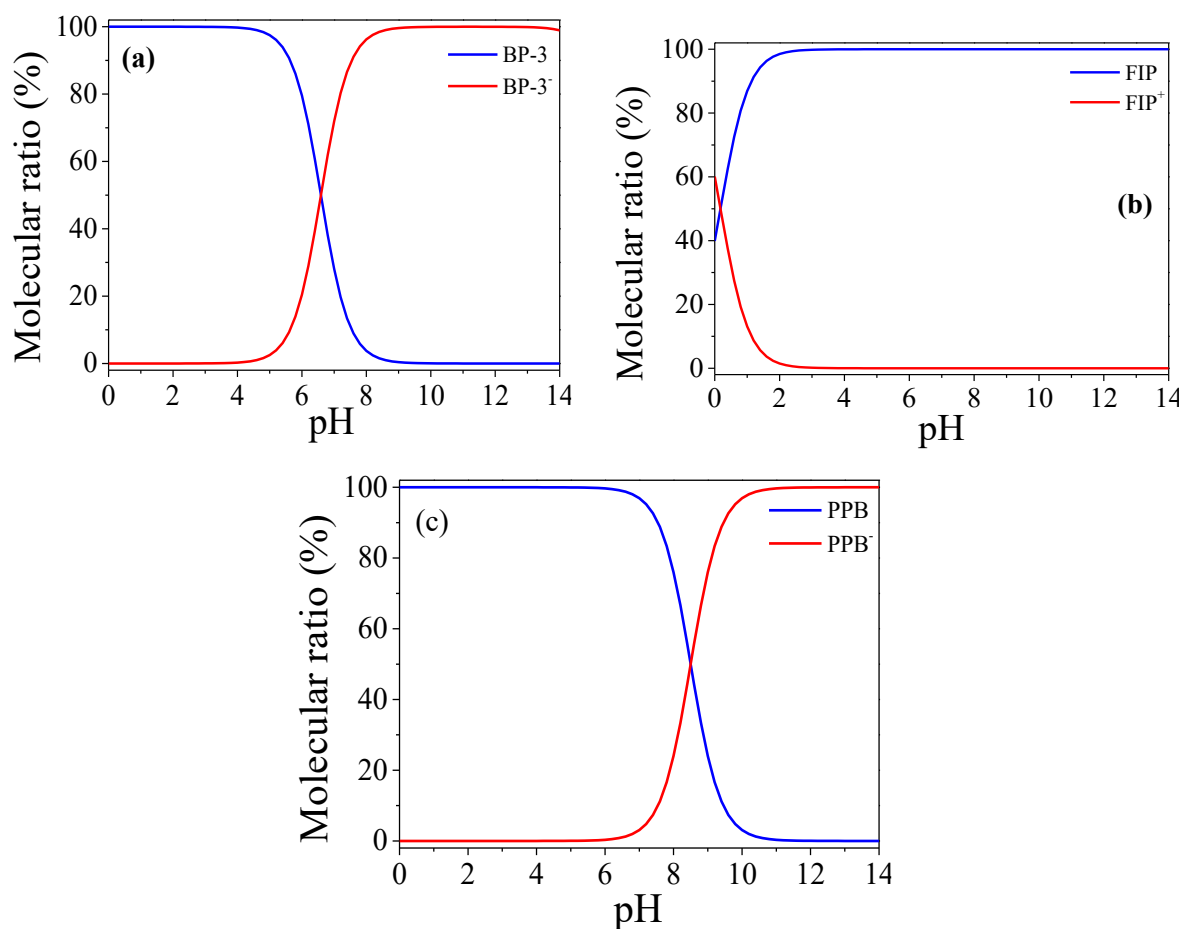
Although the pH effect in the photocatalytic reaction is generally attributed to the surface charge of the semiconductor (FENOLL et al., 2014), knowledge about the speciation of target-molecules (Figure 2.5) as a function of pH is also relevant to predict the effect of pH in this type of process. A negligible adsorption of BP-3 on the surface of photocatalysts TiO<sub>2</sub>-P25 ( $pH_{ZPC} = 6.25$  (KHAN et al., 2012)), TiO<sub>2</sub>-PC500 ( $pH_{ZPC} = 6.05$  (SINGH; MUNEER; BAHNEMANN, 2003)) and TiO<sub>2</sub>-PC105 ( $pH_{ZPC} = 3.83$  (CIAMBELLI et al., 2009)) was observed at pH 7.0 (CELEIRO et al., 2018). Although BP-3 molecule has only one  $pK_a$  (9.65) (LI et al., 2016b), its neutral form prevails at pH 7.0 (Figure 2.5a) which is the usual pH associated to natural waters. Considering the aforementioned  $pH_{ZPC}$  values for TiO<sub>2</sub> structures, TiO<sub>2</sub>-P25 and TiO<sub>2</sub>-PC500 surfaces are predominantly neutral (TiOH) at pH 7, while TiO<sub>2</sub>-PC105 surface is negatively charged (TiO<sup>-</sup>) under the same conditions. Thus electrostatic repulsion or no electrostatic interaction are expected to occur between catalyst surface and BP-3 molecule at pH 7.0 (CELEIRO et al., 2018).

Fenoll et al. (2014) studied the influence of initial pH (7.1) on the kinetics of photocatalytic degradation of FIP using TiO<sub>2</sub> ( $pH_{PZC} = 6.0$ ) and ZnO ( $pH_{PZC} = 9.0$ ). FIP is neutral over a wide pH range (Figure 2.5b). The surface of TiO<sub>2</sub> and ZnO are predominantly positively charged below pHs 6.0 and 9.0, respectively, and negatively charged above these values. Hence, electrostatic attraction or repulsion between FIP and the catalysts occurred in the reference study resulting, respectively, in increase or inhibition of FIP photodegradation rate. Since pH values ranging from 6.0 to 8.0 produce a negligible effect on TiO<sub>2</sub> and ZnO, photocatalytic treatment can be successfully carried out at an initial pH around 7.0 (FENOLL et al., 2014). It is worth mentioning that ZnO may react with a base to form Zn(OH)<sub>2</sub> at a basic

pH. This increases toxicity due to the generation of  $Zn^{2+}$  in the solution (FENOLL et al., 2014) as it is bioavailable to aquatic biota, thus its application for the treatment of real matrices prior to discharge must be supported by toxicity studies.

The adsorption of PPB is more efficient in acidic and neutral media than in basic media. Fang et al. (FANG et al., 2013) observed a rapid decrease in PPB degradation efficiency when pH was increased from 3.0 to 11.0. As the  $pK_a$  of PPB is equivalent to 8.24 (FANG et al., 2013), it tends to occur mainly in the neutral form in environmental waters showing a small dissociation. So, it may be adsorbed onto  $TiO_2$  surface which holds a positive charge below the  $pH_{pzc}$  (6.2 (FANG et al., 2013)). Furthermore, further increase in the pH to values above 8.24 led to PPB transformation to its anionic form (Figure 2.5c), which is hardly adsorbed by the negatively charged  $TiO_2$ , thus decreasing the degradation efficiencies. It is noteworthy that basic conditions can drastically increase the formation of the phenoxyl radical from PPB, which can react with hydrated electrons ( $e^-_{aq}$ ) to regenerate the original compound (FANG et al., 2013; SWOBODA; SOLAR, 1999), decreasing PPB degradation efficiency. Furthermore, decreased degradation efficiency at high pH values may also result from the transformation of  $HO^\bullet$  radical ( $pK_a = 11,9$ ) into a less reactive oxide radical ion ( $O^{\bullet-}$ ) (BUXTON et al., 1988). Similar decrease in photocatalytic degradation of metronidazole (MZ) (AZALOK; OLADIPO; GAZI, 2021a; MUSTAFA; OLADIPO, 2021) and tetracycline (TC) (AZALOK; OLADIPO; GAZI, 2021b) in the order of 50-80% were observed when pH values of respective solutions were adjusted from 3.0 to 9.0 and from 3.0 to 11.0. Therefore, at basic pH (9.0 and 11.0) there was repulsion between negatively charged photocatalysts ( $Ag-d-NZF^-$  (MUSTAFA; OLADIPO, 2021) and  $MnFe-LDO-biochar^-$  (AZALOK; OLADIPO; GAZI, 2021a, 2021b)) and anionic species of the target compounds (MZ- and TC-) (AZALOK; OLADIPO; GAZI, 2021a, 2021b; MUSTAFA; OLADIPO, 2021).

**Figure 2.5** – Effect of pH on variation of (a) BP-3, (b) FIP and (c) PPB molecular ratio. Reprinted from Ricardo et al. (2022).



Considering the intrinsic relationship between alkalinity and pH, it is also important to underline that alkalinity exerts a significant inhibitory effect on the process as it blocks active sites on the photocatalyst surface by high concentrations of organic matter (CUERDA-CORREA et al., 2016b). Therefore, the application of these processes in alkaline waters may not be efficient for the removal of target compounds.

### 2.2.3 Photo-assisted peroxidation

The exposition of H<sub>2</sub>O<sub>2</sub> to UV-C radiation generates HO<sup>•</sup> radicals through the homolytic cleavage of H<sub>2</sub>O<sub>2</sub>, thus increasing efficiency of CEC degradation when compared to UV-C radiation alone (Eq. 2.8) (ESPLUGAS et al., 2002; LEYVA et al., 2017; MONDAL; SAHA; SINHA, 2018). In general, H<sub>2</sub>O<sub>2</sub> photolysis is performed under low or medium pressure mercury vapor lamps (254 nm). However, high concentrations of H<sub>2</sub>O<sub>2</sub> were necessary to reach

satisfactory degradation efficiencies at 254 nm, due to the low absorptivity of this oxidant in this spectral region ( $\epsilon_{254} = 18.6 \text{ L mol}^{-1} \text{ cm}^{-1}$ ) (MELO et al., 2009). Xenon-doped mercury lamp emitting in the range between 210 and 240 nm may be used as an alternative despite increased costs associated to this lamp (MELO et al., 2009).

UV-C photolysis provided limited BP-3 degradation efficiency with degradation yields between 20% and 60% after 60 min of treatment in ultrapure water (CELEIRO et al., 2019). The same radiation was also applied to different real water matrices (river, sea and pool) and BP-3 degradation was lower in the presence of higher organic matter content. In contrast, UV-C/H<sub>2</sub>O<sub>2</sub> system was successful on the removal (> 90%) of 21 compounds used as UV-filters, with almost complete degradation of BP-3 after 20 min of irradiation in swimming-pool water (CELEIRO et al., 2019). Although H<sub>2</sub>O<sub>2</sub> photolysis is pH dependent (H<sub>2</sub>O<sub>2</sub> cleavage occurs mainly HO<sub>2</sub><sup>-</sup> at alkaline pH), it has numerous advantages over other AOPs such as: the absence of sludge formation, complete miscibility between H<sub>2</sub>O<sub>2</sub> and water, stability and commercial availability (MATAFONOVA; BATOEV, 2018). In addition, H<sub>2</sub>O<sub>2</sub> has no phase transfer limitations and investment costs are low (DE WITTE et al., 2009).



Table 2.2 shows the summary of papers regarding heterogeneous photocatalysis (TiO<sub>2</sub>/UV-A (CELEIRO et al., 2018; CUERDA-CORREA et al., 2016b; FANG et al., 2013), TiO<sub>2</sub>/S<sub>2</sub>O<sub>8</sub><sup>2-</sup>/UV (FENOLL et al., 2014), ZnO/S<sub>2</sub>O<sub>8</sub><sup>2-</sup>/UV (FENOLL et al., 2014), TiO<sub>2</sub>/H<sub>2</sub>O<sub>2</sub>/UV-A (CELEIRO et al., 2018; CUERDA-CORREA et al., 2016b)) and photo-assisted peroxidation (UV-C/H<sub>2</sub>O<sub>2</sub> (CELEIRO et al., 2018, 2019; DU et al., 2018; LEE; LEE; ZOH, 2021; LUCAS; PERES, 2015; WANG et al., 2021)) in the degradation of BP-3, FIP and PPB in different aqueous matrices.

**Table 2.2** – Experimental conditions applied in TiO<sub>2</sub>/UV-A, TiO<sub>2</sub>/H<sub>2</sub>O<sub>2</sub>/UV-A, TiO<sub>2</sub>/S<sub>2</sub>O<sub>8</sub><sup>2-</sup>/UV, ZnO/S<sub>2</sub>O<sub>8</sub><sup>2-</sup>/UV and UV-C/H<sub>2</sub>O<sub>2</sub> processes and efficiencies obtained for BP-3, FIP and PPB degradation in aqueous matrices.

Process	CEC/Matrix	Experimental conditions	Degradation	References
TiO <sub>2</sub> /UV-A	BP-3/deionized water	Time= 30 min; [BP-3]= 9.1 µg L <sup>-1</sup> ; pH= 7.0; UV-A radiation (6 W black light, 0.8 kJ L <sup>-1</sup> ); 25 °C.	91%	(CELEIRO et al., 2018)
	PPB/deionized water	Time= 30 min; [PPB]= 5.0 mg L <sup>-1</sup> ; [TiO <sub>2</sub> ]= 92 mg L <sup>-1</sup> ; pH= 7.0; 15 W low-pressure vapor mercury lamp (λ=254 nm).	60%	(CUERDA-CORREA et al., 2016b)
		Time= 120 min; [PPB]=18 mg L <sup>-1</sup> ; [TiO <sub>2</sub> ]= 2g L <sup>-1</sup> ; pH= 9.0; 125 W high-pressure mercury lamp (λ <sub>max</sub> =365 nm).	98%	(FANG et al., 2013)
TiO <sub>2</sub> /H <sub>2</sub> O <sub>2</sub> /UV-A	BP-3/deionized water	Time= 30 min; [BP-3]= 9.1 µg L <sup>-1</sup> ; [H <sub>2</sub> O <sub>2</sub> ]= 20 mg L <sup>-1</sup> ; pH= 7.0; UV-A lamp (λ=360 nm); 25 °C.	97.8%	(CELEIRO et al., 2018)
	BP-3/swimming pool water	Time= 6 min; [BP-3]= 9.1 µg L <sup>-1</sup> ; [H <sub>2</sub> O <sub>2</sub> ]= 20 mg L <sup>-1</sup> ; pH= 6.4-7.2; UV-A lamp (λ=360 nm); 25 °C.	97.8%	(CELEIRO et al., 2018)
	PPB/deionized water	Time= 15 min; [PPB]= 5.0 mg L <sup>-1</sup> ; [TiO <sub>2</sub> ]= 30 mg L <sup>-1</sup> ; [H <sub>2</sub> O <sub>2</sub> ]= 68 mg L <sup>-1</sup> ; 15 W low-pressure vapor mercury	86%	(CUERDA-CORREA et

		lamp ( $\lambda=254$ nm).		al., 2016b)
	PPB/ surface water reservoir	Time= 15 min; [PPB]= 5.0 mg L <sup>-1</sup> ; [TiO <sub>2</sub> ]= 30 mg L <sup>-1</sup> ; [H <sub>2</sub> O <sub>2</sub> ]= 68 mg L <sup>-1</sup> ; 15 W low-pressure vapor mercury lamp ( $\lambda=254$ nm).	80%	(CUERDA- CORREA et al., 2016b)
	PPB/river water		80%	(CUERDA- CORREA et al., 2016b)
	PPB/MWWTP effluent		77%	(CUERDA- CORREA et al., 2016b)
TiO <sub>2</sub> /S <sub>2</sub> O <sub>8</sub> <sup>2-</sup> /UV	FIP/tap water	Time= 60 min; [FIP]= 100 $\mu$ g L <sup>-1</sup> ; pH 7.1; [TiO <sub>2</sub> ]= 53 mg L <sup>-1</sup> ; [S <sub>2</sub> O <sub>8</sub> <sup>2-</sup> ]= 150 mg L <sup>-1</sup> ; 8 W low-pressure mercury lamps (8.5 mW cm <sup>-2</sup> ; $\lambda=366$ nm).	98.5%	(FENOLL et al., 2014)
ZnO/S <sub>2</sub> O <sub>8</sub> <sup>2-</sup> /UV		Time= 60 min; [FIP]= 100 $\mu$ g L <sup>-1</sup> ; pH= 7.1; [ZnO]= 200 mg L <sup>-1</sup> ; [S <sub>2</sub> O <sub>8</sub> <sup>2-</sup> ]= 150 mg L <sup>-1</sup> ; 8 W low-pressure mercury lamps (8.5 mW cm <sup>-2</sup> ; $\lambda=366$ nm).	99.2%	(FENOLL et al., 2014)
UV-C/H <sub>2</sub> O <sub>2</sub>	BP-3 /deionized water	Time= 5 min; [BP-3]= 1.0 $\mu$ mol L <sup>-1</sup> ; [H <sub>2</sub> O <sub>2</sub> ]= 100 $\mu$ mol L <sup>-1</sup> ; 6 W low pressure UV-C mercury lamp (254 nm); pH = 7.0.	~100%	(LEE; LEE; ZOH, 2021)

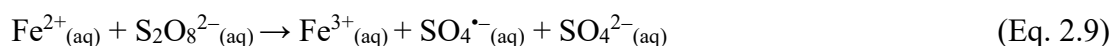
	Dose (mWh cm <sup>-2</sup> ): 1.8; [BP-3]= 5.0 mg L <sup>-1</sup> ; [H <sub>2</sub> O <sub>2</sub> ]= 8.2 mmol L <sup>-1</sup> ; low-pressure mercury lamps (UVC); pH = 7.0.	89.9%	(WANG et al., 2021)
BP-3/swimming-pool water	Time= 20 min; [BP-3]= 10 ng mL <sup>-1</sup> ; [H <sub>2</sub> O <sub>2</sub> ]= 20 mg L <sup>-1</sup> ; 8 W low-pressure mercury lamp (λ=254 nm); 25 °C.	100%	(CELEIRO et al., 2019)
	Time= 6 min; [BP-3]= 9.1 μg L <sup>-1</sup> ; [H <sub>2</sub> O <sub>2</sub> ]= 20 mg L <sup>-1</sup> ; pH 6.4-7.2; 6W UV-C lamp (λ=254 nm); 25 °C.	95%	(CELEIRO et al., 2018)
BP-3/deionized water	Time= 30 min; [BP-3]= 13.8 mg L <sup>-1</sup> ; [H <sub>2</sub> O <sub>2</sub> ]=10.20 mg L <sup>-1</sup>	74.9%	(DU et al., 2018)
PPB/deionized water	Time= 180 min; [BP-3]= 274 mg L <sup>-1</sup> ; pH= 7.2; [H <sub>2</sub> O <sub>2</sub> ] 180 mg L <sup>-1</sup> ; 15 W low-pressure mercury vapor lam (λ=253.7 nm).	71%	(LUCAS; PERES, 2015)

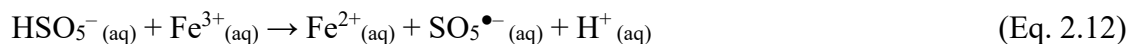
### 2.2.4 Sulfate radical based AOPs (SR-AOPs)

Sulfate radical ( $\text{SO}_4^{\bullet-}$ ) based AOPs (SR-AOPs) have become a recent trend as alternative methods for the treatment of CEC (ASIF et al., 2020; JOSÉ et al., 2014; LUO et al., 2019; PALHARIM; GRAÇA; TEIXEIRA, 2020). Persulfate ( $\text{S}_2\text{O}_8^{2-}$ ) is used as an alternative to  $\text{H}_2\text{O}_2$  in different AOPs such as UV-C/ $\text{S}_2\text{O}_8^{2-}$ , and persulfate-based Fenton and photo-Fenton. These systems result in the generation of  $\text{SO}_4^{\bullet-}$ , whose standard reduction potential (+2.60 V) is greater than that observed for  $\text{S}_2\text{O}_8^{2-}$  (+2.10 V). Thus, allowing for the degradation of contaminants at trace concentrations (LIANG et al., 2008; MIRALLES-CUEVAS et al., 2019; STARLING; AMORIM; LEÃO, 2019).

$\text{SO}_4^{\bullet-}$  is highly reactive and has an improved selectivity compared to  $\text{HO}^{\bullet}$  radical as it only reacts with organic compounds through the electron transfer mechanism. In contrast, the  $\text{HO}^{\bullet}$  radical reacts mainly by hydrogen abstraction (NOGUEIRA et al., 2007). Furthermore, a greater stability is observed for sulfate radical, which has a lifespan of 30 to 40  $\mu\text{s}$ , against 20 ns observed for  $\text{HO}^{\bullet}$  (BABU et al., 2019; BOCZKAJ; FERNANDES, 2017). Besides,  $\text{SO}_4^{\bullet-}$  standard reduction potential (+2.5 to +3.1 V) is greater than that observed for  $\text{HO}^{\bullet}$  in basic medium (+1.9 V) (ANIPSITAKIS; DIONYSIOU, 2004a; ZHANG et al., 2016). As expected, UV/ $\text{S}_2\text{O}_8^{2-}$  was a better alternative for BP-3 degradation and toxicity removal in deionized water at pH 7.0 when compared to UV/ $\text{H}_2\text{O}_2$  (LEE; LEE; ZOH, 2021).

As  $\text{SO}_4^{\bullet-}$  presents higher selectivity than  $\text{HO}^{\bullet}$ , the performance of  $\text{HO}^{\bullet}$  oxidative processes is more affected by inorganic ions and organic matter present in real waters than SR-AOPs. This is advantageous to the application of SR-AOPs for the treatment of CEC present in real matrices. In this sense, it is possible to obtain equivalent or better results via sulfate radical based AOPs (ZHANG et al., 2016). Besides,  $\text{S}_2\text{O}_8^{2-}$  and  $\text{HSO}_5^-$  may be activated by various mechanisms, such as: *i*) base activation (FURMAN; TEEL; WATTS, 2010); *ii*) UV (254 nm (HEIDT, 1942)) and IR (455 nm (DOGLIOTTI; HAYON, 1967)) light; *iii*) transition metal (Eqs. 2.9 to 2.12) (ANIPSITAKIS; DIONYSIOU, 2004b; BUXTON; MALONE; SALMON, 1997; GHANBARI; MORADI, 2017; HOUSE, 1962), and *iv*) heat (KOLTHOFF; MILLER, 1951).





Artificial UV–A light has been applied for the activation of  $\text{S}_2\text{O}_8^{2-}$  during the degradation of target compounds in real water matrices (FENOLL et al., 2014; LUO et al., 2019; PALHARIM; GRAÇA; TEIXEIRA, 2020) and in deionized water (LEE; LEE; ZOH, 2021; PAN et al., 2018), reaching >99% degradation in deionized water only. The pseudo-first-order rate constant observed for BP-3 degradation in ultrapure water was reduced by 54% in seawater for individual systems via UV/ $\text{S}_2\text{O}_8^{2-}$ . This decay in treatment efficiency was associated to the conversion of  $\text{HO}^\bullet$  and  $\text{SO}_4^{\bullet-}$  into reactive halogenated species in seawater (LUO et al., 2019). A similar effect was observed during PPB degradation, for which reaction in wastewater was 10-fold slower than in ultrapure water (MATTHAIYOU et al., 2018). Heat, transition metal ions ( $\text{Fe}^{2+}$ ,  $\text{Cu}^{2+}$  and  $\text{Co}^{2+}$ ), and UV light (254 nm) have also been used to activate  $\text{S}_2\text{O}_8^{2-}$  for BP-3 degradation. BP-3 was completely degraded at 40 °C, and all tested activation methods were significantly more efficient in aqueous solution (PAN et al., 2018). Furthermore, results showed that  $\text{Fe}^{2+}$  has the greatest promotion effect when compared to other transition metal ions (PAN et al., 2018). This finding is supported by Rastogi et al. (RASTOGI; AL-ABED; DIONYSIOU, 2009), who proposed iron as an environmentally friendly and economic species compared to other transition metals. 90% PPB degradation in the presence of  $\text{S}_2\text{O}_8^{2-}$  and magnetite nanomaterials gives further evidence of iron effectiveness to activate persulfate (MATTHAIYOU et al., 2019). In addition, zero-valent iron was more effective for persulfate activation than artificial UV-A when both activation methods were tested for PPB degradation in tap water (PALHARIM; GRAÇA; TEIXEIRA, 2020).

Special attention must also be given to red mud as a persulfate activator in the present study since it is a natural source of metal oxides rich in Fe, Al, Ti, Si, Na and Cu. This system was tested for PPB degradation in aqueous matrices (MATTHAIYOU et al., 2018). Despite high PPB degradation rates obtained in deionized (>99%) and tap water (92%) (MATTHAIYOU et al., 2018), new strategies are required to improve AOPs degradation efficiency by red mud (e.g., coupling solar or artificial radiation to the process) for the treatment of real matrices, since only 48% degradation (Table 2.3) was obtained in wastewater. Furthermore, graphene was also efficient as a catalyst in the activation of sodium persulfate, resulting in 95% degradation of PPB within 15 min of reaction (BEKRIS et al., 2017).

**Table 2.3** – Experimental conditions of SR-AOPs and efficiencies obtained for BP-3, FIP and PPB degradation in aqueous matrices.

Process	CEC/Matrix	Experimental conditions	Degradation	References
S <sub>2</sub> O <sub>8</sub> <sup>2-</sup> /UV	BP-3/deionized water	Time: ~2.5 min; [BP-3]= 1.0 μmol L <sup>-1</sup> ; [S <sub>2</sub> O <sub>8</sub> <sup>2-</sup> ]= 100 μmol L <sup>-1</sup> ; 6 W low pressure UV-C mercury lamp (254 nm); pH = 7.0.	~100%	(LEE; LEE; ZOH, 2021)
		Dose (mWh cm <sup>-2</sup> ): 6.72; [BP-3]= 5.0 mg L <sup>-1</sup> ; [S <sub>2</sub> O <sub>8</sub> <sup>2-</sup> ]= 6.4 mmol L <sup>-1</sup> ; low-pressure mercury lamps (UVC); pH = 7.0.	90.1%	(WANG et al., 2021)
	BP-3/surface water	Time= 60 min; [BP-3]= 1.14 mg L <sup>-1</sup> ; pH= 7.2; [S <sub>2</sub> O <sub>8</sub> <sup>2-</sup> ]= 96 g L <sup>-1</sup> ; 15 W low-pressure mercury lamp; 25 ± 1 °C.	59.5%	(LUO et al., 2019)
	BP-3/seawater	Time= 60 min; [BP-3]= 1.14 mg L <sup>-1</sup> ; pH= 7.6; [S <sub>2</sub> O <sub>8</sub> <sup>2-</sup> ]= 96g L <sup>-1</sup> ; 15 W low-pressure mercury lamp; 25 ± 1 °C.	54.5%	(LUO et al., 2019)
	BP-3/deionized water	Time= 180 min; [BP-3]=299 μg L <sup>-1</sup> ; pH= 7.0; [S <sub>2</sub> O <sub>8</sub> <sup>2-</sup> ]= 126 mg L <sup>-1</sup> ; 40 °C.	100%	(PAN et al., 2018)
HSO <sub>5</sub> <sup>-</sup> /UV	BP-3/deionized water	Dose (mWh cm <sup>-2</sup> ): 6.72; [BP-3]= 5.0 mg L <sup>-1</sup> ; [HSO <sub>5</sub> <sup>-</sup> ]= 6.6 mmol L <sup>-1</sup> ; low-	87%	(WANG et al., 2021)

		pressure mercury lamps (UVC); pH = 7.0.		
Nanofiltration- membrane with the Laccase/S <sub>2</sub> O <sub>8</sub> <sup>2-</sup>	BP-3/synthetic wastewater	Time= 64 h; [BP-3]= 500 µg L <sup>-1</sup> ; [S <sub>2</sub> O <sub>8</sub> <sup>2-</sup> ]= 960 mg L <sup>-1</sup> .	98%	(ASIF et al., 2020)
TiO <sub>2</sub> -P25/S <sub>2</sub> O <sub>8</sub> <sup>2-</sup> /UV	FIP/tap water	Time= 60 min; [FIP]= 100 µg L <sup>-1</sup> ; pH 7.1; [TiO <sub>2</sub> ]= 53 mg L <sup>-1</sup> ; [S <sub>2</sub> O <sub>8</sub> <sup>2-</sup> ]= 150 mg L <sup>-1</sup> ; 8 W low-pressure mercury lamps (λ=366 nm).	98.5%	(FENOLL et al., 2014)
ZnO/S <sub>2</sub> O <sub>8</sub> <sup>2-</sup> /UV		Time= 60 min; [FIP]= 100 µg L <sup>-1</sup> ; pH= 7.1; [ZnO]= 200 mg L <sup>-1</sup> ; [S <sub>2</sub> O <sub>8</sub> <sup>2-</sup> ]= 150 mg L <sup>-1</sup> ; 8 W low-pressure mercury lamps (λ=366 nm).	99.2%	(FENOLL et al., 2014)
S <sub>2</sub> O <sub>8</sub> <sup>2-</sup> /UV	PPB/tap water	[PPB]= 940 ± 70 µg L <sup>-1</sup> ; [S <sub>2</sub> O <sub>8</sub> <sup>2-</sup> ]= 1.18 g L <sup>-1</sup> ; pH= 6.8; 15 W UV-A lamp (λ <sub>max</sub> =354 nm).	77.3%	(PALHARIM; GRAÇA; TEIXEIRA, 2020)
Fe <sup>0</sup> /S <sub>2</sub> O <sub>8</sub> <sup>2-</sup>		[PPB]= 940 ± 70 µg L <sup>-1</sup> ; [Fe <sup>0</sup> ]= 40 mg L <sup>-1</sup> ; [S <sub>2</sub> O <sub>8</sub> <sup>2-</sup> ]= 961 mg L <sup>-1</sup> ; 15 W UV-A lamp (λ <sub>max</sub> =354 nm).	98.5%	(PALHARIM; GRAÇA; TEIXEIRA, 2020)

S <sub>2</sub> O <sub>8</sub> <sup>2-</sup> /iron nanomaterials	PPB/deionized water	Time= 90 min; [PPB]= 400 µg L <sup>-1</sup> ; [synthetic iron catalyst]= 50 mg L <sup>-1</sup> ; [S <sub>2</sub> O <sub>8</sub> <sup>2-</sup> ]= 1000 mg L <sup>-1</sup> .	90%	(MATTHAIYOU et al., 2019)
S <sub>2</sub> O <sub>8</sub> <sup>2-</sup> – catalyst/Graphene		Time= 20 min; [PPB]= 1.0 mg L <sup>-1</sup> ; [grafeno]= 500 mg L <sup>-1</sup> ; [S <sub>2</sub> O <sub>8</sub> <sup>2-</sup> ]= 20 mg L <sup>-1</sup> ; pH= 9.0.	95%	(BEKRIS et al., 2017)
S <sub>2</sub> O <sub>8</sub> <sup>2-</sup> – Al <sub>2</sub> O <sub>3</sub> (Red mud)		Time= 120 min; [PPB]= 800 µg L <sup>-1</sup> ; [Al <sub>2</sub> O <sub>3</sub> ]= 2 g L <sup>-1</sup> ; [S <sub>2</sub> O <sub>8</sub> <sup>2-</sup> ]= 2 g L <sup>-1</sup> ; pH= 3.0.	100%	(MATTHAIYOU et al., 2018)
	PPB/bottled water	Time= 180 min; [PPB]= 800 µg L <sup>-1</sup> ; [Al <sub>2</sub> O <sub>3</sub> ]= 2 g L <sup>-1</sup> ; [S <sub>2</sub> O <sub>8</sub> <sup>2-</sup> ]= 2 g L <sup>-1</sup> ; pH= 3.0.	92%	(MATTHAIYOU et al., 2018)
	PPB/wastewater	Time= 180 min; [PPB]= 800 µg L <sup>-1</sup> ; [Al <sub>2</sub> O <sub>3</sub> ]= 2 g L <sup>-1</sup> ; [S <sub>2</sub> O <sub>8</sub> <sup>2-</sup> ]= 2 g L <sup>-1</sup> ; pH= 3.0.	48%	(MATTHAIYOU et al., 2018)

## 2.2.5 Other AOPs

### 2.2.5.1 Sonochemistry

The propagation of ultrasound through a liquid leads to the generation of bubbles from gas cores in liquids and these bubbles grow and collapse through cycles of compression and rarefaction (CHIHA et al., 2011). During the collapse of these bubbles, temperature and pressure may reach extreme values (around 227 °C and hundreds of atmospheres) leading to the thermal dissociation of water vapor into different reactive species (CHIHA et al., 2011; ZÚÑIGA-BENÍTEZ; SOLTAN; PEÑUELA, 2016). This phenomenon allows for the formation of HO• radicals in aqueous systems from the thermal dissociation of water vapor (ZÚÑIGA-BENÍTEZ; SOLTAN; PEÑUELA, 2016). Sonochemical reactions may occur (i) inside the collapsing bubbles, (ii) in the bubble-liquid interfacial region where HO• radicals are predominant and (iii) in most solutions (CHIHA et al., 2010, 2011; HENGLEIN, 1987; ZÚÑIGA-BENÍTEZ; SOLTAN; PEÑUELA, 2016). During sonolysis, non-volatile and hydrophilic compounds are oxidized by radicals at the interface of bubbles or in the solution, while volatile and hydrophobic pollutants are generally pyrolyzed within bubble cavity (CHIHA et al., 2010; HOFFMANN; HUA; HÖCHEMER, 1996; ZÚÑIGA-BENÍTEZ; SOLTAN; PEÑUELA, 2016). Since BP3 is a non-volatile compound with low water solubility, its degradation occurs either in the solution or on the surface of bubbles, being higher in the former as the concentration of HO• radicals is higher on bubble surface. Acidic medium (pH 2) enhances BP-3 hydrophobicity (ionic fraction  $8.71 \times 10^{-5}$  %), thus favoring its accumulation in the interfacial region and increasing degradation rate (ZÚÑIGA-BENÍTEZ; SOLTAN; PEÑUELA, 2016).

Sonochemical treatment efficiency may be affected by the presence of inorganic ions and different dissolved gases. As previously described, anions negatively affect the performance of several AOPs, yet no consensus has been reached on how they affect sonochemical treatments. Bicarbonate ( $\text{HCO}_3^-$ ) ion reacts with HO• radicals to produce carbonate ( $\text{CO}_3^{\bullet-}$ ) radical (GAO et al., 2013), which can migrate to the bulk solution and promote pollutant degradation. Migration capacity is not observed for HO• radicals and, although the  $\text{CO}_3^{\bullet-}$  radical is less reactive than the HO• radical, it attacks BP-3 molecules in solution (ZÚÑIGA-BENÍTEZ; SOLTAN; PEÑUELA, 2016). In contrast, nitrate ( $\text{NO}_3^-$ ) and

chloride ( $\text{Cl}^-$ ) ions show a scavenging effect, thus competing with BP-3 for  $\text{HO}^\bullet$  radicals (ZÚÑIGA-BENÍTEZ; SOLTAN; PEÑUELA, 2016).

Ozone treatment enhanced by ultrasound was more efficient in the degradation of BP-3 when compared to conventional ozonation (ZÚÑIGA-BENÍTEZ; SOLTAN; PEÑUELA, 2016). This is justified by the fact that ultrasound promotes the transfer of the ozone mass to the liquid and ozone also decomposes thermolytically in the vapor phase of bubbles cavity, thus increasing the efficiency of  $\text{HO}^\bullet$  radical formation (JI; ZHANG; WU, 2012; ZÚÑIGA-BENÍTEZ; SOLTAN; PEÑUELA, 2016). The presence of  $\text{O}_2$  in the ultrasonic treatment increased the degradation of BP-3 by 6.7%, while  $\text{N}_2$  inhibited the degradation efficiency of the same pollutant by 18.3% (ZÚÑIGA-BENÍTEZ; SOLTAN; PEÑUELA, 2016). Two main reasons are pointed out for this behavior: (i) generation of additional  $\text{HO}^\bullet$  radicals by the dissociation of molecular oxygen inside the cavitation bubble (PÉTRIER; COMBET; MASON, 2007) and (ii) free radical scavenging by molecular nitrogen (CHIHA et al., 2011). Furthermore, degradation by ultrasound does not require additives and no waste is generated. The effect of frequency and power density on BP-3 ( $1.0 \text{ mg L}^{-1}$ ) degradation efficiency was analyzed and best degradation rate (98%) was obtained using 574 kHz and  $200 \text{ W L}^{-1}$  (VEGA; PEÑUELA, 2018).

#### 2.2.5.2 Ozonation and electrochemical oxidation

The principles of ozonation and electrochemical oxidation were recently reviewed (MAZIVILA et al., 2019). In ozonation,  $\text{HO}^\bullet$  radicals are generated through (i) photolysis of  $\text{O}_3$  in aqueous medium, (ii) reaction between  $\text{O}_3$  and  $\text{H}_2\text{O}_2$  in basic medium, and (iii) reaction between  $\text{O}_3$  and  $\text{OH}^-$  ions present in the water (JUNG et al., 2017; LUCAS et al., 2009). Furthermore, molecular ozone may react directly with dissolved contaminants through the electrophilic attack mechanism (HOIGNÉ; BADER, 1983). The degradation of different parabens, including PPB, was investigated using single ozonation and various ozone-combined processes in ultrapure water.  $\text{O}_3/\text{UV}/\text{TiO}_2/\text{H}_2\text{O}_2$  process was the most efficient in the degradation of parabens at pH 8 (CUERDA-CORREA et al., 2016a).

In electrochemical AOPs, transfer of electrons or oxygen atoms may oxidize electrochemical species in aqueous solutions (MARTÍNEZ-HUITLE; BRILLAS, 2009). For example, in the case of a photo-electron-Fenton process,  $\text{H}_2\text{O}_2$  is continuously generated *in situ*

by electrochemical  $O_2$  reduction on the cathode and Fe(II) is continuously regenerated on the cathode, allowing for the formation of  $HO^\bullet$  radicals (MAZIVILA et al., 2019). FIP degradation was evaluated in aqueous solution using advanced electrochemical oxidation and process efficiency was evaluated based on COD removal (79%), chlorine (52%), and fluorine reduction (52%) (THANGAMANI et al., 2019).

A recent study has shown that a cell configuration based on solid polymer electrolyte, which avoids the addition of salt to increase solution conductivity, was more efficient in the degradation of parabens (COD removal of 91%) than the conventional system based on a boron doped diamond (81%) (ABIDI et al., 2019).

#### 2.2.5.3 Photolysis of monochloramine and hypochlorite ion

Oxidants such as monochloramine and hypochlorite have been investigated and introduced in a photolytic process for the generation of hydroxyl radicals and other reactive species. The combination of chlorine and UV radiation is one of the newest alternatives under investigation for the treatment of contaminated water (DEBORDE; VON GUNTEN, 2008). Although chlorine gas is commonly used in this process, monochloramine has been identified to replace as it is able to control the possible formation of disinfection by-products, such as trihalomethanes and haloacetic acids (SHAH et al., 2012). Another advantage of using chloramine in the degradation of CEC is the production of  $HO^\bullet$  radicals and other reactive species. Changes in reaction pH can cause the conversion of monochloramine into dichloramine and trichloramine, which can also be decomposed into reactive species by UV irradiation with high values of quantum yields. UV irradiation of inorganic chloramines produces the chlorine radical ( $Cl^\bullet$ ) (SOLTERMANN et al., 2014) and monochloramine, which is more stable compared to chlorine, thus providing lasting residual chlorine in the reaction system (HE et al., 2016).

UV light can effectively activate hypochlorite to produce  $HO^\bullet$  radicals (LI et al., 2016a; QIN et al., 2014). The optimal pH range for this process is 3-6 (KISHIMOTO; NISHIMURA, 2015). It has been found that the contribution of  $HO^\bullet$  radicals for the degradation of BP3 increases at acidic pH values, while reactivity of chlorine species, such as  $Cl^\bullet$ , increases at neutral and basic pH values (LEE et al., 2020).

Table 2.4 summarizes studies related to the application of AOPs mentioned in this section for the degradation of BP-3, FIP and PPB in aqueous matrices. Satisfactory degradation

efficiencies were achieved in most cases as most studies were carried out in deionized water (Table 2.4). Hence, it would be convenient to direct efforts towards the application of these techniques in real matrices.

**Table 2.4** – Experimental conditions and efficiencies obtained during the degradation of BP-3, FIP and PPB in aqueous matrices by various AOPs.

Process	CEC/Matrix	Experimental conditions	Degradation	References
Ultrasound	BP-3/deionized water	Time= 60 min; [BP-3] = 3.9 mg L <sup>-1</sup> ; pH= 6.5; Power: 80.1 W; Frequency: 20 kHz.	91.4%	(ZÚÑIGA-BENÍTEZ; SOLTAN; PEÑUELA, 2016)
		Time= 30 min; [BP-3]= 1.0 mg L <sup>-1</sup> ; pH= 6.9; Power density: 200 W L <sup>-1</sup> ; Frequency: 574 kHz.	98%	(VEGA; PEÑUELA, 2018)
O <sub>3</sub> /US		Time= 60 min; [BP-3]= 3.9 mg L <sup>-1</sup> ; pH= 6.5; Power: 80.1 W; Frequency: 20 kHz; O <sub>3</sub> flow: 0.5 mL min <sup>-1</sup> .	100%	(ZÚÑIGA-BENÍTEZ; SOLTAN; PEÑUELA, 2016)
UVC/CIO <sup>-</sup>		Time= 15 min; [BP-3]= 1.0 mg L <sup>-1</sup> ; [CIO <sup>-</sup> ]= 0.64 mg L <sup>-1</sup> ; pH= 8.0; 6 W low-pressure UV-C mercury lamp (254 nm).	100%	(LEE et al., 2020)
Electrochemical oxidation	FIP/Wastewater	Time= 70 min; [FIP]= 1000 mg L <sup>-1</sup> ; pH= 9.0; Current density: 2.5 mA cm <sup>-2</sup> ; Graphite electrode with	48% COD	(THANGAMANI et al., 2019)

	electrolytic support (2.5 g L <sup>-1</sup> ).		
	Time= 70 min; [FIP]= 1000 mg L <sup>-1</sup> ; pH= 9.0; Current density: 7.5 mA cm <sup>-2</sup> ; Graphite electrode with electrolytic support (2.5 g L <sup>-1</sup> ).	73% COD	(THANGAMANI et al., 2019)
	PPB/deionized water	Time= 120 min; [PPB]= 100 mg L <sup>-1</sup> ; [S <sub>2</sub> O <sub>8</sub> <sup>2-</sup> ]= 9.6g L <sup>-1</sup> ; Current density: 5.0 mA cm <sup>-2</sup> .	97% (ABIDI et al., 2019)
O <sub>3</sub>	Time= 20 min; [PPB]= 5.0 mg L <sup>-1</sup> ; pH= 8.0.	80%	(CUERDA-CORREA et al., 2016a)
O <sub>3</sub> /UV	Time= 20 min; [PPB]= 5.0 mg L <sup>-1</sup> ; pH= 8.0; 15 W low-pressure vapor mercury lamp (λ=254 nm).	100%	(CUERDA-CORREA et al., 2016a)
O <sub>3</sub> /H <sub>2</sub> O <sub>2</sub>	Time= 20 min; [PPB]= 5.0 mg L <sup>-1</sup> ; pH= 8.0.	71%	(CUERDA-CORREA et al., 2016a)
O <sub>3</sub> /UV/H <sub>2</sub> O <sub>2</sub>	Time= 20 min; [PPB]= 5.0 mg L <sup>-1</sup> ; pH= 8.0; 15 W low-pressure vapor mercury lamp (λ=254 nm).	96%	(CUERDA-CORREA et al., 2016a)
O <sub>3</sub> /Fenton	Time= 20 min; [PPB]= 5.0 mg L <sup>-1</sup> ; pH= 3.5.	67%	(CUERDA-CORREA et al.,

---

			2016a)
O <sub>3</sub> /photo-Fenton	Time= 20 min; [PPB]= 5.0 mg L <sup>-1</sup> ; pH= 3.5; 15 W low-pressure vapor mercury lamp ( $\lambda$ =254 nm).	92%	(CUERDA-CORREA et al., 2016a)
O <sub>3</sub> /UV/TiO <sub>2</sub> /H <sub>2</sub> O <sub>2</sub>	Time= 20 min; [PPB]= 5.0 mg L <sup>-1</sup> ; pH= 3.5; 15 W low-pressure vapor mercury lamp ( $\lambda$ =254 nm).	97%	(CUERDA-CORREA et al., 2016a)

---

## 2.3 Degradation pathways, transformation products (TPs) and toxicity

Identification and monitoring of TPs play a key role in the degradation of CEC, since degradation products formed during treatment may be more toxic than target-compounds. Therefore, it is important to monitor the generation and degradation of these TPs, which is made possible by applying analytical techniques such as liquid chromatography–mass spectrometry (LC-MS/MS), liquid chromatography quadrupole time-of-flight mass spectrometry (LC-QTOF/MS) and gas chromatography time-of-flight mass spectrometry (GC-QTOF/MS).

### 2.3.1 *Benzophenone-3*

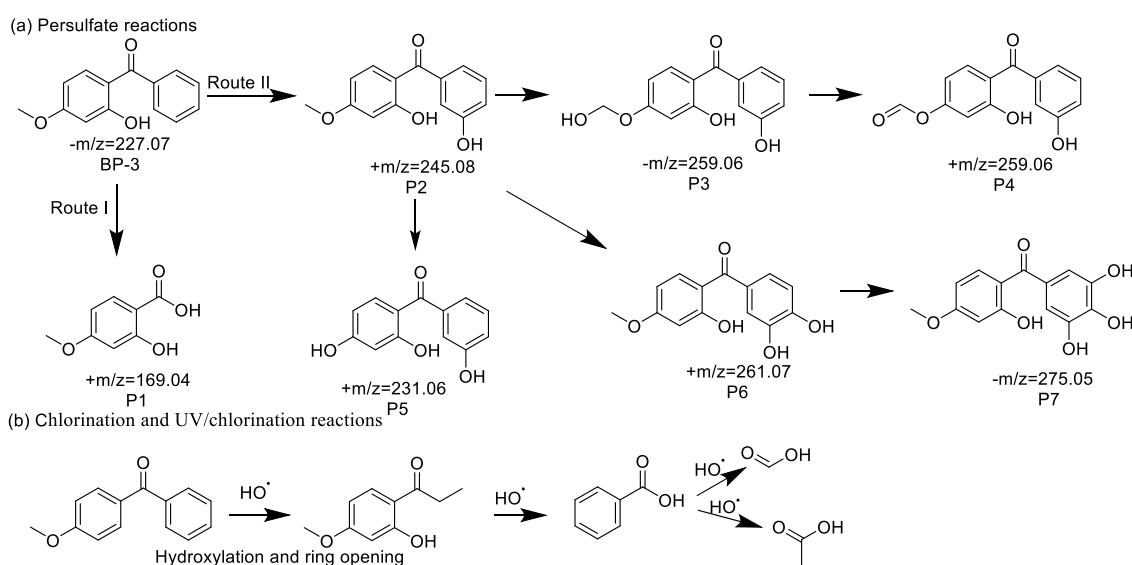
Lee et al. (2020) investigated BP-3 transformation pathway under chlorination and UV/chlorination. Chlorinated derivatives were observed in both cases as a consequence of the electrophilic substitution of one or two H atoms by chlorine, a typical reaction for phenolic compounds. In the UV/chlorination reaction, an additional oxidation reaction by HO<sup>•</sup> was observed to yield the formation of hydroxylated derivatives and promote the conversion of the carbonyl group to an ester. Further transformation steps including the formation of halogenated methoxyphenols and chloroform were only detected during chlorination. The formation of chlorinated derivatives could be responsible for toxicity increase observed in the early stages of both reactions, which was lower during UV/chlorination treatment, thus indicating that TPs generated by this process are less toxic than those produced by chlorination alone. This behavior is due to additional oxidation by reactive radicals produced by UV radiation coupled to the process, which results in further mineralization of BP-3.

BP-3 treatment in the presence of persulfate yielded the formation of 7 main TPs (PAN et al., 2018). Hydroxylation of the molecule in several positions was identified as the main route (Figure 2.6a). Up to 4 mono-, di- and trihydroxylated derivatives could be detected. Demethylation and direct oxidation reactions, as well as the loss of the non-substituted benzene ring were also observed. HO<sup>•</sup> and SO<sub>4</sub><sup>•-</sup> were identified as responsible for the degradation of BP-3 by persulfate. The evaluation of toxicity associated to TPs by ECOSAR software suggested a significant decrease in toxicity after treatment in the presence of persulfate. However, it is important to highlight, that this software considers individual TP structure to predict acute and chronic toxicity and does not enable the evaluation of effects which may be promoted by the mixture nor by the interaction between TPs and other components present in

environmental waters such as sulfate, carbonate and other ions.

TPs identified during sonochemical degradation of BP-3 are shown in Figure 2.6b (VEGA; PEÑUELA, 2018). The TP identified as 1-(2-hydroxy-4-methoxyphenyl) propan-1-on was generated by HO<sup>•</sup> attack on the unsubstituted benzene fraction, which led to ring opening. The formation of benzoic acid formation was previously reported during photochemical degradation of BP3 (VIONE et al., 2013) via oxidation by HO<sup>•</sup>. Acetic and formic acid also arise from the non-specific attack of HO<sup>•</sup> on oxidized BP-3 intermediates. In this study, toxicity profile decreased at the beginning of sonochemical treatment, growing after 30% degradation.

**Figure 2.6** – Proposed BP-3 transformation pathways via oxidation by (a) persulfate, (b) chlorination and UV/chlorination reactions. Adapted from (a) Pan et al. (2018) and (b) Lee et al. (2020). Copyright 2017, 2020 Elsevier.



### 2.3.2 Fipronil

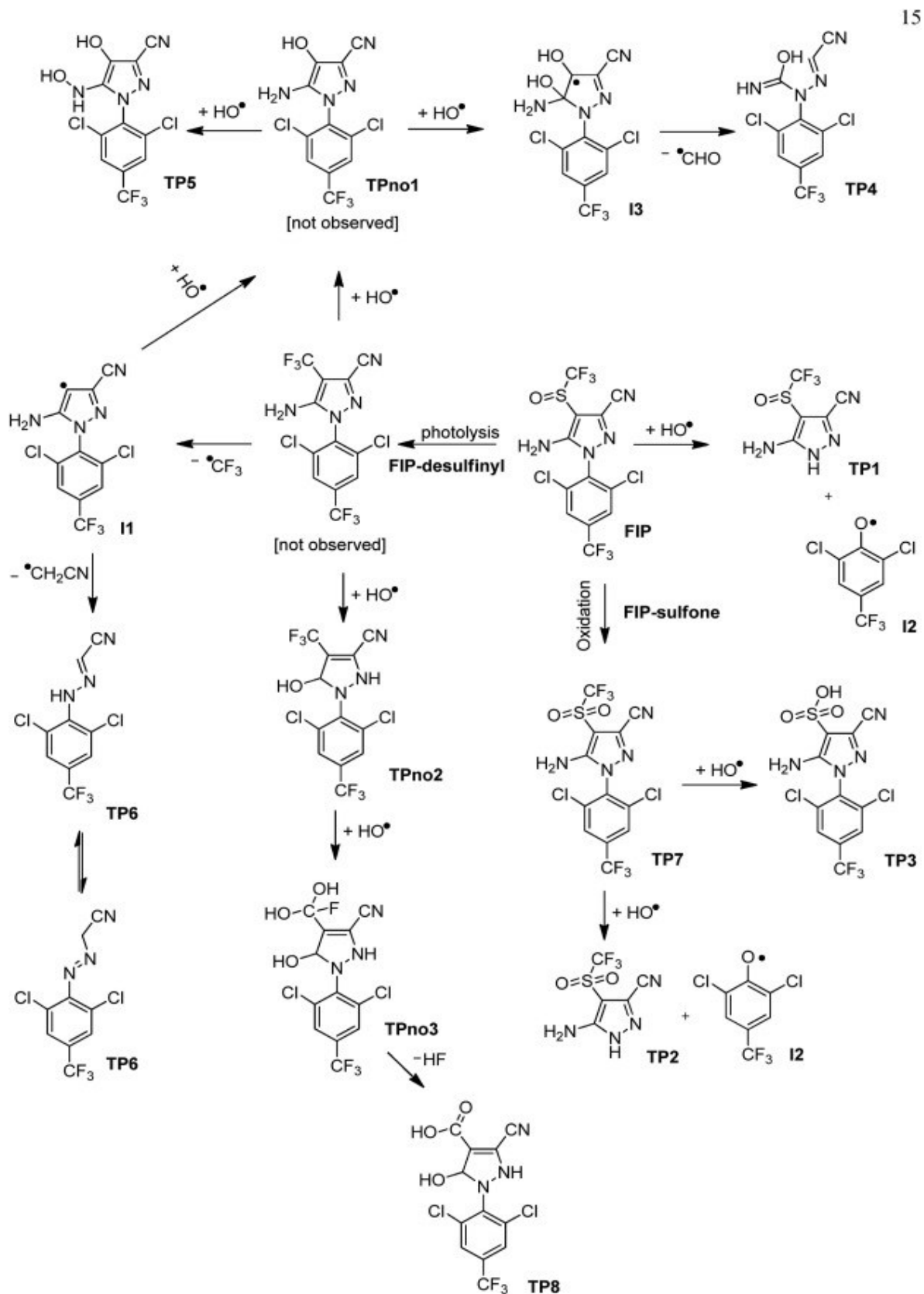
The formation of several TPs has been reported to occur during FIP degradation by different treatments (DA COSTA FILHO et al., 2016; FENOLL et al., 2014; GOMES JÚNIOR et al., 2017, 2020; THANGAMANI et al., 2019). FIP degradation in the environment (soil, sediments and water) occurs by means of oxidation, reduction, hydrolysis and photolysis reactions to yield FIP – sulfone, FIP – sulfide, FIP – carboxamide, FIP – desulfinyl, and FIP – difluoromethylsulfinyl as main TPs (GUNASEKARA et al., 2007). All or part of these compounds have also been detected in MWWTP effluents (MCMAHEN et al., 2016) and

during the application of AOPs.

In all cases, the transformation occurs preferentially in the pyrazole ring, thus indicating greater stability of the 2,6-dichloro-4-(trifluoromethyl)phenyl moiety. FIP – sulfone is the main TP identified in all reported treatments (GUNASEKARA et al., 2007; MCMAHEN et al., 2016), and was observed during photocatalytic degradation (FENOLL et al., 2014; GOMES JÚNIOR et al., 2017) and also by photo-Fenton process (GOMES JÚNIOR et al., 2020). The main mechanism of generation of this intermediate was oxidation (FENOLL et al., 2014; GOMES JÚNIOR et al., 2020) initiated by HO<sup>•</sup> attack on the sulfur atom (GOMES JÚNIOR et al., 2020). Recent studies (GOMES JÚNIOR et al., 2020) have evidenced the formation of new TPs by photo-Fenton treatment of FIP, as shown in Figure 2.7. The formation of these TPs includes the opening of the pyrazole ring (TP4 and TP6), the rupture between the pyrazole and phenyl rings (TP1 and TP2), and sequential HO<sup>•</sup> attacks in the amino and trifluoromethyl groups from FIP-desulfinyl (TP5 and TP8). Finally, chloramination reaction of FIP-sulfone takes place as a consequence of the treatment with NaOCl in reclaimed water (MCMAHEN et al., 2016). Potential risks associated to the disinfection of this by-product are still unknown.

FIP and its main TPs are reported as being highly toxic for many species, such as insects, birds, aquatic organisms, among others (GUNASEKARA et al., 2007). Nonetheless, this toxicity may be reduced or eliminated by the application of AOPs if treatment time and conditions are properly optimized. For instance, reduction of acute toxicity towards *Drosophila melanogaster* flies by solar photo-Fenton was obtained (pH = 6) in an MWWTP effluent (GOMES JÚNIOR et al., 2020). Besides, Da Costa Filho et al. (2016) demonstrated a reduction in acute toxicity for *A. salina* from 100% to 13% during the photo-Fenton treatment applied to an industrial effluent containing high loads of FIP. In contrast, FIP and its TPs did not show significant inhibitory effect to the bioluminescence of *V. fischeri* monitored during FIP degradation by TiO<sub>2</sub> heterogeneous photocatalysis (GOMES JÚNIOR et al., 2017), thus evidencing the critical need to perform toxicity tests with organisms from different trophic levels.

**Figure 2.7** – Mechanism proposed for FIP degradation via FeCit/photo-Fenton process at pH 6 and main TPs. Reprinted from Gomes Júnior et al. (2020). Copyright 2020 Elsevier.



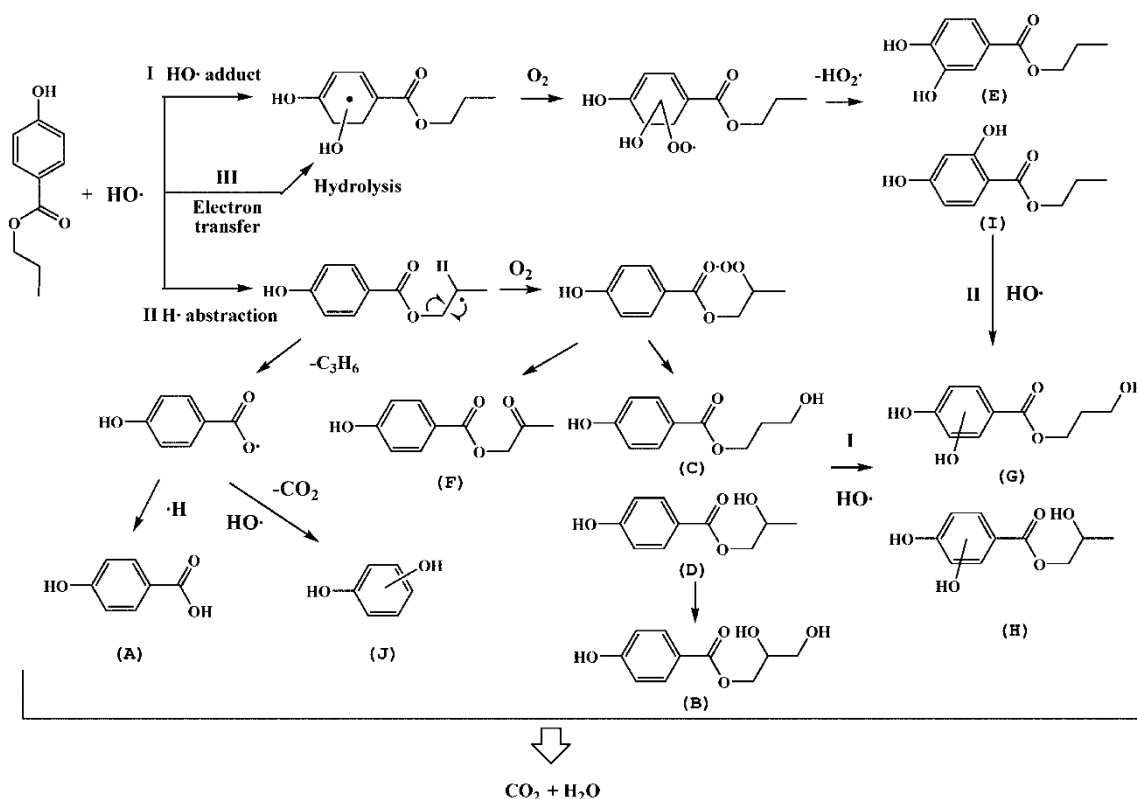
### 2.3.3 Propylparaben

Dehydroxylation and dealkylation of PPB side chains have resulted in TPs as reported in studies involving UVC/H<sub>2</sub>O<sub>2</sub> systems (GMUREK et al., 2015), ozonation (TAY; RAHMAN; ABAS, 2010), ferrate (VI) (AN et al., 2018) and UVA- and zero-valent iron-activated persulfate processes (PALHARIM; GRAÇA; TEIXEIRA, 2020). Some of these TPs include propyl benzoate, methyl benzoate, 4-hydroxybenzoic acid and methylparaben (PALHARIM; GRAÇA; TEIXEIRA, 2020). In the presence of HO<sup>•</sup> radicals, hydroxylation has been reported as the main transformation pathway (GMUREK et al., 2015). Mono- and hydroxylated derivatives mainly result from the HO<sup>•</sup> attack in the -ortho position of the phenolic ring, and, subsequently, in the propyl ester chain (MATTHAIYOU et al., 2019). The formation of di- and tri- hydroxylated isomers at the aromatic ring have also been reported during ozonation.

Concerning toxicity, theoretical predictions calculated by the ECOSAR software indicated that all TPs identified during PPB degradation are less toxic to fish, daphnid, and green algae than the parent compound (PALHARIM; GRAÇA; TEIXEIRA, 2020). PPB and methyl benzoate are harmful to all the aforementioned aquatic organisms, while 4 – hydroxybenzoic acid and methylparaben were harmful to *Daphnia sp.* and green algae. In contrast, propyl benzoate is not considered a threat to any of the aforementioned organisms (PALHARIM; GRAÇA; TEIXEIRA, 2020).

On the other hand, TPs of greater toxicity to *P. phosphoreum*, *S. capricornutum*, and *D. magna* compared to PPB have been identified (FANG et al., 2013). In addition, it has been demonstrated that TPs formed by hydroxylation in the aromatic ring of the HO<sup>•</sup>-adduct pathway (Figure 2.8) have greater toxicity than those formed by the H abstraction pathway. Based on this finding and added to the increase in initial acute toxicity observed during degradation, it can be inferred that (i) each degradation pathway has a specific contribution to total toxicity and (ii) a careful determination of optimum treatment time during AOPs is necessary to ensure toxicity removal during CEC treatment in aqueous matrices.

**Figure 2.8** – Proposed photocatalytic degradation pathways and mechanism of PPB in water. Reprinted from Fang et al. (2013).



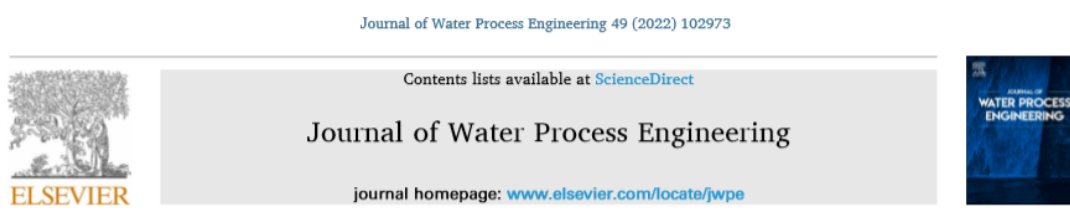
## 2.4 Concluding remarks and future trends

This review highlights recent developments in the application of AOPs for the removal of BP-3, FIP and PPB in aqueous matrices, with an estimate of only 40% in real matrices. In general, TPs identified during BP-3 and PPB were less toxic than parent compound and the main degradation mechanisms which led to their generation for all of the three target compounds were: hydroxylation, dealkylation and oxidation. Furthermore, toxicity reduction was also reported after the treatment of matrices containing these target-compounds by AOPs. Although it has been shown that each degradation pathway has a specific contribution to total toxicity, mechanistic aspects related to toxicity reduction and interaction between parent compounds, TPs, matrix components and aquatic biota remain unclear. In addition, despite the fact that several studies have reported satisfactory performance and innovative findings (in example: the use of red mud as a natural and alternative source of metals for persulfate ion activation, improvement of optical properties of photocatalysts, among others) towards the application of AOPs for the removal of these compounds, low degradation efficiencies (~48-60%) were achieved in real matrices. Thus, reinforcing the need for studies with this type of

matrix to better understand the influence of matrix composition and toxicity of treated sample aiming the application of these technologies as tertiary treatment in wastewater treatment plants for the removal of refractory and toxic organic compounds, toxicity reduction and disinfection of the effluent prior to reuse in crop irrigation.

## 2.5 Attachment

Results of the literature review outlined here in Chapter 2 were published on July, 2022, in the Journal of Water Process Engineering (Elsevier®), as shown in this attachment (<https://doi.org/10.1016/j.jwpe.2022.102973>) (RICARDO et al., 2022).



A critical review of trends in advanced oxidation processes for the removal of benzophenone-3, fipronil, and propylparaben from aqueous matrices: Pathways and toxicity changes

Ivo A. Ricardo<sup>a,b,\*</sup>, Cleiseano E.S. Paniagua<sup>a</sup>, Edna A. Alberto<sup>a,c</sup>, Maria Clara V.M. Starling<sup>d</sup>, Ana Agüera<sup>e,f</sup>, Alam G. Trovó<sup>a,\*\*</sup>

<sup>a</sup> Institute of Chemistry, Federal University of Uberlândia, 38400-902 Uberlândia, MG, Brazil

<sup>b</sup> Faculty of Natural and Exact Sciences, Save University, 0301-01 Chongoene, Gaza, Mozambique

<sup>c</sup> District Service of Education, Youth and Technology of Bilene, 0304-02 Macia, Gaza, Mozambique

<sup>d</sup> Federal University of Minas Gerais, Department of Sanitary and Environmental Engineering, 31270-010 Belo Horizonte, MG, Brazil

<sup>e</sup> Department of Chemistry and Physics, University of Almería, Carretera de Sacramento s/n, Almería 04120, Spain



### 3 CHAPTER III: EFFECT OF IRON COMPLEX SOURCE ON MWWTP EFFLUENT TREATMENT BY SOLAR PHOTO-FENTON: MICROPOLLUTANT DEGRADATION, TOXICITY REMOVAL AND OPERATING COSTS

#### 3.1 Introduction

Studies have demonstrated that conventional municipal wastewater treatment plants (MWWTP) are not designed to remove organic compounds such as pesticides, pharmaceutical drugs and personal care products, among others (KRZEMINSKI et al., 2019). These compounds occur in concentration ranging from  $\text{ng L}^{-1}$  to  $\mu\text{g L}^{-1}$ , and are known as micro-pollutants or contaminants of emerging concern (CEC) as they are potentially harmful to ecosystems and human health (BIELSKÁ; HALE; ŠKULCOVÁ, 2021; MA et al., 2019; TSUI et al., 2017; WNUK et al., 2018). Thus, recent studies have evaluated new technologies, i.e., advanced oxidation processes (AOPs) as complementary treatment stages in MWWTP aiming at the degradation of these micro-pollutants (MAZIVILA et al., 2019). Although photo-Fenton (Eq. 3.1 – 3.2) is an effective process for CEC removal (AMILDON RICARDO et al., 2018a; HABER; WEISS, 1934), one of its main drawbacks is the narrow optimal pH range of operation (pH 2.5-3.0) (AHILE et al., 2020; CLARIZIA et al., 2017). Thus, requiring a previous step of acidification followed by neutralization before discharge of the treated effluent into the environment since natural water matrices, such as MWWTP effluent and surface waters usually have neutral pH.



The use of iron chelating agents such as oxalate (Ox), oxalic acid (OA), tartaric acid (TA), citrate (Cit), nitrilotriacetic acid (NTA), ethylene diaminetetraacetic acid (EDTA) and ethylenediamine-N,N'-disuccinic (EDDS) is one of the strategies used to apply the photo-Fenton process at near-neutral conditions (DE LUCA; DANTAS; ESPLUGAS, 2014; SILVA et al., 2021). A comparison between the use of EDTA, NTA, OA and TA as chelating agents for the degradation of sulfamethoxazole ( $20 \text{ mg L}^{-1}$ ) in distilled water (DW) at neutral pH and under black-light irradiation (8W,  $\lambda_{\text{max}} = 365 \text{ nm}$ ) demonstrated that FeNTA (molar iron/ligand ratio of 1:1.5) appears to be the most appropriate chelator considering its benefits (high

degradation and biodegradability) and limitations (lower total organic carbon input and low electricity consumption). In contrast, FeOx could allow for a efficiency (~ 65%) even in the presence of iron/ligand ratios up to 1:20 (DE LUCA; DANTAS; ESPLUGAS, 2014). A similar study was performed to compare Ox, Cit, EDDS, EDTA and NTA as Fe-chelating agents for naproxen ( $200 \mu\text{g L}^{-1}$ ) degradation via photo-Fenton in DW at neutral pH and under black-light irradiation (8W,  $\lambda_{\text{max}} = 365 \text{ nm}$ ). Best performance was obtained for FeCit at a molar ratio of 1:3 (SILVA et al., 2021).

Considering that micro-pollutants occur in MWWTP effluents (FANG et al., 2019; SADARIA et al., 2019) and matrix components affect degradation efficiency and route, thus influencing the structure and concentration of transformation products generated during degradation of organic matter from micro-pollutants, chelating agents and matrix itself (AMILDON RICARDO et al., 2018a; PANIAGUA et al., 2020), more studies using real effluents are needed. Only one study has evaluated the efficiency and operating costs associated to the use of different iron sources (EDDS and NTA) on the degradation of a target micropollutant (sulfamethoxazole,  $50 \mu\text{g L}^{-1}$ ) in MWWTP effluent at neutral pH (SORIANO-MOLINA et al., 2021). Besides, as effluents vary in composition, toxicity must also be used as response variable for a comprehensive evaluation of the efficiency of each chelating agent in terms of environmental footprint (CLARIZIA et al., 2017).

Until now, evaluations on the effect of these chelating agents has been limited to EDDS and NTA (PÉREZ et al., 2020; SORIANO-MOLINA et al., 2021), which are more expensive than EDTA, Cit and Ox (SILVA et al., 2021), in two studies involving DW and one with MWWTP (DE LUCA; DANTAS; ESPLUGAS, 2014; SILVA et al., 2021; SORIANO-MOLINA et al., 2021). To investigate the feasibility of scaling-up the photo-Fenton process at near neutral conditions using these agents, it is critical to perform more in-depth studies comparing efficiencies obtained for simultaneous degradation of micro-pollutants and toxicity removal in MWWTP in the presence of each of these agents. Besides, an appropriate comparison must define best operational conditions for each complex agent (iron concentration, iron/ligand molar ratio and oxidant concentration) in MWWTP to provide deep knowledge about chemical and biological responses monitored as well as treatment costs.

Therefore and as described in chapter I, this study focused on the effect of solar photo-Fenton applied in the presence of different chelating agents (Cit and NTA) for the degradation and toxicity removal of a mixture of micro-pollutants at neutral pH in MWWTP effluent and under solar irradiation. The personal care products (benzophenone-3 (BP-3) and propylparaben (PPB)) and the insecticide fipronil (FIP) were selected as model pollutants and were added to

the matrix at an initial concentration of  $100 \mu\text{g L}^{-1}$  for each of them. These contaminants were selected because they have been detected in surface water (BASIN et al., 2016), raw wastewater (CANOSA et al., 2006; LEE; PEART; SVOBODA, 2005; LI et al., 2015a), treated effluent (HANEKAMP; BAST, 2014; HOPKINS; BLANEY, 2016; SADARIA et al., 2019), groundwater (SEMONES et al., 2017) and drinking water (MONTAGNER; VIDAL; ACAYABA, 2017) and associated to toxic effects (DA COSTA FILHO et al., 2016; SADARIA et al., 2019).

## 3.2 Experimental

### 3.2.1 Reagents

All chemical solutions were prepared in ultrapure water ( $18.2 \text{ M}\Omega \text{ cm}$ ) produced by a Milli-Q water purification system. FIP (98.77 wt%) was acquired from Sinochem Ningbo (Lian Yun Gang City, Jiangsu Province, China). PPB ( $\text{C}_{10}\text{H}_{12}\text{O}_3$ , 99 wt%), BP-3 ( $\text{C}_{14}\text{H}_{12}\text{O}_3$ , 98 wt%), NTA ( $\text{C}_6\text{H}_6\text{NNa}_3\text{O}_6$ ) and potassiumtitanium oxide oxalate ( $\text{C}_4\text{K}_2\text{O}_9\text{Ti}\cdot 2\text{H}_2\text{O}$ ,  $\geq 90$  wt%) were purchased from Sigma-Aldrich (São Paulo, Brazil). Ferric nitrate nonahydrate ( $\text{Fe}(\text{NO}_3)_3\cdot 9\text{H}_2\text{O}$ ), ferrous sulfate heptahydrate ( $\text{FeSO}_4\cdot 7\text{H}_2\text{O}$ ), sodium citrate dihydrate ( $\text{Na}_3\text{C}_6\text{H}_5\text{O}_7\cdot 2\text{H}_2\text{O}$ ), hydrogen peroxide ( $\text{H}_2\text{O}_2$ ) (30 wt%), sodium sulfite ( $\text{Na}_2\text{SO}_3$ ), 1.10-phenanthroline ( $\text{C}_{12}\text{H}_8\text{N}_2\cdot \text{H}_2\text{O}$ ) were provided by Synth (Diadema, Brazil). Hydroxylamine hydrochloride ( $\text{NH}_2\text{OH}\cdot \text{HCl}$ ) was obtained from Êxodo (Sumaré, Brazil), HPLC-grade methanol ( $\text{CH}_3\text{OH}$ ) from J. T. Baker (Aparecida de Goiânia, Brazil), acetic acid ( $\text{CH}_3\text{COOH}$ ) from Panreac (Barcelona, Spain), anhydrous sodium acetate ( $\text{CH}_3\text{COONa}$ ) and sulfuric acid ( $\text{H}_2\text{SO}_4$ ) were both furnished by Dinâmica (Indaiatuba, Brazil).

### 3.2.2 MWWTP effluent

MWWTP effluent samples were collected at the Municipal Department of Water and Sewage located in Uberlândia, Brazil ( $18^\circ 55' 08'' \text{ S}$ ,  $48^\circ 16' 37'' \text{ W}$ ). Sampling was carried out in the flotation channels after the following stages: preliminary treatment (bar screens + desanders), upflow anaerobic sludge blanket (UASB), coagulation-flocculation (ferric chloride,  $\text{FeCl}_3$ ) and flotation. After sampling, physicochemical characterization of the collected effluent matrix was carried out (Table 3.1) and samples were stored in amber bottles and kept under refrigeration at  $4^\circ \text{ C}$  before and during the period of degradation experiments.

### 3.3 Photodegradation experiments

All photodegradation experiments were conducted in a dark-glass vessel (5.5 cm depth, 0.13 cm width and 5.0 cm of optical path) under magnetic stirring. 500 mL of the MWWTP effluent were spiked with a mixture containing the target compounds (500 mg L<sup>-1</sup> each CEC prepared in acetonitrile) in order to obtain a final concentration of 100 µg L<sup>-1</sup> of each CEC.

Experiments were carried out under solar radiation between 10 a.m. and 2 p.m. An aliquot was taken from the initial solution (-10 min) for HPLC-DAD analysis. Iron-complex solutions at the desirable iron/ligand ratios were prepared in the dark and apart from the mixture by mixing the organic ligand to Fe<sup>3+</sup> solutions at the appropriate concentration. In the sequence, solutions were stirred for 5 minutes in order to ensure the formation of iron complexes (SORIANO-MOLINA et al., 2018). Subsequently, the iron complex solution was added to the mixture. After five minutes of stirring in the dark, another sample was collected (-5 min) for chromatographic analysis and total iron analyses. The oxidant was then added to the solution, and after five minutes of stirring (Fenton process, 0 min), samples were taken for chromatographic analysis, total iron and H<sub>2</sub>O<sub>2</sub> concentration quantification. From this moment, effluent was exposed to solar irradiation, and aliquots were sampled for the former mentioned analyses at pre-established times (5, 10, 20, 30, 40, 50 and 60 min). Incident irradiation (W m<sup>-2</sup>) was monitored by a radiometer (MU-100) containing an ultraviolet sensor (250-400 nm), and registered data were used to calculate the normalized irradiation time ( $t_{30W}$ ) (Eq. 3.3) (MIRALLES-CUEVAS et al., 2019).

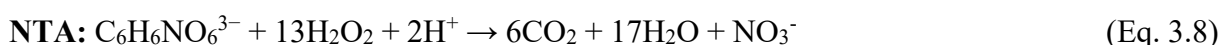
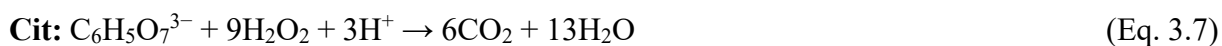
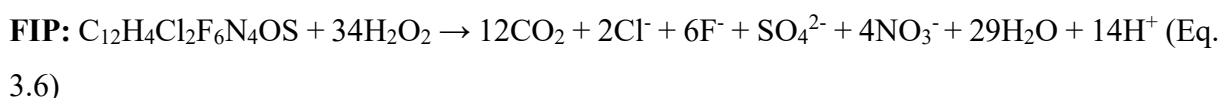
$$t_{30W(n)} = t_{30W(n-1)} + (t_{(n)} - t_{(n-1)}) \times \frac{I_n}{30} \quad (\text{Eq. 3.3})$$

Where:  $t_{30W(n)}$  and  $t_{30W(n-1)}$  represent the normalized times for an irradiance of 30 W m<sup>-2</sup> after n and n-1 minutes, respectively;  $t_n$  e  $t_{n-1}$  as the sampling times at n and n-1 minutes, respectively and  $I_n$ , represented the solar irradiance measured by the radiometer for a given time n. Thus, the time refers to a constant solar UV power of 30 W m<sup>-2</sup> (typical solar UV power on a perfectly sunny day around noon). This calculation allows comparison with other photocatalytic experiments (LAPERTOT et al., 2007).

Three sets of experiments were performed at initial pH 7.4 (natural pH of the MWWTP matrix) in order to determine the best operational parameters conditions for each ligand: (i) the effect of iron concentration (12.5, 25, 50 and 100 µmol L<sup>-1</sup>) at fixed Fe/Ligand (Fe/L) molar

ratio (1:1) and fixed initial concentration of 5.9 mmol L<sup>-1</sup> H<sub>2</sub>O<sub>2</sub> (200 mg L<sup>-1</sup> H<sub>2</sub>O<sub>2</sub>) (SILVA et al., 2021); (ii) the effect of the Fe/L molar ratio (1:2 for FeCit and FeNTA; 1:3, 1:4, 1:5 and 1:6 for FeCit) using the best iron concentration (100 μmol L<sup>-1</sup>) and 5.9 mmol L<sup>-1</sup> H<sub>2</sub>O<sub>2</sub>, (iii) the influence of H<sub>2</sub>O<sub>2</sub> concentration (0.74, 1.5, 2.9, 5.9 and 11.8 mmol L<sup>-1</sup> H<sub>2</sub>O<sub>2</sub>, equivalent to 25, 50, 100 and 400 mg L<sup>-1</sup>, respectively) under the best iron concentration (100 μmol L<sup>-1</sup>) and molar ratios (1:1 for FeNTA and 1:5 for FeCit).

Considering the Chemical Oxygen Demand (COD) (COD = 200 mg L<sup>-1</sup>; it requires 12.5 mmol L<sup>-1</sup> of H<sub>2</sub>O<sub>2</sub> to lead to complete mineralization) of the matrix, it is expected that there is greater competition of organic matter with the target compounds by hydroxyl radicals (HO•). This justifies the fixed initial H<sub>2</sub>O<sub>2</sub> concentration used in (i), which was approximately 434, 462 and 758 – fold than the theoretical value (0.0139, 0.0128 and 0.00778 mmol L<sup>-1</sup>) required to mineralise BP-3, PPB and FIP, respectively (Eq. 3.4 – 3.6). In addition, the organic ligands (citrate and NTA) also consume H<sub>2</sub>O<sub>2</sub> (Eq. 3.7 – 3.8).



Control experiments using the best Fe/L molar ratios and, iron and H<sub>2</sub>O<sub>2</sub> concentrations were also performed under solar irradiation (photolysis, Fe/L and H<sub>2</sub>O<sub>2</sub>) and in the dark (H<sub>2</sub>O<sub>2</sub> and FeL/H<sub>2</sub>O<sub>2</sub>) at pH 7.4 (natural of the MWWTP matrix).

### 3.4 Chemical and bioassay analysis

The efficiency of the photo-Fenton degradation process of the target compounds was determined and evaluated through the following chemical and bioassays analyses: monitoring of the concentration of the target compounds, quantification of the concentrations of the oxidants (H<sub>2</sub>O<sub>2</sub>), total dissolved iron and monitoring of acute toxicity to *drosophila melanogaster* (*D. melanogaster*) flies due to the response/sensitivity of this organism to FIP (GOMES JÚNIOR et al., 2020; GONÇALVES et al., 2020).

### 3.4.1 Target Compound

A LC-6AD High-Performance Liquid Chromatograph (Shimadzu) equipped with a UV-DAD detector, model SPD-M20A (Shimadzu) containing a Phenomenex C-18 column (Luna 5  $\mu\text{m}$ ,  $250 \times 4.6$  mm) was used to monitor the concentration of each CEC. Isocratic elution was applied using a mobile phase composed of 25% of acetic acid (0.01% v/v) in Milli-Q water and 75% methanol. The flow rate was  $1 \text{ mL min}^{-1}$ . The analytical curve was obtained by injection into the chromatograph, of 13 solutions of the mixture of the target compounds at different concentrations ( $0.625$  to  $120 \mu\text{g L}^{-1}$ ), prepared from a stock solution of the mixture of the target compounds ( $500 \text{ mg L}^{-1}$ ) in  $10 \text{ mL}$  volumetric flasks for each concentration.

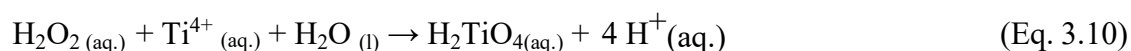
The average degradation of the mixture ( $C/C_0$ ) was evaluated by calculating the difference between average of initial concentrations compared to average of concentrations after a certain reaction time ( $t_{30W}$ ) for the sum of target compounds (Eq. 3.9):

$$C/C_0 = \frac{\sum C_0 - \sum C_{t_{30W}} w_i}{\sum C_0} \quad (\text{Eq. 3.9})$$

where:  $C_0$  is the initial concentration of each target compound,  $w_i$  is the % in weight of each contaminant, and  $C_{t_{30W}}$  is the concentration of each target compound at  $t_{30W}$ .

### 3.4.2 Hydrogen peroxide

The concentration of  $\text{H}_2\text{O}_2$  was determined by the spectrophotometric method using titanium oxalate (USP TECHNOLOGIES, 2015). The principle of the method consists in the reaction of  $\text{H}_2\text{O}_2$  with titanium potassium oxalate oxide dihydrate in acidic solution ( $\text{H}_2\text{SO}_4/\text{H}_2\text{O}$ ) to form the yellow complex of pertitanic acid (Eq. 3.10). The coloured complex is measured spectrophotometrically at  $400 \text{ nm}$ .



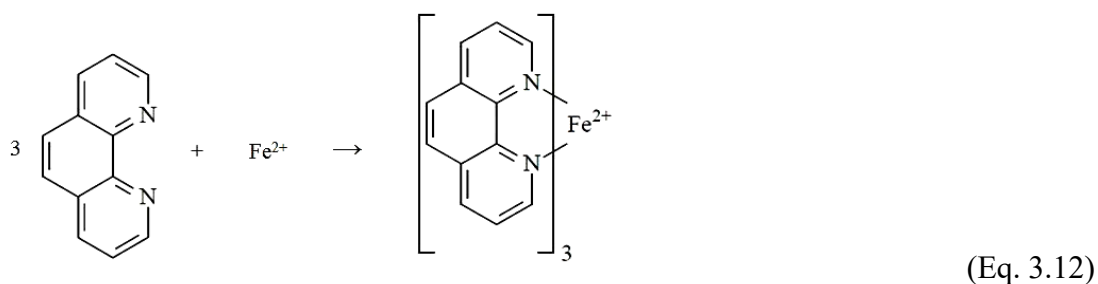
For hydrogen peroxide determination,  $500.0 \mu\text{L}$  of sulphuric acid (1:17) (v/v),  $400.0 \mu\text{L}$  of titanium potassium oxalate and  $4100 \mu\text{L}$  of the sample containing the oxidant were added to a tube. Residual  $\text{H}_2\text{O}_2$  was removed from aliquots prior to HPLC analysis by adding excess of  $\text{Na}_2\text{SO}_3$  ( $1 \text{ g L}^{-1}$ ) (Eq. 3.11). In contrast, excess  $\text{H}_2\text{O}_2$  present in samples submitted to toxicity

assays was removed by the addition of bovine catalase ( $2 \text{ g L}^{-1}$ ) prior to sample filtration and exposition to test-organisms. (GOMES JÚNIOR et al., 2020).

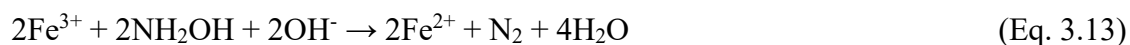


### 3.4.3 Total iron dissolved ( $\text{Fe}^{3+}$ and $\text{Fe}^{2+}$ )

Total dissolved iron was measured by Standard Method 3500-Fe B (EATON et al., 2005). The methodology is based on the reaction between  $\text{Fe}^{2+}$  and 1,10 – phenanthroline, originating a red colored complex ( $[\text{Fe}(1,10\text{ – phenanthroline})_3]^{2+}$ ) (Eq. 3.12) called ferroin, whose colour intensity is independent of pH in the range of 2 to 9. The concentration of  $\text{Fe}^{2+}$  was determined spectrophotometrically by monitoring the absorption maximum at 510 nm.



$\text{Fe}^{3+}$  concentration was estimated by the difference between the total iron (determined after reduction with hydroxylamine (Eq. 3.13) and the  $\text{Fe}^{2+}$  content.



The equipment used for the quantification of  $\text{H}_2\text{O}_2$  and total iron dissolved was the UV-Vis spectrophotometer, model UV-1800 (SHIMADZU).

### 3.4.4 Bioassays with *Drosophila melanogaster*

Acute toxicity of treated and untreated samples towards *Drosophila melanogaster* (*D. melanogaster*) was estimated according to the methodology described by Gomes Júnior et al. (2020) and Gonçalves et al. (2020). All *D. Melanogaster* bioassays were also performed in triplicates.

*D. melanogaster*, an invertebrate also termed as fruit fly, has some desirable characteristics (short lifespan, fully known genome sequence and ease of genetic manipulation) that are not characteristic of higher organisms and stimulate its use as a model for acute toxicity assays. Furthermore, metabolic pathway for the metabolism of environmental toxins observed in this organism is similar to that presented by vertebrates, including humans (LI et al., 2015b; LIU; LI; WANG, 2019; RAJAK et al., 2017). Lifespan of *D. melanogaster* was used to assess acute toxicity in many studies, using leachates from municipal solid wastes (BHARGAV et al., 2008), MWWTP effluent containing pesticides (GOMES JÚNIOR et al., 2020; GONÇALVES et al., 2020), aqueous solutions of parabens (GAO et al., 2020; LI et al., 2015b) and antibiotics (LIU; LI; WANG, 2019).

In this study, Canton S. strain flies were used for the acute toxicity test, in which mortality between 0-4 days old wild-type *D. melanogaster* was monitored. The mortality of flies was evaluated for initial solution of MWWTP effluent containing BP-3, FIP and PPB (100 µg L<sup>-1</sup> each), and for photo-Fenton (20 and 60 min) processes evaluated under better experimental conditions for FeCit and FeNTA. For each bioassay, 30 flies (n=30) (15 females and equal number of males) were exposed to of treated and untreated samples by mixing samples to fly food. The food was made in a medium enriched with mashed potato (1.5 g, 75% instant mashed potato, 15% yeast extract, 9.3% glucose, 0.07% nipagin) and 5 mL of each sample of the treated and untreated solutions. Fly food was replaced every 2 to 3 days and the number of dead flies was registered until the 15 days corresponding to the experiment.

For control experiments, fly lifespan was assessed when exposed to distilled water, acetonitrile (0.01%), MWWTP effluent (in the absence of target-compounds) and MWWTP effluent degradation samples (at the same sampling time for target-compounds degradation, 20 and 60 min) using the FeCit and FeNTA systems were also verified. In addition, solutions containing only FIP or PPB or BP-3 in the MWWTP effluent were also tested. Flasks containing flies were kept at 25 °C in a light/dark cycle (12 h/12 h) during experiments. Mean life span was calculated using the Kaplan-Meier test using the *Graph Pad Prism* 8.02 software.

### **3.5 Results and discussion**

#### *3.5.1 Characterization of MWWTP effluent water*

The effluent water sample from MWWTP Uberabinha, which receives and treats 95% of the effluent generated by the population of Uberlândia, was collected to simulate a real

contamination with the compounds BF-3, FIP and PPB. The physicochemical parameters regarding the characterization of this matrix are presented in Table 3.1. Some of this data were carried out by the laboratory Bioética Ambiental (Environmental Bioethics) and supplied by the DMAE, while others were carried out at the Laboratório de Química Ambiental (Environmental Chemistry Laboratory) - UFU.

**Table 3.1** – Physicochemical characterization of MWWTP effluent sample.

<b>Parameter</b>	<b>Unit</b>	<b>Value</b>	<b>CONAMA 430/2011</b>
pH	-	7.4	5.0 – 9.0
Color	mg L <sup>-1</sup> Pt/Co	440	-
Turbidity	NTU	47.5	-
Total solids	mg L <sup>-1</sup>	601	-
Dissolved solids	mg L <sup>-1</sup>	523	-
Suspended solids	mg L <sup>-1</sup>	36	-
Conductivity	μS cm <sup>-1</sup>	1040	-
Chemical oxygen demand	mg O <sub>2</sub> L <sup>-1</sup>	200	-
Biochemical oxygen demand	mg O <sub>2</sub> L <sup>-1</sup>	80	-
Alkalinity	mg CaCO <sub>3</sub> L <sup>-1</sup>	312	-
Chloride	mg L <sup>-1</sup>	200	-
Iron	mg L <sup>-1</sup>	0.7	<15
Total carbon	mg C L <sup>-1</sup>	95.3	-
Organic carbon	mg C L <sup>-1</sup>	38.1	-
Total Sulfate*	mg L <sup>-1</sup>	73.5	-
Ammoniacal Nitrogen *	mg L <sup>-1</sup>	20.7	20
Total Phosphorus *	mg L <sup>-1</sup>	1.39	-
Total Fluoride *	mg L <sup>-1</sup>	0.23	-
Surfactants *	mg L <sup>-1</sup>	3.40	-
<i>Escherichia Coli</i> *	MPN/100 mL	6,14 x 10 <sup>5</sup>	-

\* – Conducted by the Environmental Bioethics Laboratory

**NTU:** Nephelometric Turbidity Unit      **μS cm<sup>-1</sup>:** microsiemens per centimetre

**MPN:** most probable number

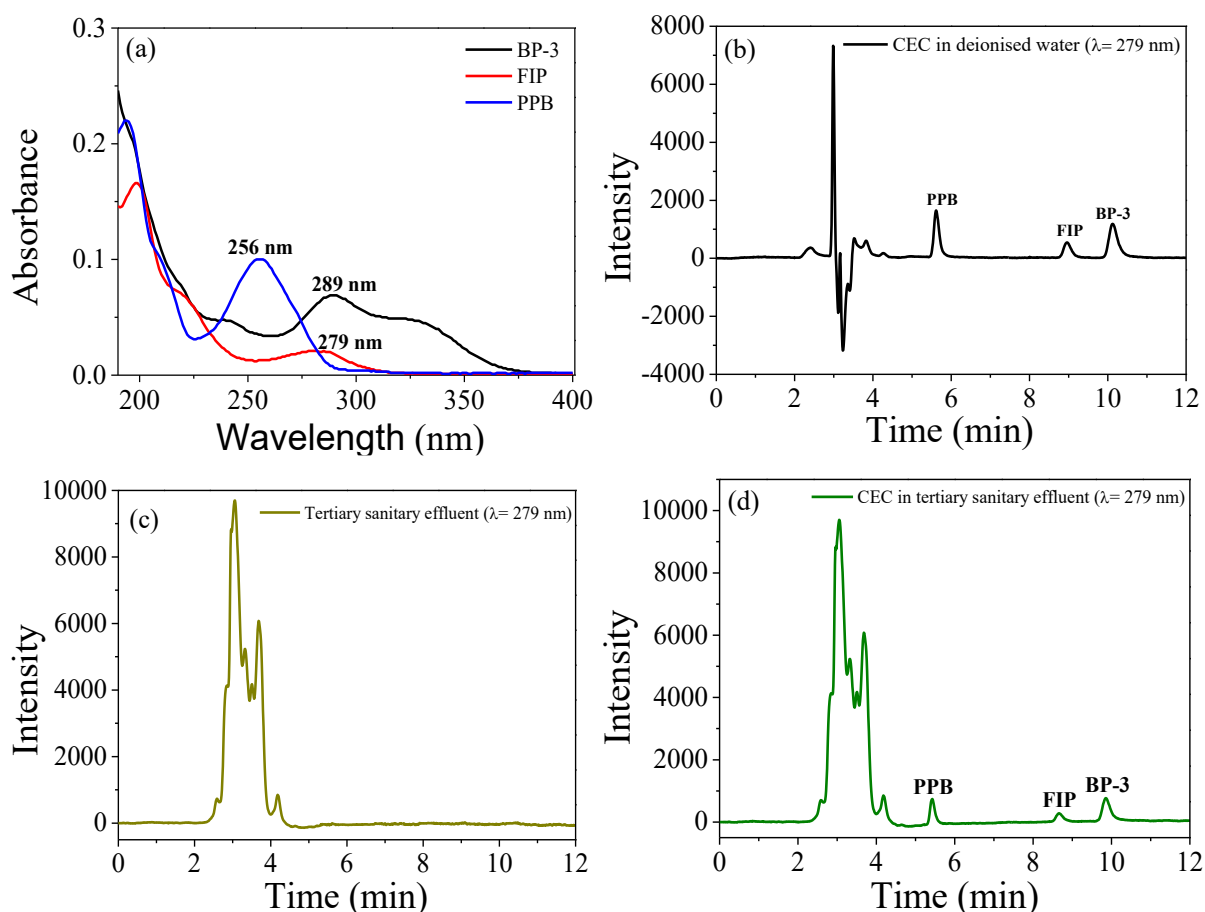
The effluent water presents a complex composition characterized by the presence of organic matter and inorganic ions, especially carbonate, chloride and total and dissolved solids, which can interfere in the degradation process. The chromatographic determination of each target compound was made based on the analytical curve made in this matrix.

### 3.5.2 Analytical method by HPLC - DAD for determination of BP-3, FIP, PPB

Initially, absorption spectra between 190 and 400 nm were obtained from the samples of the target compounds in natural pH solutions (7.4) of deionized water in order to determine the wavelengths of maximum absorption to be used in the chromatographic analysis of each target compound. BP-3 and FIP showed bands with maximum absorption at 289 and 279 nm respectively, and PPB showed a single band with maximum absorption at 256 nm (Figure 3.1a).

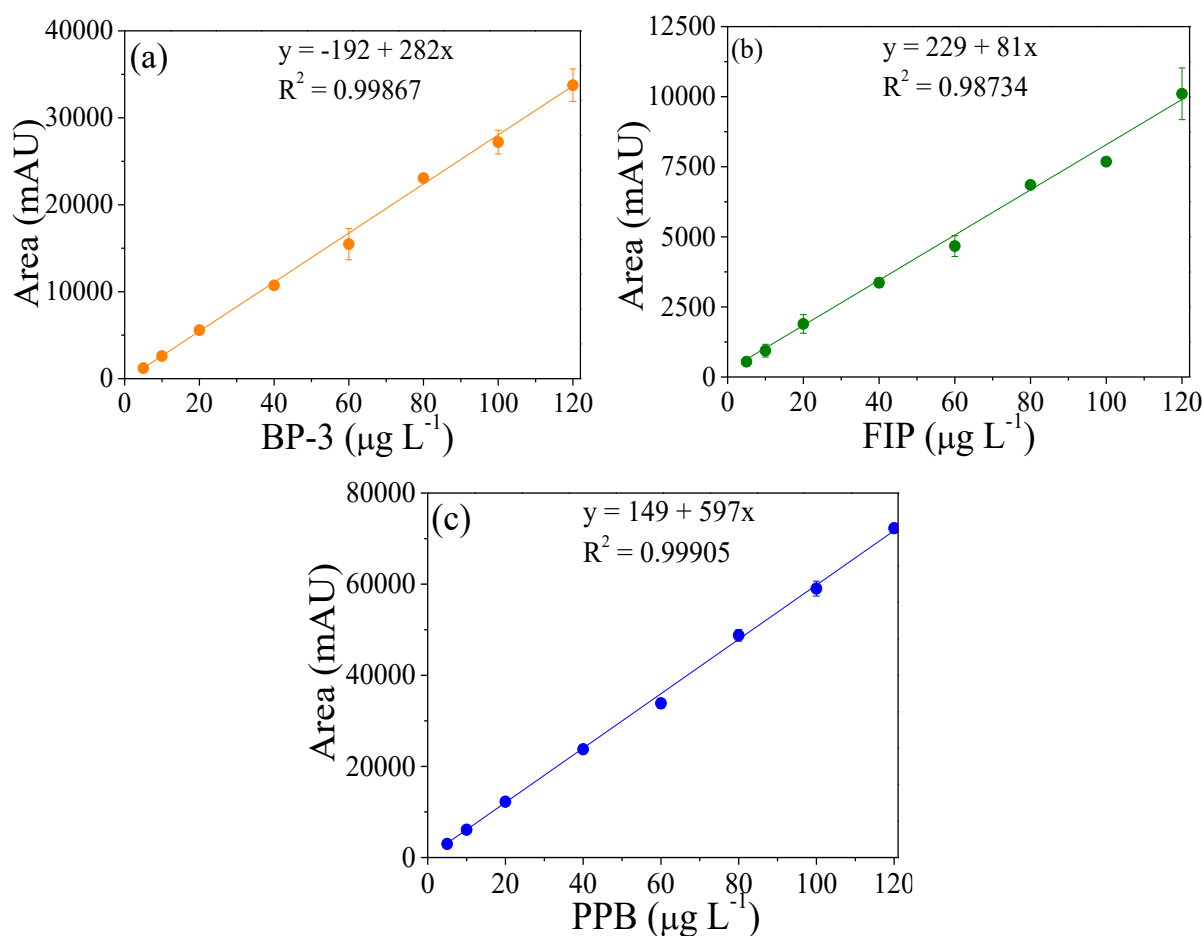
Subsequently, the chromatographic conditions of each target compound were tested using, respectively, the wavelength of 289, 279 and 256 nm for BP-3, FIP and PPB and as mobile phase an isocratic mixture of methanol/acetic acid (0.01 % v/v) in different proportions in % (v/v) (60:40, 65:35, 70:30 and 75:25). In the 60:40 (% v/v) ratio, there was similarity in the retention time ( $t_r$ ) of BP-3 (25.9 min) and FIP (25 min), generating co-elution. Similar phenomenon was also observed for the same compounds (BP-3 (13.8 min) and FIP (13.29 min)) when using the 70:30 (% v/v) ratio. At the 65:35 (% v/v) ratio, FIP ( $t_r = 23.88$  min) showed an extended peak, compromising the separation with BP-3 peak ( $t_r = 21.07$  min). The 75:25 (% v/v) ratio was selected due to good chromatogram resolution, relatively short run time and good separation between the target compounds (Figure 3.1b). In addition, a relatively favourable time interval between the dead volume peak and the target compounds was observed, allowing the formation of intermediates, which are generally more polar and come out in a shorter retention time, to be verified. It was also observed that the tertiary sanitary effluent generates some compounds near the dead volume of the column (figure 3.1c). Thus, the output of the first compound (PPB) at 5.6 min (figures 3.1b and 3.1d) is extremely important, since there is no coelution of PPB with such compounds. Moreover, it was observed that there is no presence of peaks in the retention times of the target compounds (figure 3.1d). The flow rate was  $1 \text{ mL min}^{-1}$  and retention times of  $5.6 \pm 0.1$  (PPB),  $9.0 \pm 0.1$  (FIP) and  $10.2 \pm 0.1$  (BP-3) min were obtained.

**Figure 3.1** – (a) Absorption spectra of the target compounds ( $1000 \mu\text{g L}^{-1}$  each, in deionised water at pH 7.0) and (b) Chromatogram for a solution containing FIP, PPB and BP-3 ( $100 \mu\text{g L}^{-1}$ ) in deionised water and near neutral pH (7.0), (c) tertiary sanitary effluent and (d) solution containing FIP, PPB and BP-3 ( $100 \mu\text{g L}^{-1}$  each) in tertiary sanitary effluent (pH= 7.4 (natural effluent)) using the mobile phase 75% MeOH : 25% HAc (% v/v) for the wavelength ( $\lambda$ ) of 279 nm.



After defining the best ratio based on retention time, analytical curves were obtained for quantification of BP-3, FIP and PPB (Figure 3.2) during the degradation experiments.

**Figure 3.2** – Analytical curves for quantification of (a) BP-3, (b) FIP and (c) PPB in MWWTP effluent at pH 7.4 (natural of the matrix).



Since the performance parameters should be clearly described in the validation procedure, the above curves were used for description/estimation of selectivity, linearity, working range, linear working range, sensitivity, limit of detection (LOD), limit of quantification (LOQ) and precision (repeatability, intermediate precision and reproducibility).

The limit of detection (LOD) of an individual analytical procedure is the smallest amount of analyte in the sample that can be detected, but not necessarily quantified under the conditions established for the test (INMETRO, 2020). When measurements are performed in samples with low levels of the analyte or of a property, such as trace analysis, it is important to know the lowest concentration value of the analyte or of the property that can be detected by the method. The LOD was calculated based on the signal-to-noise ratio. The signal-to-noise ratio is determined by comparing the measured signals from samples with known low concentrations of the analyte and the noise from sample blanks and defining the minimum concentration at which the analyte can be reliably detected. A signal-to-noise ratio of 2:1 was

considered for the estimation of the LOD. It is worth mentioning that the noise region of the blank was the same as the measured signal. To guarantee the reliability of the LOD values adopted for each compound, 7 injections of the same concentration were made. Once the LOD was established, this was confirmed through the analysis of independent samples at the same concentration level of the LOD and a number of 6 replicates was adopted for the effect. In this context, all replicates were detected, meaning that the LOD determined was not underestimated.

The limit of quantification (LOQ) of an individual analytical procedure is the smallest amount of the analyte in the sample that can be quantitatively determined with acceptable precision and accuracy (INMETRO, 2020). The LOQ obtained from equation 3.14 were: 4.2  $\mu\text{g L}^{-1}$  for FIP (279 nm) and BP-3 (289 nm) and, 1.3  $\mu\text{g L}^{-1}$  for PPB (256 nm), thus allowing the evaluation of up to 96 -99% degradation.

$$LOQ = LOD \times 3,3 \quad (\text{Eq. 3.14})$$

The straight line equation of the analytical curve of BP-3, FIP and PPB as well as the figures of merit, correlation coefficient ( $R^2$ ) and the linear working range are presented in Table 3.2.

**Table 3.2** – Straight line equations of the analytical curves, linear ranges, linear correlation coefficient ( $R^2$ ), limit of detection (LOD) and limit of quantification (LOQ) for the target compounds.

CEC	Analytical curve	Linear range ( $\mu\text{g L}^{-1}$ )	$R^2$	LOD ( $\mu\text{g L}^{-1}$ )	LOQ ( $\mu\text{g L}^{-1}$ )
PPB	$y = 149 + 597x$	1.3 – 120	0.99905	0.4	1.3
FIP	$y = 229 + 81x$	4.2 – 120	0.98734	1.3	4.2
BP-3	$y = -192 + 282x$	4.2 – 120	0.99867	1.3	4.2

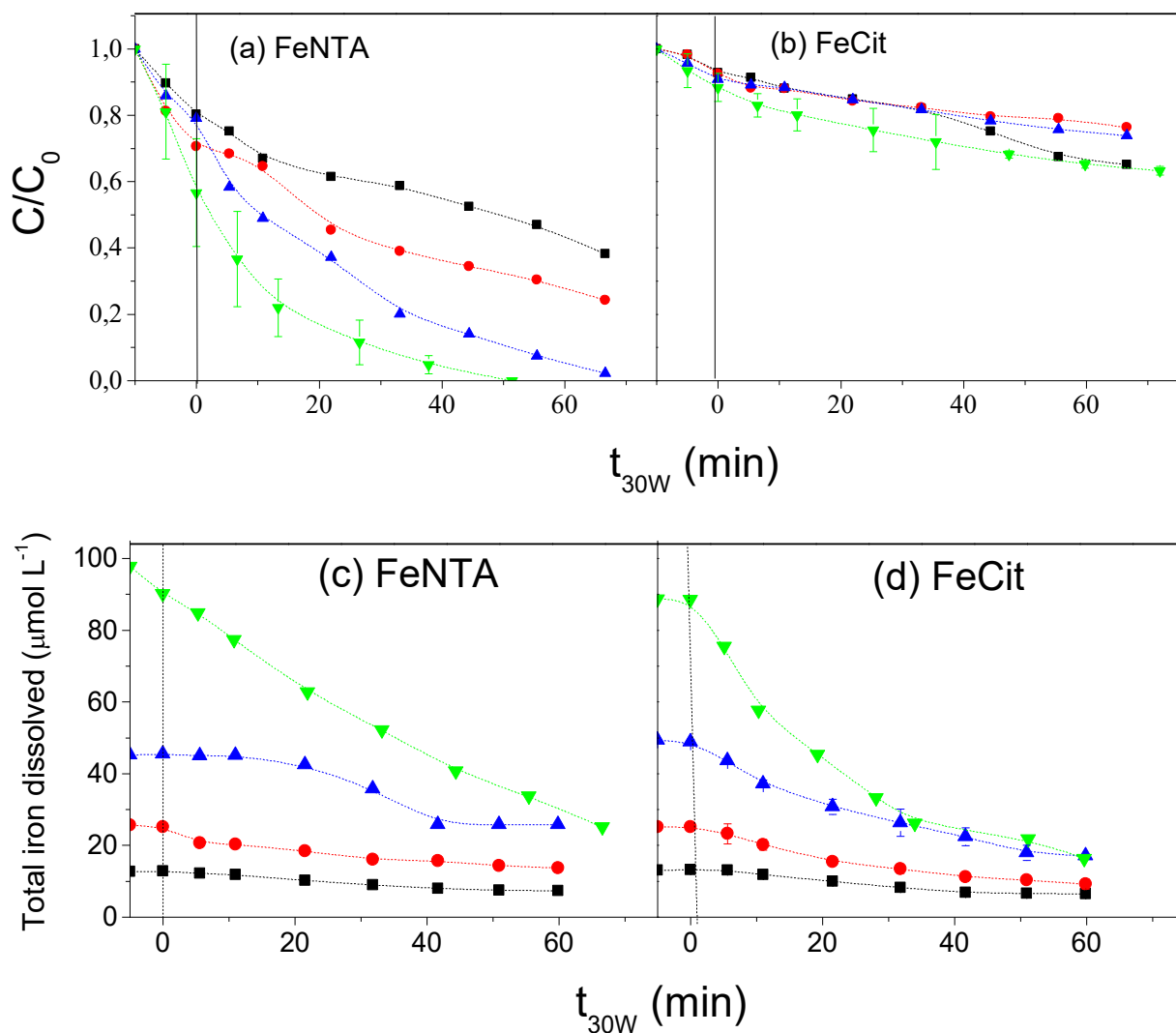
### 3.5.3 Influence of the source and concentration of the iron on the degradation of BP-3, FIP and PPB

The sources and concentration of iron constitute one of the operational parameters for photo-Fenton efficiency, since excessive doses of iron contribute to the elimination of HO<sup>•</sup> radicals (RAHIM POURAN; ABDUL AZIZ; WAN DAUD, 2015). On the other hand, the use of organic iron complexes in this process contributes to the increase of light absorption efficiency, since they extend the absorption band into the visible region (RAHIM POURAN; ABDUL AZIZ; WAN DAUD, 2015).

In this context, the influence of iron sources and concentration on the degradation of the target compounds was evaluated (Figure 3.3). The source and concentration of the iron complex strongly influenced the degradation of the mixture (Figure 3.3). An expressive improvement in degradation was observed by increasing the iron complex concentration from 12.5 to 100 μmol L<sup>-1</sup> for FeNTA (Figure 3.3a), due to the high concentration of soluble iron in the first 30 min in the presence of this ligand (Figure 3.3c), thus contributing to the enhanced Fenton reaction (Eq. 3.15 and 3.16).



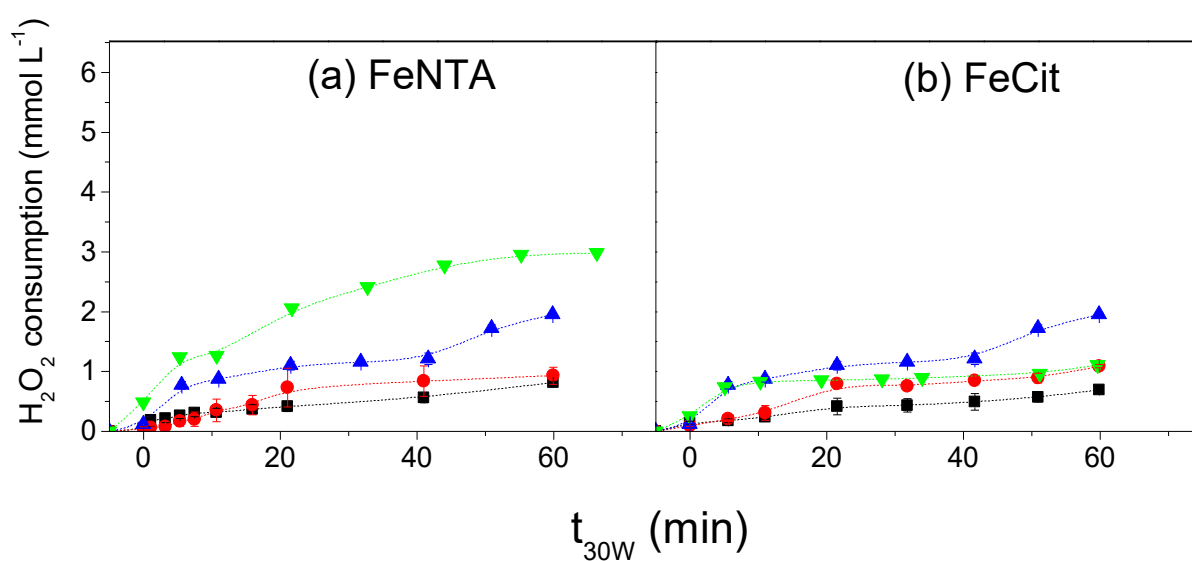
**Figure 3.3** – Influence of iron complex source and concentration (■ 12.5  $\mu\text{mol L}^{-1}$ , ● 25  $\mu\text{mol L}^{-1}$ , ▲ 50  $\mu\text{mol L}^{-1}$  and ▼ 100  $\mu\text{mol L}^{-1}$ ) on the degradation of the mixture of BP-3, FIP and PPB using the iron complexes (a) FeNTA and (b) FeCit and ((c) and (d)) on the concentration of total dissolved iron during the solar photo-Fenton. Initial conditions:  $[\text{CEC}] = 100 \mu\text{g L}^{-1}$  (for each compound),  $[\text{H}_2\text{O}_2] = 5.9 \text{ mmol L}^{-1}$ ,  $\text{Fe/L} = 1:1$ ;  $\text{pH} = 7.4$  (natural of the MWWTP effluent).



However, this behaviour was not observed for FeCit, as, the degradation efficiency was limited to 30% degradation for all iron concentrations (Figure 3.3b). This is justified by the presence of less photoactive iron species. At  $\text{pH} 7.4$  (natural of the WWTP matrix), the predominant iron species are  $\text{FeOHCit}^-$  (90%) and  $\text{Fe}_2(\text{OH})_2(\text{Cit})_2^{2-}$  (10%), which show lower photoreactivity compared to FeCit (CLARIZIA et al., 2017). These results are in agreement

with the similar  $\text{H}_2\text{O}_2$  consumption observed for the different FeCit concentrations (Figure 3.4b).

**Figure 3.4** – Influence of iron complex source and concentrations ( $\blacksquare$   $12.5 \mu\text{mol L}^{-1}$ ,  $\bullet$   $25 \mu\text{mol L}^{-1}$ ,  $\blacktriangle$   $50 \mu\text{mol L}^{-1}$  and  $\blacktriangledown$   $100 \mu\text{mol L}^{-1}$ ) on  $\text{H}_2\text{O}_2$  consumption during the degradation of BP-3, FIP and PPB by solar photo-Fenton using the iron complexes (a) FeNTA and (b) FeCit. Initial conditions:  $[\text{CEC}] = 100 \mu\text{g L}^{-1}$  (for each compound),  $[\text{H}_2\text{O}_2] = 5.9 \text{ mmol L}^{-1}$ ,  $\text{Fe:L} = 1:1$ ;  $\text{pH} = 7.4$  (natural of the MWWTP effluent).



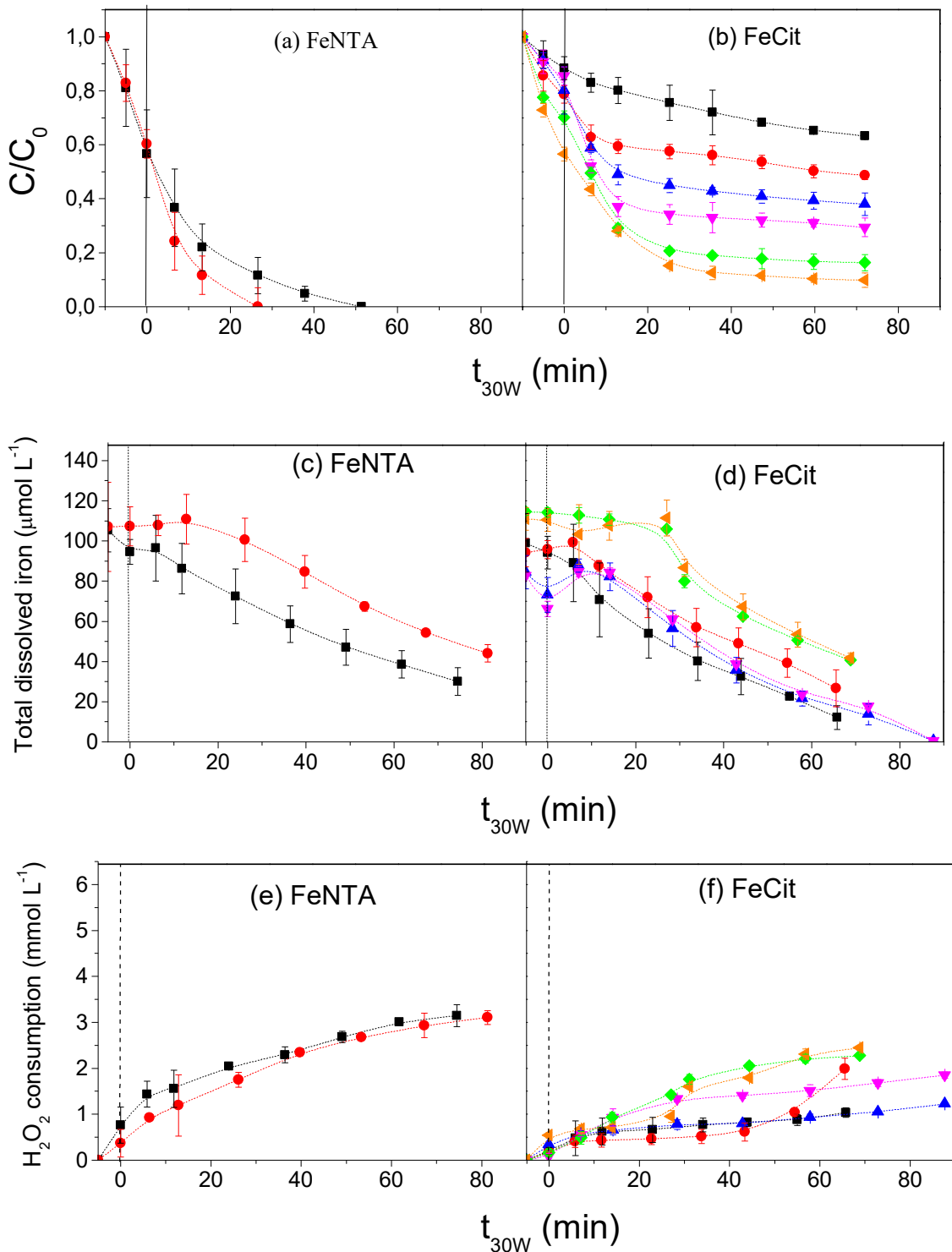
Moreover, the low efficiency of the process can be attributed to the low stability of the Fe(III)-Cit complex ( $\beta = 1.9 \times 10^{14}$ ) (ZHANG; ZHOU, 2019) and its lower molar absorptivity at wavelengths above 300 nm (solar spectrum region) (Figure 1.3) compared to Fe(III)-NTA ( $\beta = 7.9 \times 10^{15}$ ) (HOWSAWKENG et al., 2001). Therefore, the experiments were performed using the best iron concentration ( $100 \mu\text{mol L}^{-1}$ ) and in the presence of increased Fe/L molar ratio (Figure 3.5).

#### 3.5.4 Influence of Fe/L molar ratio on the degradation of BP-3, FIP and PPB

No improvement in the degradation of the target compounds was observed by increasing the Fe/L molar ratio from 1:1 to 1:2 for FeNTA (Figure 3.5a), as the molar ratio of 1:1 was sufficient to ensure high concentration of total dissolved iron (Figure 3.5c) during the Fenton reaction. Moreover, excess chelating ligands compete with micro-pollutants for HO•, thus decreasing the efficiency of the process (MEJRI et al., 2019). In contrast, the degradation efficiency increased from 37% to 84% by increasing the Fe/L molar ratio from 1:1 to 1:5 for FeCit (Figure 3.5b) since higher concentrations of the ligand increased the availability of total dissolved iron (Figure 3.5d) and consequently the consumption of H<sub>2</sub>O<sub>2</sub> (Figure 3.5f).

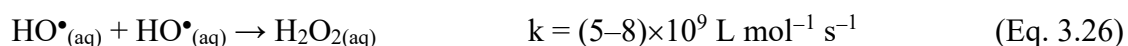
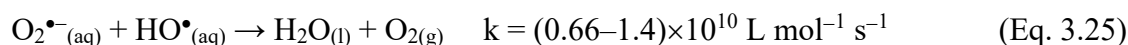
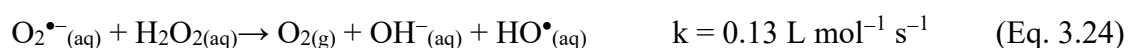
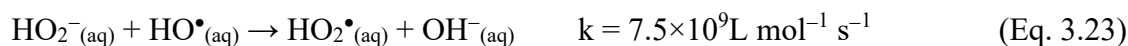
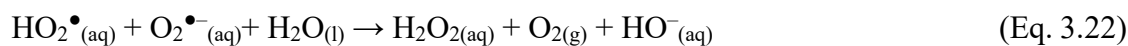
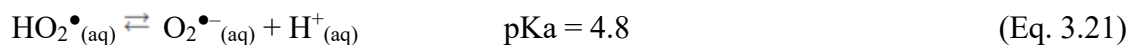
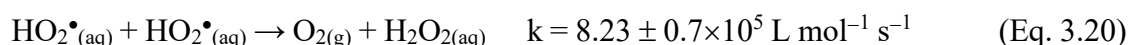
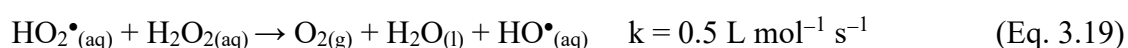
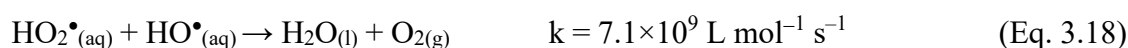
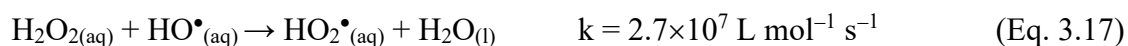
However, no increase was observed using higher molar ratios of FeCit (1:6) (Figure 3.5b) due to the elimination of HO• by excess chelating agents (MEJRI et al., 2019). Therefore, 100 µmol L<sup>-1</sup> of each iron complex and Fe/L molar ratios equivalent to 1:1 (FeNTA) and 1:5 (FeCit) were chosen as the best conditions for each ligand. These conditions were then used to evaluate the influence of H<sub>2</sub>O<sub>2</sub> concentration (ranged from 0.74 to 11.8 mmol L<sup>-1</sup> H<sub>2</sub>O<sub>2</sub>) on the removal of the target compounds (Figure 3.6).

**Figure 3.5** – Influence of Fe/L molar ratio (■ 1:1, ● 1:2, ▲ 1:3, ▼ 1:4, ◆ 1:5 and ◀ 1: 6) in the degradation of the mixture of BP-3, FIP and PPB using the iron complexes (a) FeNTA and (b) FeCit, ((c) and (d)) dissolved iron concentration, and ((e) and (f)) H<sub>2</sub>O<sub>2</sub> consumption during the solar photo-Fenton process. Initial conditions: [CEC]= 100 μg L<sup>-1</sup> (for each compound), [H<sub>2</sub>O<sub>2</sub>] = 5.9 mmol L<sup>-1</sup>, [Fe<sup>3+</sup>] = 100 μmol L<sup>-1</sup>; pH= 7.4 (natural of the MWWTP effluent).



### 3.5.5 Influence of $H_2O_2$ concentration on the degradation of BP-3, FIP and PPB

In the presence of FeNTA, increased concentrations of  $H_2O_2$  (0.74 to 11.8 mmol L<sup>-1</sup>) enhanced the degradation of the target compounds reaching the LOQ (< 4.2 µg L<sup>-1</sup> for FIP and BP-3 and < 1.3 µg L<sup>-1</sup> for PPB) after 51 and 70 min of reaction using 5.9 and 11.8 mmol L<sup>-1</sup>  $H_2O_2$ , respectively (Figure 3.6a). However,  $H_2O_2$  concentrations above 5.9 and up to 11.8 mmol L<sup>-1</sup> increased the treatment time required to reach the LOQ (< 4.2 µg L<sup>-1</sup> for FIP and BP-3 and < 1.3 µg L<sup>-1</sup> for PPB) (Figure 3.6a) by 37% due to inefficient parallel reactions between excess  $H_2O_2$  and  $HO^\bullet$  (Eq. 3.17) and other inefficient reactions driven by secondary radicals (Eq. 3.18-3.26), hindering the degradation of the target compounds (SILVA et al., 2021; TROVÓ et al., 2013).



Regarding FeCit, increasing the concentration of  $H_2O_2$  from 0.74 to 2.9 mmol L<sup>-1</sup> improved the degradation rates, reaching the LOQ (< 4.2 µg L<sup>-1</sup> for FIP and BP-3 and < 1.3 µg L<sup>-1</sup> for PPB) after 19 min of reaction (Figure 3.6b). On the other hand, a further increase in  $H_2O_2$  concentration from 2.9 to 5.9 and to 11.8 mmol L<sup>-1</sup> resulted in a decrease in degradation efficiency (Figure 3.6b) and, as reported for FeNTA, due to the occurrence of inefficient parallel reactions (Eqs. 3.18-3.27) (SILVA et al., 2021; TROVÓ et al., 2013). In addition, a lower concentration of  $H_2O_2$  was required for FeCit compared to FeNTA, since photolysis of the main predominant iron species ( $FeOHCit^-$ , 90%) at pH 7.4 (natural of the MWWTP matrix) produces  $H_2O_2$  (Eq. 3.20-3.22 and 3.27-3.28), thus requiring a lower concentration of this reagent (RUALES-LONFAT et al., 2016):

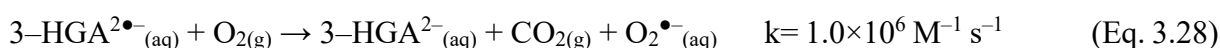
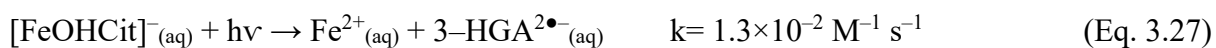
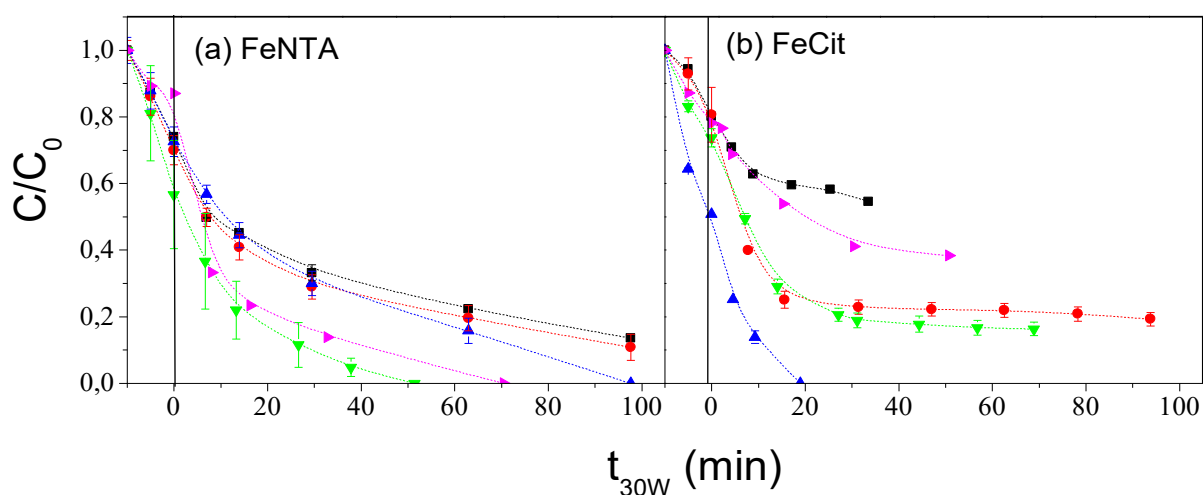
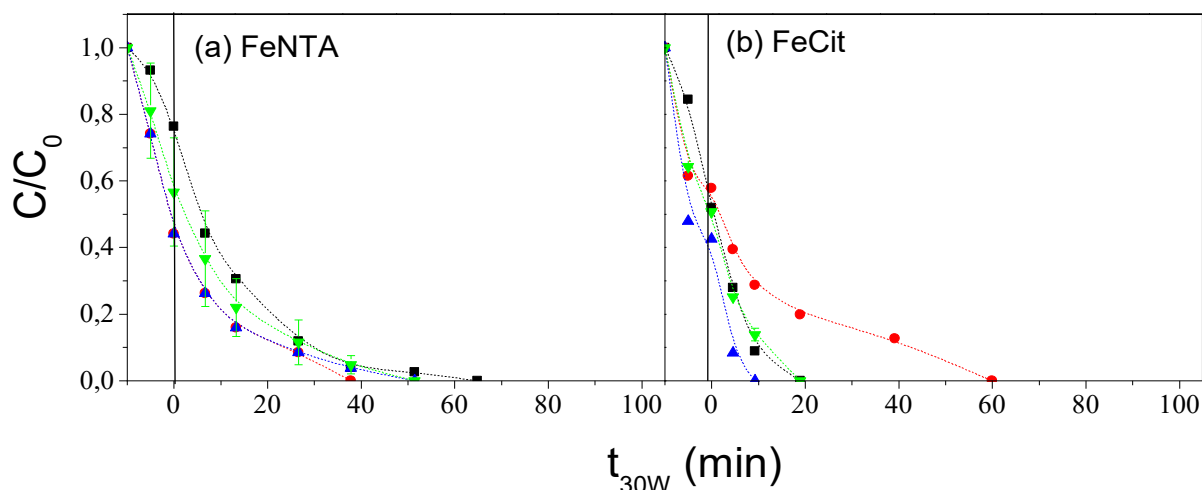


**Figure 3.6** – Influence of  $\text{H}_2\text{O}_2$  concentration (■ 0.74 mmol  $\text{L}^{-1}$ , ● 1.5 mmol  $\text{L}^{-1}$ , ▲ 2.9 mmol  $\text{L}^{-1}$ , ▼ 5.9 mmol  $\text{L}^{-1}$ , ► 11.8 mmol  $\text{L}^{-1}$ ) on the degradation of the mixture of BP-3, FIP and PPB using the iron complexes (a) FeNTA and (b) FeCit. Initial conditions:  $[\text{CEC}] = 100 \mu\text{g L}^{-1}$  (for each compound),  $\text{Fe:L} = 1:1$  (FeNTA) and  $1:5$  (FeCit),  $[\text{Fe}^{3+}] = 100 \mu\text{mol L}^{-1}$ ;  $\text{pH} = 7.4$  (natural of the MWWTP effluent).



Kinetically, the use of FeCit was apparently efficient when compared to FeNTA (19 min for FeCit and 51 min for FeNTA) (Figures 3.6 and 3.7). However, a synergism regarding the degradation efficiency of FIP in the mixture was observed using FeCit (Figure 3.7b), extending the treatment time from 19 to 60 min. Therefore, kinetic aspects alone are not sufficient to evaluate the efficiency of solar photo-Fenton in the treatment of real MWWTP effluents containing BP-3, FIP and PPB, because other variables (acute toxicity after treatment and reagent costs) are fundamental to define the best iron complex to be proposed for full-scale photo-Fenton application.

**Figure 3.7** – Degradation efficiencies per compound (■ PPB, ● FIP, ▲ BP-3, ▼ Mixture) obtained during the degradation of the mixture of BP-3, FIP and PPB using the iron complexes (a) FeNTA and (b) FeCit. Initial conditions: [CEC]= 100  $\mu\text{g L}^{-1}$  (for each compound), Fe:L= 1:1 (FeNTA) and 1:5 (FeCit),  $[\text{Fe}^{3+}] = 100 \mu\text{mol L}^{-1}$ ;  $[\text{H}_2\text{O}_2] = 5.9 \text{ mmol L}^{-1}$  (for FeNTA) and 2.9  $\text{mmol L}^{-1}$  (for FeCit); pH= 7.4 (natural of the MWWTP effluent).



### 3.5.6 Acute toxicity assays: *Drosophila melanogaster* lifespan

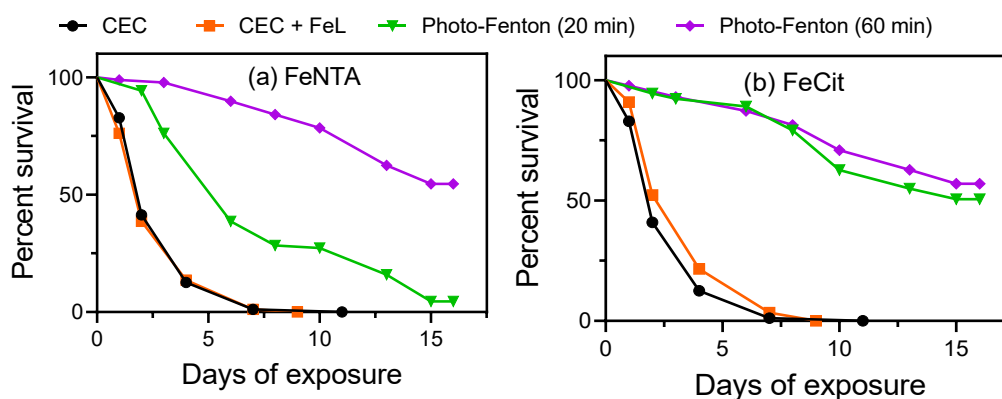
The MWWTP effluent containing the CEC was highly toxic to *D. melanogaster*, as almost all flies were dead after 7 days (Figure 3.8 and Figure 3.9a). This effect can be attributed to FIP, as no flies survived after 7 days of exposure to the MWWTP effluent enriched exclusively with FIP (Figure 3.9b). In contrast, exposure of test-organisms to MWWTP effluent enriched exclusively with BP-3 or PPB resulted in 70% and 64% survival, respectively, after 15 days of exposure (Figure 3.9b).

Samples collected after 20 min of photo-Fenton in the presence of the FeCit system showed a considerable percentage of survival of the flies (50%) after 15 days of exposure (Figure 3.8b). This result suggests that the by-products generated during this treatment were less toxic than the original compounds. Increasing the reaction time (60 min) showed no improvement in the survival percentage of the flies (56% survival after 15 days of exposure to FeCit) (Figure 3.8b). These results were expected, since no increase in the degradation efficiency of the target compounds was observed between 20 min ( $t_{30W} = 19$  min for FeCit) and 60 min ( $t_{30W} = 60$  min for FeCit) of treatment performed in the presence of FeCit (Figure 3.8b).

A different behaviour regarding toxicity was observed for samples obtained in the presence of FeNTA. The samples obtained after 20 min ( $t_{30W} = 13$  min) of solar photo-Fenton

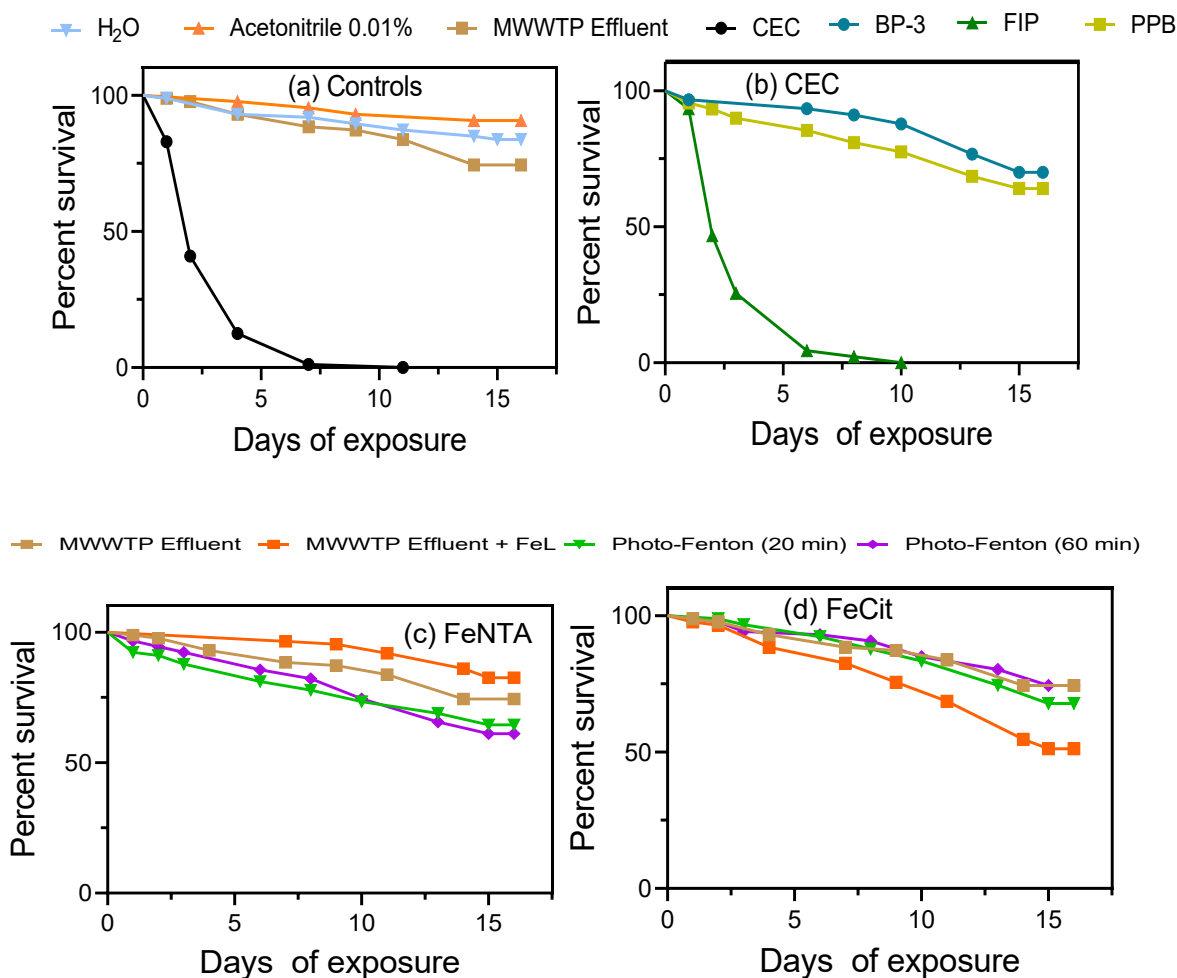
treatment reached 95% fly mortality (Figure 3.8a), which can also be attributed to the incomplete degradation (78%) of FIP ( $22.0 \mu\text{g L}^{-1}$  residual concentration) (Figure 3.7a). Samples obtained after 60 min ( $t_{30\text{W}} = 51$  min) reached the LOQ ( $< 4.2 \mu\text{g L}^{-1}$  for FIP and BP-3 and  $< 1.3 \mu\text{g L}^{-1}$  for PPB) (Figure 3.6a) and resulted in 54% fly survival after 15 days of exposure (Figure 3.8a).

**Figure 3.8** – *D. melanogaster* survival assay for MWWTP effluent samples enriched with the mixture of BP-3, FIP and PPB before and after solar/photo-Fenton treatment using different iron complexes: (a) FeNTA and (b) FeCit. Initial conditions: [CEC]=  $100 \mu\text{g L}^{-1}$  (for each compound), Fe/L= 1:1 (FeNTA) and 1:5 (FeCit),  $[\text{Fe}^{3+}] = 100 \mu\text{mol L}^{-1}$ ;  $[\text{H}_2\text{O}_2] = 5.9 \text{ mmol L}^{-1}$  (for FeNTA) and  $2.9 \text{ mmol L}^{-1}$  (for FeCit).



Exposure of flies to controls containing  $\text{H}_2\text{O}$  and MWWTP effluent without the CEC showed 90% and 80% survival of flies after 15 days of exposure (Figure 3.9a). In addition, control experiments performed to assess the degradation of the effluent in the absence of CEC using each of the iron complexes (Figure 3.9c-d) resulted in 70%-80% fly survival after 15 days, indicating that non-toxic transformation products were generated from MWWTP effluent and iron complexes. These results suggest that the residual concentration of FIP ( $< 4.2 \mu\text{g L}^{-1}$ ) implied toxicity to the test- organisms even after LOQ was reached ( $< 4.2 \mu\text{g L}^{-1}$  for FIP and BP-3 and  $< 1.3 \mu\text{g L}^{-1}$  for PPB), resulting in almost 50% fly survival after 15 days.

**Figure 3.9** – Results obtained during *D. melanogaster* survival assay for (a) control experiments; (b) individual solutions of the target compounds and ((c) and (d)) samples of MWWTP effluent in the absence of BP3, FIP and PPB but in the presence of iron complexes before and after solar photo-Fenton treatment. Initial conditions: [CEC] = 100  $\mu\text{g L}^{-1}$  (for each compound), Fe/L= 1:1 (FeNTA) and 1:5 (FeCit),  $[\text{Fe}^{3+}] = 100 \mu\text{mol L}^{-1}$ ;  $[\text{H}_2\text{O}_2] = 2.94 \text{ mmol L}^{-1}$  (for FeCit,  $\text{Fe}^{3+}$ ,  $\text{H}_2\text{O}_2$  (in the dark) and  $\text{H}_2\text{O}_2/\text{solar}$ ) and 5.9  $\text{mmol L}^{-1}$  (for FeNTA), pH = 7.4 (natural of the MWWTP effluent).



### 3.5.7 Cost assessment

Ligand and oxidant costs were calculated for the treatment of 1 m<sup>3</sup> of MWWTP effluent and the values were obtained considering the concentrations of the best performing reagents and at their commercial price, respectively (Table 3.3). One of the advantages of the solar photo-Fenton process is the use of sunlight as a source of radiation, which is economically attractive, since the costs with artificial radiation are dispensed (SILVA et al., 2021). In this work, electrical costs were not considered in the calculations and all ligands were quoted at Sigma-Aldrich. Even so, the prices for other companies may be different from those presented in this work.

**Table 3.3** – Reagents prices (iron, chelating agents and oxidant) for the photo-Fenton process, as according to Sigma-Aldrich®.

Reagent	Price (US\$ kg <sup>-1</sup> )
Fe(NO <sub>3</sub> ) <sub>3</sub> ·9H <sub>2</sub> O	137
Cit	86
NTA	173
H <sub>2</sub> O <sub>2</sub>	14

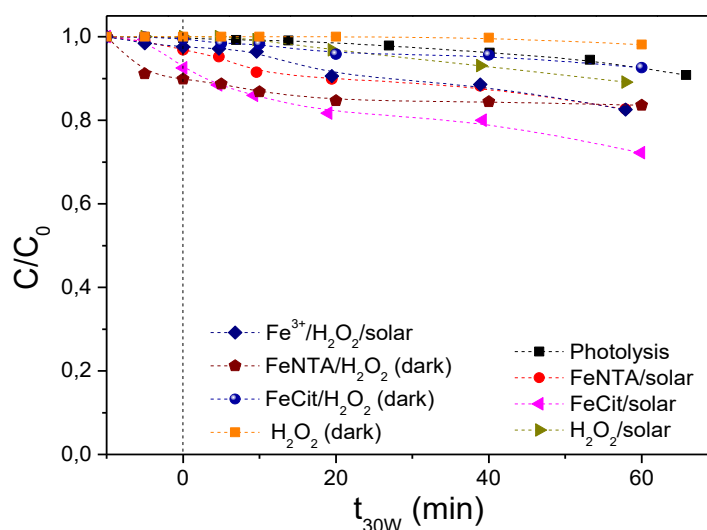
Considering that this is a comparative study, the prices revealed in Table 3.3 are estimates and presented in relative form by comparison with the lowest price (price equal to 1.0). The costs associated with iron concentration were the same for all iron complexes (Table 3.3), because the best iron concentration was the same for all complexes tested (100 μmol L<sup>-1</sup>). Although citrate is the cheapest complex (US\$ 86 kg<sup>-1</sup>) (Table 3.3), the costs with this ligand were the highest, as a higher Fe:Cit molar ratio (1:5) is required to achieve LOQ. Thus, the costs associated with the processes evaluated in this study follow the increasing order: FeNTA < FeCit. The kinetic constants obtained for photo-Fenton (k) were calculated considering a pseudo - first order model for the target compounds. High values of coefficient of determination (R<sup>2</sup>) were obtained, indicating that all ligands follow the pseudo - first order model (Table 3.4).

**Table 3.4** – Pseudo-first kinetic constants and cost assessment for solar photo-Fenton using different iron complexes.

Parameter	FeCit	FeNTA
k (min <sup>-1</sup> )	0.10	0.063
R <sup>2</sup>	0.96	0.99
t <sub>1/2</sub> (min)	6.6	11
Cost <sub>Iron</sub> (US\$ m <sup>-3</sup> )	5.6	5.6
Cost <sub>Ligand</sub> (US\$ m <sup>-3</sup> )	13	4.5
Cost <sub>Oxidant</sub> (US\$ m <sup>-3</sup> )	1.4	2.8
Cost <sub>Total</sub> (US\$ m <sup>-3</sup> )	20	13

The kinetic constants also indicate the increasing order: FeNTA < FeCit. In other words, FeCit presented the fastest degradation rate and shorter half-life (t<sub>1/2</sub>) when compared to FeNTA. Moreover, the addition of ligands to the effluent adds total organic carbon (TOC) to the MWWTP matrix which is equivalent to 36 mg L<sup>-1</sup> for FeCit and 7 mg L<sup>-1</sup> for FeNTA. As the original TOC of the effluent is 38 mg L<sup>-1</sup> (Table 3.1), Cit represents a TOC increase of 95%, while NTA contributes in the order of 7%, respectively. Although the TOC of the effluent increases, the use of these ligands allows conducting the treatment at almost neutral pH, which is a disadvantage of the conventional photo-Fenton, and improves the degradation of CEC (the treatment in the absence of complexes reached only 17% degradation efficiency) (Figure 3.10). However, the choice of the best ligand should also consider kinetic constant, added TOC content and lower costs. Thus, although FeCit showed the highest kinetic constant, higher Fe/L molar ratio (1:5) associated with this ligand implied higher TOC increase and costs associated with the ligand.

**Figure 3.10** – Control experiments for the degradation of BP-3, FIP and PPB using the iron complexes FeNTA and FeCit. Initial conditions: [CEC]= 100  $\mu\text{g L}^{-1}$  (for each compound), Fe:L= 1:1 (FeNTA) and 1:5 (FeCit),  $[\text{Fe}^{3+}]$ = 100  $\mu\text{mol L}^{-1}$ ;  $[\text{H}_2\text{O}_2]$ = 2.94  $\text{mmol L}^{-1}$  (for FeCit,  $\text{Fe}^{3+}$ ,  $\text{H}_2\text{O}_2$  (in the dark) and  $\text{H}_2\text{O}_2/\text{solar}$ ) and 5.9  $\text{mmol L}^{-1}$  (for FeNTA), pH= 7.4 (natural of the MWWTP effluent).



Thus, considering the kinetic parameters, TOC increase, total process costs and toxicity to *D. melanogaster*, FeNTA presented the most cost-effective alternative for the treatment of CEC in MWWTP effluent at pH close to neutral using solar photo-Fenton. However, it is worth noting that this work was carried out in laboratory scale experiments and for an industrial scale application, the costs change completely using commercial reagents. Thus, an analysis on a larger scale is also necessary to confirm these results and verify the economic feasibility of the application of these processes. Soriano-Molina et al. (2021) investigated the removal of sulfamethoxazole in real MWWTP effluents using FeNTA and FeEDDS for the continuous flow solar photo-Fenton and also concluded that FeNTA was the most economical ligand to use in solar photo-Fenton, even when compared to classical photo-Fenton, because it presented higher costs associated with the iron source ( $\text{FeSO}_4 \cdot 7\text{H}_2\text{O}$ ) and acidification (6% of the total treatment cost), resulting in lower efficiency associated with higher costs (30% more expensive) when compared to FeNTA.

### 3.6 Conclusions

The efficiency of solar photo-Fenton using two iron ligands was assessed for simultaneous degradation of benzophenone-3, fipronil and propylparaben at MWWTP effluent. Treatment systems were compared in terms of kinetics, toxicity and costs. Although, both iron complexes were efficient for the degradation of benzofenone-3, fipronil and propylparaben, best operational conditions for each system were different. In the presence of  $100 \mu\text{mol L}^{-1}$  of ferric ions, best Fe/L molar ratio and oxidant concentrations were 1:1 and  $5.9 \text{ mmol L}^{-1} \text{ H}_2\text{O}_2$  for FeNTA; 1:5 and  $2.9 \text{ mmol L}^{-1} \text{ H}_2\text{O}_2$  FeCit. These results reveal the need to optimize treatment conditions for each system, since distinct iron complexes species associated to different photo-activity and stability are present in each system and impact the degradation efficiency. Besides, the acute toxicity to Canton S. strain flies *D. melanogaster* reduced significantly after treatment for all iron complexes evaluated, which indicates the formation of low toxic transformations products in the process. Considering results obtained for simultaneous degradation of benzofenone-3, fipronil and propylparaben at MWWTP effluent, toxicity and costs, FeNTA is presented as the best option for the application of solar photo-Fenton at near-neutral pH.



### 3.7 Attachment

Results delineated here in Chapter 3 were published in *Molecules* (MDPI) (see print).



Article

## Effect of Iron Complex Source on MWWTP Effluent Treatment by Solar Photo-Fenton: Micropollutant Degradation, Toxicity Removal and Operating Costs

Eduardo O. Marson <sup>1</sup>, Ivo A. Ricardo <sup>1,2</sup>, Cleiseano E. S. Paniagua <sup>1</sup>, Serena M. Malta <sup>3</sup> , Carlos Ueira-Vieira <sup>3</sup>, Maria Clara V. M. Starling <sup>4</sup>, José Antonio Sánchez Pérez <sup>5</sup>  and Alam G. Trovó <sup>1,5,\*</sup>

<sup>1</sup> Instituto de Química, Universidade Federal de Uberlândia, Uberlândia 38400-902, Brazil

<sup>2</sup> Faculdade de Ciências Naturais e Exatas, Universidade Save, Chongoene 0301-01, Mozambique

<sup>3</sup> Instituto de Biotecnologia, Universidade Federal de Uberlândia, Uberlândia 38405-319, Brazil

<sup>4</sup> Departamento de Engenharia Sanitária e Ambiental, Universidade Federal de Minas Gerais, Belo Horizonte 31270-010, Brazil

<sup>5</sup> Solar Energy Research Centre (CIESOL), University of Almería, Ctra. de Sacramento s/n, ES04120 Almería, Spain

\* Correspondence: alamtrovo@ufu.br; Tel.: +55-34-3291-6380

## 4 CHAPTER IV – PERSULFATE AND MONOPERSULFATE IONS AS PEROXIDE SOURCES IN SOLAR PHOTO-FENTON MODIFIED WITH ORGANIC IRON COMPLEXES FOR THE DEGRADATION OF MICRO-CONTAMINANTS IN A TERTIARY EFFLUENT FROM A MUNICIPAL WASTEWATER TREATMENT PLANT

### 4.1 Introduction

Municipal wastewater treatment plants (MWWTP) are considered the main entrance of pharmaceuticals and personal care products, pesticides, drugs among others organic compounds in environmental water matrices, since they are not designed for removal or degrading this type of micropollutants. Even present in concentrations levels from ng to  $\mu\text{g L}^{-1}$ , these compounds may contribute to the development of endocrine disrupting effects in some target-organisms (MARSON et al., 2022a; RICARDO et al., 2022). So, new technologies must be evaluated as alternatives of complementary treatment in MMWTP aiming the degradation of these micropollutants.

In a previous work of our group, the modified photo-Fenton process using different organic ligands (i.e. nitriloacetic acid (NTA), ethylene diaminetetraacetic acid (EDTA), ethylenediamine-N,N'-disuccinic (EDDS) and citrate (Cit)) was evaluated to apply the photo-Fenton treatment at neutral pH as an alternative of tertiary treatment of MWWTP effluents using hydrogen peroxide ( $\text{H}_2\text{O}_2$ ). The iron complex FeNTA presented as the best option for micro-pollutants degradation, toxicity and costs (MARSON et al., 2022b). However, more studies with FeNTA and FeCit are needed involving the use of other oxidants, i.e., persulfate ion ( $\text{S}_2\text{O}_8^{2-}$ , source of sulphate radicals  $\text{SO}_4^{\bullet-}$ ) and peroxymonosulphate ion ( $\text{HSO}_5^-$ , source of  $\text{HO}^{\bullet}$  and  $\text{SO}_4^{\bullet-}$ ), to verify how the peroxide source affects the degradation of the micropollutants and to understand better the effects of the matrix composition using three different peroxide sources ( $\text{H}_2\text{O}_2$ ,  $\text{S}_2\text{O}_8^{2-}$  and  $\text{HSO}_5^-$ ), since  $\text{HO}^{\bullet}$  and  $\text{SO}_4^{\bullet-}$  are considered non- and selective radicals, respectively (NOGUEIRA et al., 2007).

The degradation of organic compounds by  $\text{HO}^{\bullet}$  involve three main mechanisms: electrophilic addition, electron transfer or hydrogen abstraction (NOGUEIRA et al., 2007), while  $\text{SO}_4^{\bullet-}$  preferably reacts via electron transfer mechanisms with organic compounds that have electron rich active sites, being a more selective oxidant (GHANBARI; MORADI, 2017; WACŁAWEK et al., 2017). For, example, best degradation results of the herbicide tebuthiuron

in MWWTP effluent occurred in the presence of  $S_2O_8^{2-}$  compared to  $H_2O_2$  (GONÇALVES et al., 2023) justified by the presence of electron-donating groups (two amino groups and one aromatic ring containing N and S atoms) in the structure of the target herbicide. Similar behavior was obtained in other studies involving these same peroxide sources during the degradation of sulfamethoxazole (YANG et al., 2017), diclofenac, venlafaxine and metoprolol (NIHEMAITI et al., 2018) and naproxen (SILVA et al., 2021). In addition, it has been highlighted that  $SO_4^{\bullet-}$  reacts with inorganic and organic components of the matrix with one order lower when compared to those with  $HO^{\bullet}$ , being an advantage (GHANBARI; MORADI, 2017; WACŁAWEK et al., 2017; WACŁAWEK; GRÜBEL; ČERNÍK, 2015). However, more studies must be done using other types of organic compounds, mainly them that present low affinity in react by electron transfer to understanding better the different mechanisms of degradation by different peroxide sources and as the matrix composition affects the degradation and operational conditions.

Hence, for this first time, this study aimed to compare the mixture degradation of the personal care products (benzophenone-3 (BP-3) and propylparaben (PPB)) and the insecticide fipronil (FIP), at an initial concentration of  $100 \mu\text{g L}^{-1}$  for each of them. These compounds were selected based in previous published work of our group (MARSON et al., 2022b).

## 4.2 Experimental

### 4.2.1 Reagents

All chemical solutions were prepared in ultrapure water ( $18.2 \text{ M}\Omega \text{ cm}$ ) produced by a Milli-Q water purification system. FIP (98.77 wt%) was acquired from Sinochem Ningbo (Lian Yun Gang City, Jiangsu Province, China). Naproxen (NAP) ( $C_{14}H_{13}NaO_3$ , 99.0 wt%), PPB ( $C_{10}H_{12}O_3$ , 99 wt%), BP-3 ( $C_{14}H_{12}O_3$ , 98 wt%), NTA ( $C_6H_6NNa_3O_6$ ), barium nitrate ( $Ba(NO_3)_2$ , 99.0 wt%) and potassium peroxymonosulphate (oxone®) ( $HKO_5S.0.5HKO_4S.0.5K_2O_4S$ ) were purchased from Sigma-Aldrich (São Paulo, Brazil). Ferric nitrate nonahydrate ( $Fe(NO_3)_3.9H_2O$ ), ferrous sulfate heptahydrate ( $FeSO_4.7H_2O$ ), sodium citrate dihydrate ( $Na_3C_6H_5O_7.2H_2O$ ), silver nitrate ( $AgNO_3$ , 99,8 wt%), mercury sulphate ( $HgSO_4$ , 99.0 wt%), silver sulphate ( $Ag_2SO_4$ , 99.0 wt%), sodium sulfite ( $Na_2SO_3$ ), 1.10-phenanthroline ( $C_{12}H_8N_2.H_2O$ ) and sodium hydroxide (NaOH) were provided by Synth (Diadema, Brazil). Hydroxylamine hydrochloride ( $NH_2OH.HCl$ ) was obtained from Êxodo

(Sumaré, Brazil), Methanol (CH<sub>3</sub>OH) and acetonitrile (CH<sub>3</sub>CN), both HPLC-grade, were obtained from J. T. Baker (Aparecida de Goiânia, Brazil), acetic acid (CH<sub>3</sub>COOH) from Panreac (Barcelona, Spain). Anhydrous sodium acetate (CH<sub>3</sub>COONa), sodium bicarbonate (NaHCO<sub>3</sub>) and sulfuric acid (H<sub>2</sub>SO<sub>4</sub>) were furnished by Dinâmica (Indaiatuba, Brazil). Sodium thiosulphate pentahydrate (Na<sub>2</sub>S<sub>2</sub>O<sub>3</sub>·5H<sub>2</sub>O, 99.5 wt%) was obtained from Carlo Erba, potassium dichromate (K<sub>2</sub>Cr<sub>2</sub>O<sub>7</sub>, 99 wt%) from Vetec and sodium persulfate (Na<sub>2</sub>S<sub>2</sub>O<sub>8</sub>) and potassium iodide (KI) were both purchased from Neon Comercial Ltda.

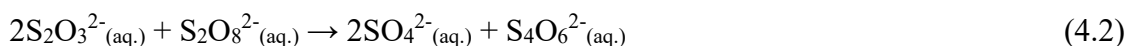
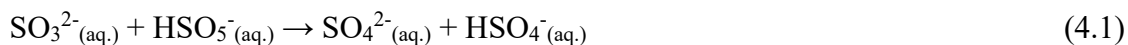
#### 4.2.2 MWWTP effluent

The MWWTP effluent samples used in this work were the same as those used in our previous work (MARSON et al., 2022b) and/or section 3.2.2. However, it is worth noting that currently, the Uberabinha Sewage Treatment Plant (the supplier of the effluent samples) has a maximum treatment capacity of 2.2 m<sup>3</sup> s<sup>-1</sup> of sewage and receives to treat on average 1.5 m<sup>3</sup> s<sup>-1</sup> of raw sewage, which corresponds to 95% of the sewage collected in Uberlândia, a city with more than 670.000 inhabitants (AMILDON RICARDO et al., 2018b). Thus, the municipality of Uberlândia continues to be a reference in basic sanitation with outstanding indicators on a national level, being the second best in water and sewage treatment in the country, remaining first in the state of Minas Gerais for more than 10 consecutive years. Furthermore, the collection was carried out in the flotation channel after preliminary (grading, sieving and desanding), anaerobic (biological treatment) and tertiary (coagulation-flocculation (ferric chloride (FeCl<sub>3</sub>)) and flotation) treatment stages, due to the fact that the technology evaluated in this work could be a good complementary treatment alternative to improve effluent quality in terms of degradation of contaminants of emerging concern and disinfection.

### 4.3 Photodegradation experiments

All photodegradation experiments were performed as described by Marson et al. (2022b) (subsection 3.3 of this manuscript). For the chromatographic analyses, the samples were previously filtered on 0.45 µm pore size membranes (PTFE/L) and an excess of sodium sulfite (Na<sub>2</sub>SO<sub>3</sub>) or sodium thiosulfate (Na<sub>2</sub>S<sub>2</sub>O<sub>3</sub>) was added to the samples, which act as reducing agents for HSO<sub>5</sub><sup>-</sup> (Equations 4.1) and S<sub>2</sub>O<sub>8</sub><sup>2-</sup> (Equations 4.2) in solution respectively, preventing the formation of reactive radicals, thus ceasing the degradation of the target compounds. It is worth noting that before the PTFE/L filters, nylon membrane filters were

initially tested, which did not provide adequate results due to adsorption of the target compounds on the membrane surface.



Under the same optimal conditions of ferric ion concentration ( $100 \mu\text{mol L}^{-1}$ ) and Fe:L molar ratios (1:1 for FeNTA and 1:5 for FeCit) established for  $\text{H}_2\text{O}_2$  (MARSON et al., 2022b), three sets of experiments were performed to determine the best initial concentrations of the oxidants ( $\text{S}_2\text{O}_8^{2-}$  and  $\text{HSO}_5^{-}$ ) aiming to facilitate the comparison of the results obtained for all peroxide sources ( $\text{H}_2\text{O}_2$ ,  $\text{S}_2\text{O}_8^{2-}$  and  $\text{HSO}_5^{-}$ ): effect of initial *i*)  $\text{S}_2\text{O}_8^{2-}$  and *ii*)  $\text{HSO}_5^{-}$  concentrations at initial pH 7.4 (natural pH of the MWWTP matrix) and *iii*) pH (2.5, 4.0, 5.5 and 7.4) effect in the presence of  $2.98 \text{ mmol L}^{-1}$  of  $\text{S}_2\text{O}_8^{2-}$ . To compare the efficiency of the different peroxide sources, the last three highest concentrations initially evaluated for  $\text{H}_2\text{O}_2$  ( $1.5$ ,  $2.9$  and  $5.9 \text{ mmol L}^{-1}$ ) were also evaluated equimolarly for  $\text{S}_2\text{O}_8^{2-}$  and  $\text{HSO}_5^{-}$ . Subsequently, two sets of experiments were performed in the presence of  $5.9 \text{ mmol L}^{-1}$  of  $\text{S}_2\text{O}_8^{2-}$  under optimized FeNTA conditions ( $[\text{Fe}^{3+}] = 100 \mu\text{mol L}^{-1}$ ; Fe:NTA molar ratio = 1:1) (best iron complex in the presence of  $\text{H}_2\text{O}_2$  (MARSON et al., 2022b)) in order to evaluate the operational parameters (inorganic ions) of the process involving  $\text{S}_2\text{O}_8^{2-}$  and identify the main mechanisms of the reactions involved in each process: *i*) influence of inorganic ions (bicarbonate ( $\text{HCO}_3^{-}$ ), chloride ( $\text{Cl}^{-}$ ) and sulfate ( $\text{SO}_4^{2-}$ )) on the degradation efficiency of the mixture of the target compounds; and *ii*) comparison of the degradation efficiency of the target compounds with NAP ( $100 \mu\text{mol L}^{-1}$ ) (which reacts preferentially by electron transfer (SILVA et al., 2021)) at natural pH of the MWWTP matrix. The choice of FeNTA ( $\beta = 7.9 \times 10^{15}$  (HOWSAWKENG et al., 2001)) to evaluate the effect of inorganic ions and the molecular structure of BP-3, FIP and PPB on the degradation efficiency using  $\text{S}_2\text{O}_8^{2-}$  is due to its higher stability compared to FeCit ( $\beta = 1.9 \times 10^{14}$  (ZHANG; ZHOU, 2019)). In addition, Fe(III)-NTA has a different photolysis mechanism than FeCit complex, i.e. it does not form  $\text{HO}^{\bullet}$  that also oxidize the target compounds.

The removal of  $\text{HCO}_3^{-}$  was carried out by adjusting the pH of the effluent using nitric acid ( $\text{HNO}_3$ ), since the pH reduction guarantees the removal of  $\text{HCO}_3^{-}$  and  $\text{CO}_3^{-}$  through the generation of  $\text{CO}_2$  (AMILDON RICARDO et al., 2018b). To better compare the results and avoid the influence of pH on the evaluated process, the acid pH (2.5) of the effluent resulting

from the adjustment was subsequently readjusted to a pH close to the natural pH of the effluent (7.4) after 40 min of stirring, adding sodium hydroxide (NaOH). The removal of  $\text{HCO}_3^-$  was certified through analysis of inorganic carbon (bicarbonates and carbonates) of the sample, carried out in a carbon analyzer available at the Chemical Engineering Faculty of the Universidade Federal de Uberlândia. Excess silver nitrate ( $\text{AgNO}_3$ ) and barium nitrate ( $\text{Ba}(\text{NO}_3)_2$ ) were respectively used for the precipitation of  $\text{Cl}^-$  and  $\text{SO}_4^{2-}$ . The use of excess of these salts aimed to avoid the interference of the matrix components. The combined removal of anions was done by first removing the  $\text{HCO}_3^-$  ions and then adjusting the pH to a value close to the natural value of the effluent and subsequent addition of  $\text{AgNO}_3$  for precipitation of  $\text{Cl}^-$ . Then, the solution was left to stand to ensure complete precipitation and decanting to the bottom of the beaker. Finally,  $\text{Ba}(\text{NO}_3)_2$  was used to remove  $\text{SO}_4^{2-}$  and, after decantation of the precipitate formed for both salts, the supernatant was separated to perform the photodegradation experiments and characterization of the matrix.

#### 4.4 Chemical analysis

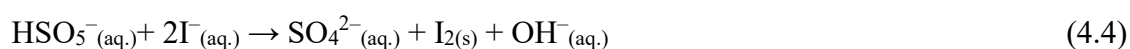
The efficiency of the degradation processes of the target compounds was determined and evaluated through the following chemical analyses: concentration of the target compounds, total iron dissolved and consumption of the oxidants ( $\text{S}_2\text{O}_8^{2-}$  and  $\text{HSO}_5^-$ ). Concentrations of target compounds and total dissolved iron were determined as described in sections 3 of this manuscript. An isocratic mixture of methanol/HAc (0.01 % v/v) was also used for chromatographic determinations of NAP at 230 nm, however, in the ratio 65:35 (% v/v). The average degradation of the mixture ( $C/C_0$ ) was also assessed as described in section 3 (equation 3.10).

##### 4.4.1 Persulfate and monopersulfate ions

$\text{S}_2\text{O}_8^{2-}$  was quantified spectrophotometrically, using a solution with potassium iodide (KI). In the presence of excess iodide,  $\text{S}_2\text{O}_8^{2-}$  is reduced to sulfate ions while iodide is converted to iodine, generating a yellow colored solution ( $\text{I}_2$ ) (equation 4.3). The  $\text{S}_2\text{O}_8^{2-}$  concentration is proportional to the iodine concentration which can be determined by spectrophotometry, monitoring the absorbance at 400 nm and converting the analytical signal into concentration using an analytical curve.



$\text{HSO}_5^-$  was determined by the spectrophotometric method that allows determining the active part of Oxone without performing iodometric titration (WACŁAWEK; GRÜBEL; ČERNÍK, 2015). When  $\text{HSO}_5^-$  is added to an iodide solution, it is possible to observe a yellow color resulting from the transformation of iodide into iodine (Equation 4.4), forming a complex with maximum absorption at 400 nm. The intensity of the color is pH independent in the range of 2.5 to 10.0.



The oxidation of KI by air can be avoided by adding sodium bicarbonate ( $\text{NaHCO}_3$ ) to the solution (LIANG et al., 2008). For determination of  $\text{S}_2\text{O}_8^{2-}$  and  $\text{HSO}_5^-$  concentrations, 3000  $\mu\text{L}$  of the KI solution containing  $\text{NaHCO}_3$  and 2000  $\mu\text{L}$  of the sample containing  $\text{S}_2\text{O}_8^{2-}$  and/or  $\text{HSO}_5^-$  were added and spectrophotometric readings of the samples were performed after 15 min of the reactions of equations 4.3 and 4.4.

## 4.5 Results and discussion

### 4.5.1 Analytical method by HPLC - DAD for determination of BP-3, FIP, PPB and NAP

The analytical method for the determination of target compounds (BP-3, FIP, PPB) was described in subsection 3 and the results were presented in subsection 3.5.1 of this manuscript. As described, the chromatographic conditions of FIP, BP-3 and PPB were tested using, respectively, the wavelengths of 279 nm, 289 nm and 256 nm and as mobile phase an isocratic mixture of methanol/HAc (0.01 % v/v) in the proportion 75:25 (% v/v). This isocratic mixture, but in the ratio 65:35 (% v/v), was also used for chromatographic determinations of NAP at 230 nm (SILVA et al., 2021)). Table 4.1 shows the proportions tested between the mobile phases, as well as the dead volume and retention time of the NAP.

**Table 4.1** – Influence of the ratio between the mobile phases (methanol and HAc) on the retention time of NAP and dead volume, in tertiary sanitary effluent.

Compound	MeOH:HAc (% v/v)	Dead volume (min)	Retention time (min)
NAP	65:35	3,5	10.6 ± 0.0

The linear equation of the analytical curve of NAP, as well as the figures of merit, correlation coefficient ( $R^2$ ) and the linear working range are presented in Table 4.2.

**Table 4.2** – Straight line equations of the analytical curves, linear ranges, linear correlation coefficient ( $R^2$ ), limit of detection (LOD) and limit of quantification (LOQ) for the target compounds.

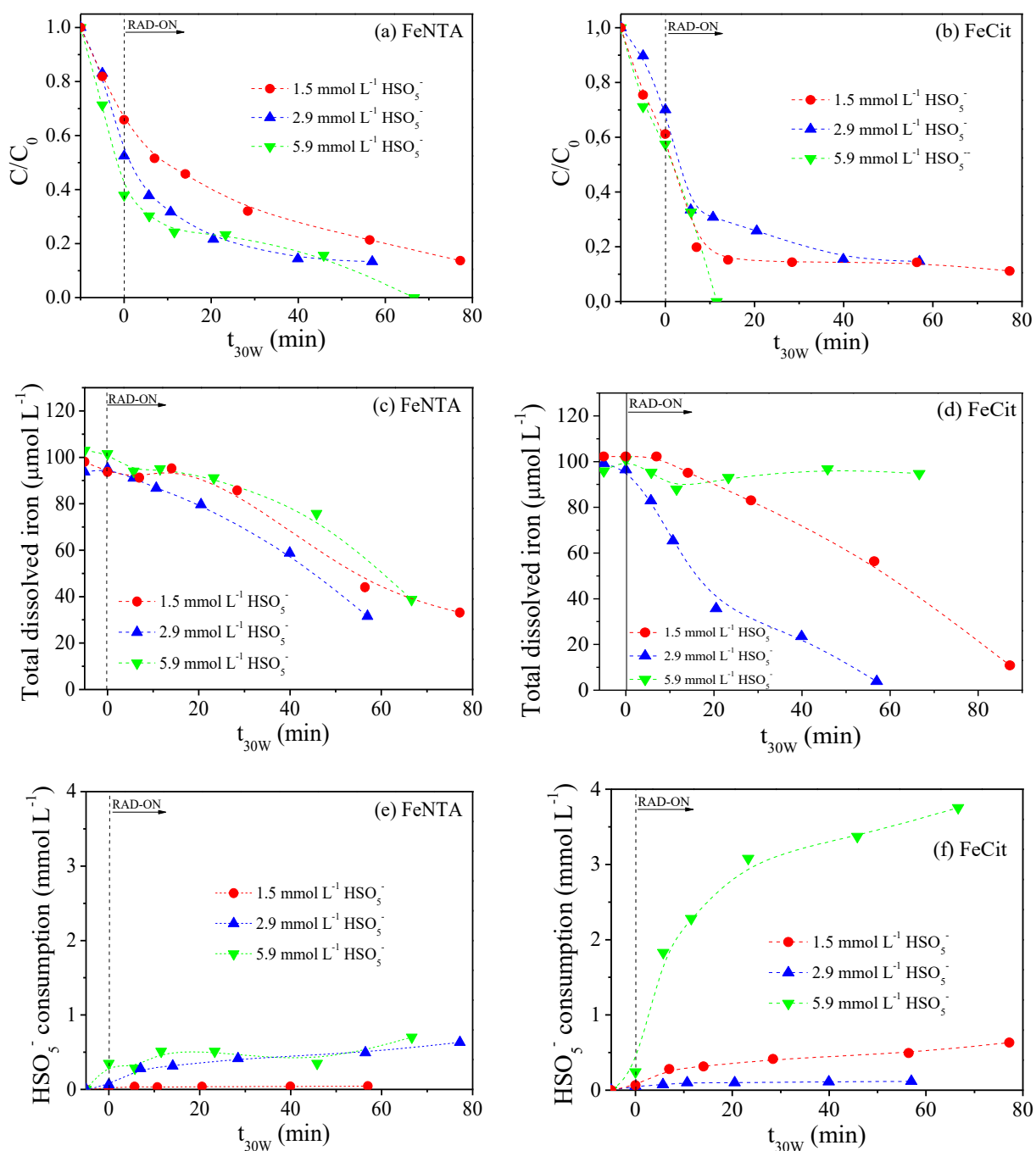
Compound	Analytical curve	Linear range ( $\mu\text{g L}^{-1}$ )	$R^2$	LOD ( $\mu\text{g L}^{-1}$ )	LOQ ( $\mu\text{g L}^{-1}$ )
NAP	$y = 5590 + 355x$	2.4 – 120	0.9984	0.6	2.1

#### 4.5.2 Effect of $S_2O_8^{2-}$ and $HSO_5^-$ concentration on the degradation of BP-3, FIP and PPB

In the presence of FeNTA, increasing concentrations of  $HSO_5^-$  (1.5 to 5.9 mmol L<sup>-1</sup>) increased the degradation efficiency of the mixture of the target compounds, reaching the LOQ (< 4.2  $\mu\text{g L}^{-1}$  for FIP and BP-3 and < 1.3  $\mu\text{g L}^{-1}$  for PPB) after 77 min of reaction using 5.9 mmol L<sup>-1</sup> of  $HSO_5^-$  (Figure 4.1a). These results are consistent with the availability of total dissolved iron during the process (Figures 4.1c) and the relatively higher consumption of  $HSO_5^-$  observed at the higher oxidant concentration (Figures 4.1e). For the FeCit system, increasing the concentration of  $HSO_5^-$  from 1.5 to 2.9 mmol L<sup>-1</sup> did not cause synergism in the degradation efficiency of the mixture of the target compounds and degradation rates around 85% were obtained (Figure 4.1b). However, a rapid degradation of the mixture of the target compounds was observed using the highest concentration of the oxidant (5.9 mmol L<sup>-1</sup>), reaching the LOQ (< 4.2  $\mu\text{g L}^{-1}$  for FIP and BP-3 and < 1.3  $\mu\text{g L}^{-1}$  for PPB) after 12 min of reaction (Figure 4.1b). The higher availability of total dissolved iron (99% of the initial concentration) (Figure 4.1d) and the higher consumption of  $HSO_5^-$  (64% of the concentration initially added) (Figure 4.1f) after the reaction in the presence of FeCit and 5.9 mmol L<sup>-1</sup> of the oxidant corroborate with the degradation result obtained.

Comparing these results based on the best  $\text{H}_2\text{O}_2$  concentrations ( $5.9 \text{ mmol L}^{-1}$  for FeNTA and  $2.9 \text{ mmol L}^{-1}$  for FeCit), it was observed that the use of  $\text{H}_2\text{O}_2$  resulted in better degradation efficiencies since for this oxidant, shorter reaction time and oxidant concentration were respectively required in FeNTA and FeCit systems. As described (subsection 2.2.4), the activation of  $\text{HSO}_5^-$  by ferric and ferrous ions generates  $\text{SO}_4^{\bullet-}$  (Equations 2.11 and 2.12), this being the predominant radical species in the reaction system. This allows inferring that the low degradation efficiencies of the mixture of BP-3, FIP and PPB using  $\text{HSO}_5^-$  when compared to  $\text{H}_2\text{O}_2$  (Figure 3.6) can be justified by the selectivity of  $\text{SO}_4^{\bullet-}$ , which react preferentially with compounds of high electronic density.

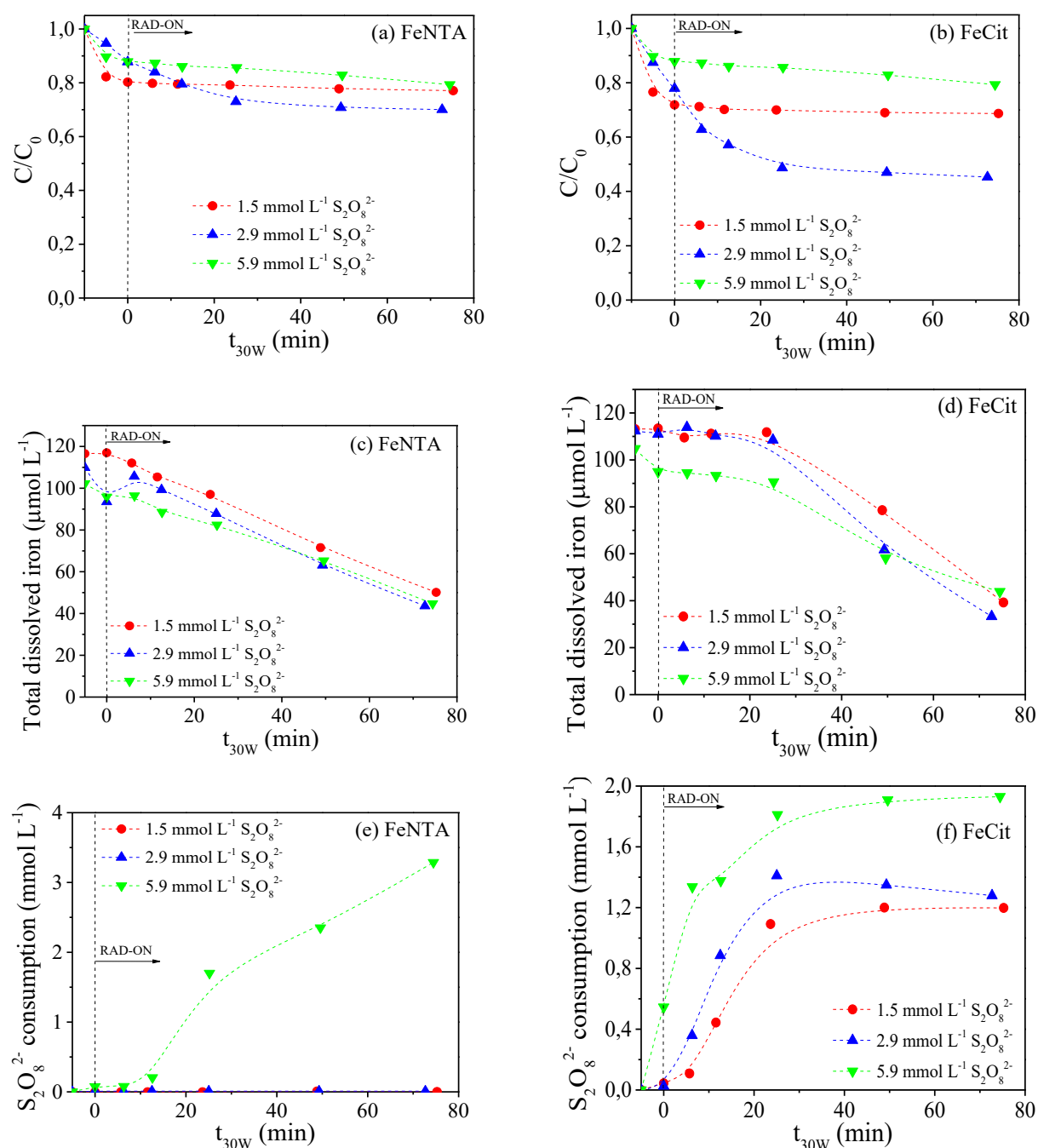
**Figure 4.1** – Influence of  $\text{HSO}_5^-$  concentration on the degradation of the mixture of BP-3, FIP and PPB using the iron complexes (a) FeNTA and (b) FeCit, ((c) and (d)) dissolved iron concentration, and ((e) and (f))  $\text{HSO}_5^-$  consumption. Initial conditions:  $[\text{CEC}] = 100 \mu\text{g L}^{-1}$  (for each compound),  $\text{Fe:L} = 1:1$  (FeNTA) and  $1:5$  (FeCit),  $[\text{Fe}^{3+}] = 100 \mu\text{mol L}^{-1}$ ;  $\text{pH} = 7.4$  (natural of the MWWTP effluent).



Regarding  $\text{S}_2\text{O}_8^{2-}$ , its use in all concentrations evaluated was not effective for the degradation of the target compounds. There were average degradation rates between 21% and

30% (Figure 4.2a) for FeNTA and 21% to 55% for FeCit. Similar to the FeCit/H<sub>2</sub>O<sub>2</sub> system (Figure 3.6), the highest degradation rate for this complex was obtained using 2.9 mmol L<sup>-1</sup> of S<sub>2</sub>O<sub>8</sub><sup>2-</sup> (Figure 4.2b). For FeCit there was a higher degradation efficiency when compared to FeNTA and the degradation rate was maximum after 24 min of reaction (Figures 4.2a-b). To some extent, this is consistent with the data for total dissolved iron and S<sub>2</sub>O<sub>8</sub><sup>2-</sup> consumption in this time interval (Figures 4.2c-f). In contrast, although there was an increased consumption of S<sub>2</sub>O<sub>8</sub><sup>2-</sup> for the highest concentrations evaluated (Figures 4.2e-f), there was no increase in the degradation efficiency, i.e. there was a reduction (Figures 4.2a-b). The reduction in degradation efficiency when increasing the S<sub>2</sub>O<sub>8</sub><sup>2-</sup> concentration from 2.9 to 5.9 mmol L<sup>-1</sup> can be attributed to inefficient parallel reactions resulting from the excess concentration of the oxidant (YANG et al., 2019). The higher degradation efficiency in the presence of FeCit may also be associated with the contribution of this complex in the generation of HO• and other radical species, as discussed by Marson et al. (2022b).

**Figure 4.2** – Influence of  $S_2O_8^{2-}$  concentration on the degradation of the mixture of BP-3, FIP and PPB using the iron complexes (a) FeNTA and (b) FeCit, ((c) and (d)) dissolved iron concentration, and ((e) and (f))  $S_2O_8^{2-}$  consumption. Initial conditions:  $[CEC]= 100 \mu\text{g L}^{-1}$  (for each compound),  $\text{Fe:L}= 1:1$  (FeNTA) and  $1:5$  (FeCit),  $[\text{Fe}^{3+}] = 100 \mu\text{mol L}^{-1}$ ;  $\text{pH}= 7.4$  (natural of the MWWTP effluent).



Overall, compared to  $H_2O_2$  and  $HSO_5^-$ , the degradation involving  $S_2O_8^{2-}$  was low for both iron complexes. On the other hand, activation of  $S_2O_8^{2-}$  by ferrous ions also generates

$\text{SO}_4^{\bullet-}$  in the reaction medium, so the degradation efficiencies involving  $\text{HSO}_5^-$  and  $\text{S}_2\text{O}_8^{2-}$  were expected to be equal and/or similar (Eq. 2.9). The difference in degradation efficiencies involving these two peroxide sources can be supported on the basis of pH. In the presence of  $\text{S}_2\text{O}_8^{2-}$ , there was no significant change in the pH of the reaction medium for any  $\text{S}_2\text{O}_8^{2-}$  concentration evaluated (Figures 4.3a-b). In contrast, for the highest concentration of  $\text{HSO}_5^-$  evaluated ( $5.9 \text{ mmol L}^{-1}$ ), there was a decrease in the pH value, reaching up to 3.5 for both iron complexes (FeNTA and FeCit) (Figures 4.3c-d). The decrease in pH value when adding  $\text{HSO}_5^-$  is due to the presence of bisulfate ion ( $\text{HSO}_4^-$ ) (strong acid) in the oxone composition ( $\text{KHSO}_5 \cdot 0,5\text{KHSO}_4 \cdot 0,5\text{K}_2\text{SO}_4$ ) (GHANBARI; MORADI, 2017). Therefore, for the highest concentration of  $\text{HSO}_5^-$  evaluated, the presence of the strong acid becomes significant, surpassing the bicarbonate and carbonate buffer of the tertiary sanitary effluent. The application of the photo-Fenton process in acid medium enables a greater availability of soluble iron in the reaction system (Figure 4.1c-d), which contributes to the greater generation of  $\text{SO}_4^{\bullet-}$  and a higher efficiency of degradation. For example, high quantum yield values of Fe(II) generation from UV-A photolysis of Fe(III)-NTA in acidic medium (pH 4.0) have already been reported (0.46 and 0.28 at 313 nm and 325 nm, respectively versus 0.16 and 0.04 at pH 6.0 in the same sequence of wavelengths) (ABIDA et al., 2006; CLARIZIA et al., 2017). Moreover, the better degradation at acidic pH can also be justified by the reduction of bicarbonate ( $\text{HCO}_3^-$ ) and carbonate ( $\text{CO}_3^{2-}$ ) ions concentration and soluble organic load (precipitation of humic acids), which compete with the target compounds for  $\text{HO}^{\bullet}$  and  $\text{SO}_4^{\bullet-}$  (Equations 4.5-4.8) (RATHI; KUMAR; SHOW, 2021; WACŁAWEK et al., 2017).

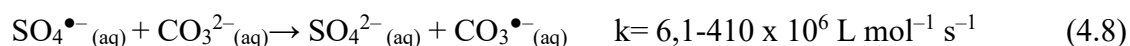
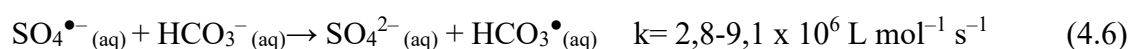
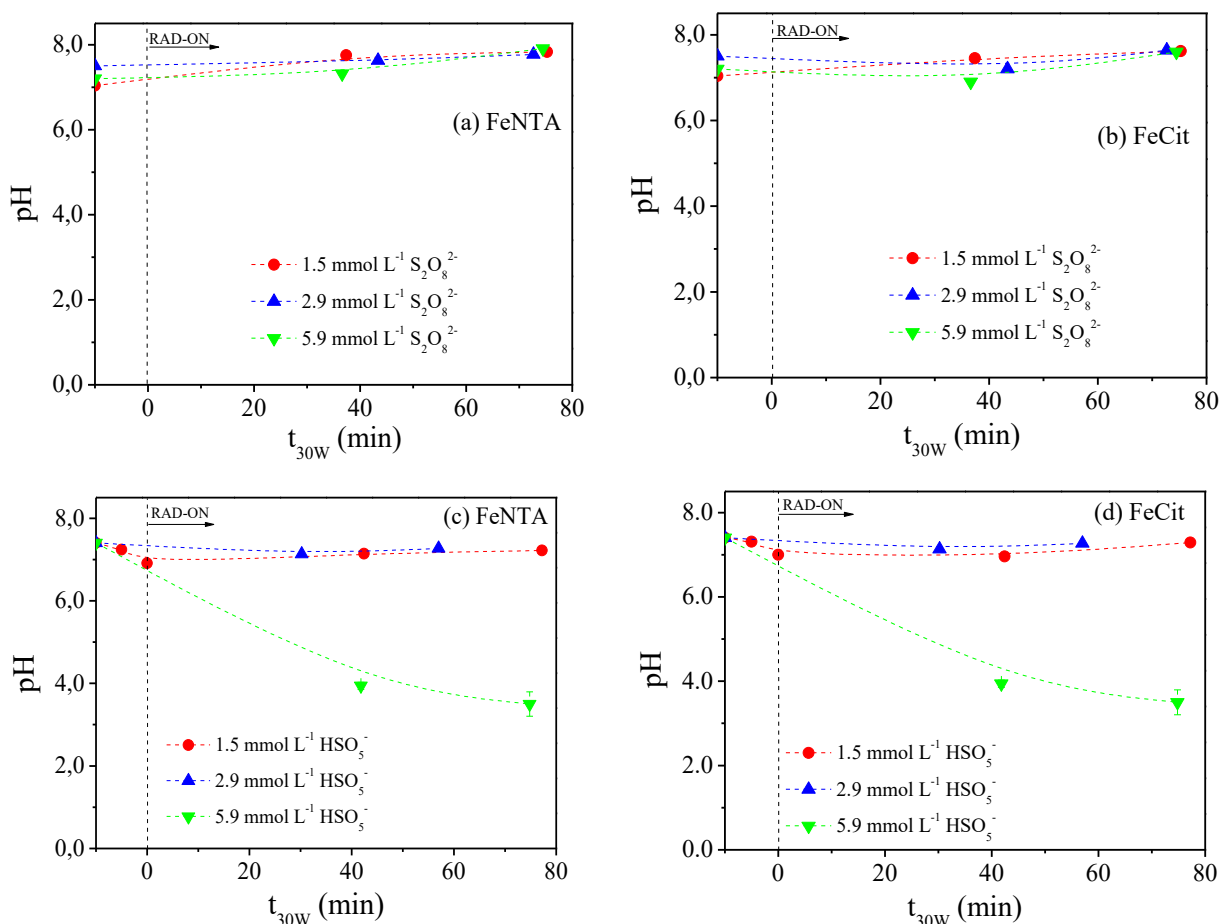


**Figure 4.3** – Influence of  $S_2O_8^{2-}$  and  $HSO_5^-$  concentrations on the pH of the reaction medium during the degradation of the mixture of BP-3, FIP and PPB using FeNTA and FeCit complexes. Initial conditions:  $[CEC]= 100 \mu\text{g L}^{-1}$  (for each compound), Fe:L= 1:1 (FeNTA) and 1:5 (FeCit),  $[\text{Fe}^{3+}] = 100 \mu\text{mol L}^{-1}$ ; pH= 7.4 (natural of the MWWTP effluent).



The results of the pH effect in the presence of  $S_2O_8^{2-}$  (next subsection) also support the above explanation concerning the higher degradation efficiency of the mixture of BP-3, FIP and PPB at high  $HSO_5^-$  concentrations.

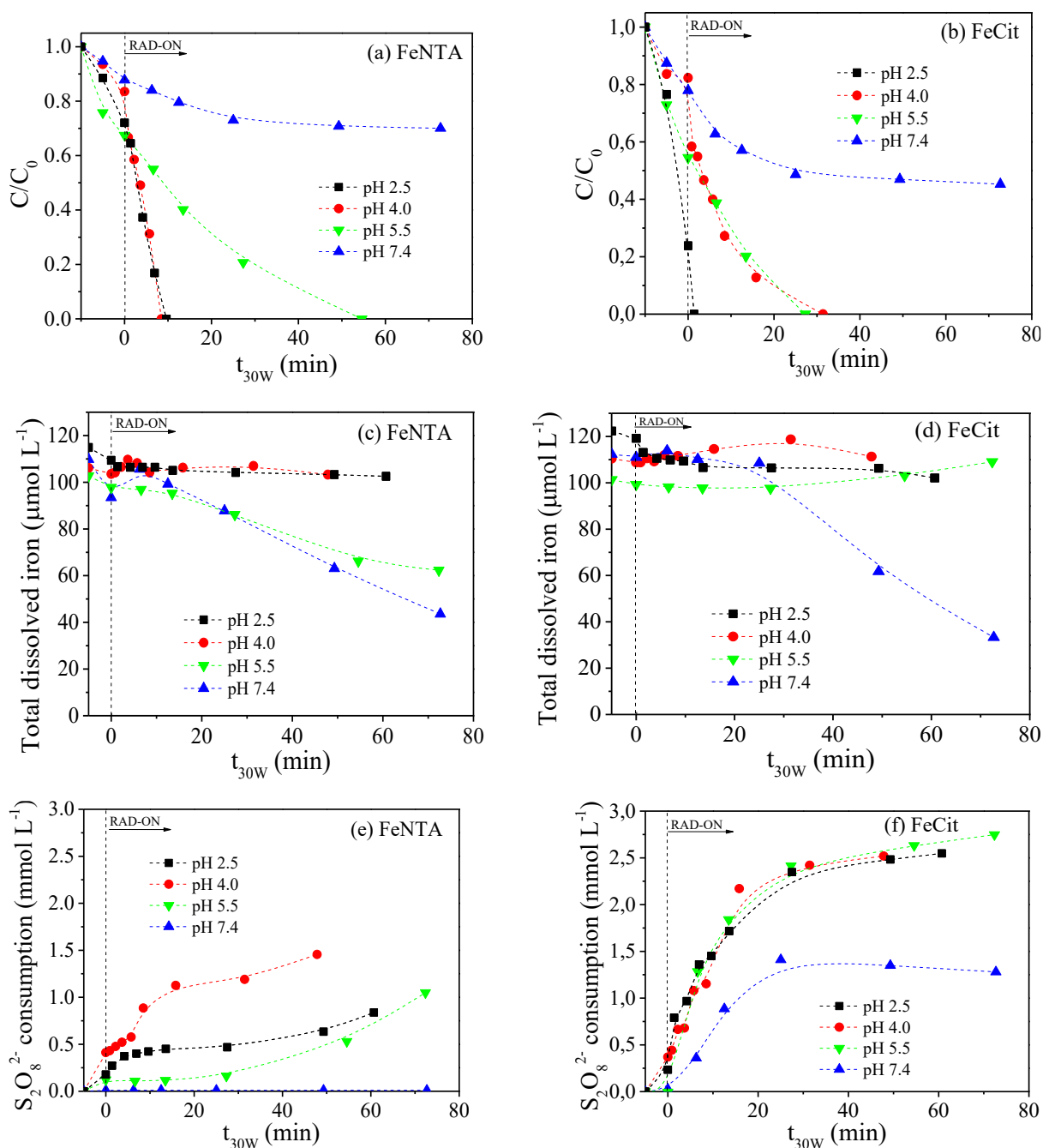
#### 4.5.3 Effect of pH on the degradation of BP-3, FIP and PPB using $S_2O_8^{2-}$

For both complexes (FeNTA and FeCit), there was an increase in degradation efficiency with decreasing pH and even at pH 5.5, it was possible to reach the LOQ of the mixture ( $1.3 \mu\text{g L}^{-1}$  for PPB and  $4.2 \mu\text{g L}^{-1}$  for FIP and BP-3) (Figure 4.4a-b). Furthermore, lower initial pH values (2.5 and 4.0) of the solution resulted in shorter effective degradation times of the mixture of target compounds and the decreasing order of degradation efficiency was: pH 2.5 > pH 4.0

> pH 5.5 > pH 7.4 (natural matrix) (Figures 4.4a-b). As described (subsection 4.5.2), these results are within expectations due to the higher availability of soluble iron in acidic medium (Figures 4.4c-d), which allows a higher consumption of  $S_2O_8^{2-}$  (Figures 4.4e-f) and increased concentration of  $SO_4^{\bullet-}$ . A rapid degradation (around 1 min of treatment) was obtained in the presence of FeCit at pH 2.5. This can be attributed to the presence of part of iron in the form of  $Fe(OH)^{2+}$  (Figure 2.3b) at this pH, a highly photoactive species whose photolysis results in the regeneration of ferrous ions and production of  $HO^{\bullet}$  (Eq. 2.2) (BABUPONNUSAMI; MUTHUKUMAR, 2014; CLARIZIA et al., 2017).

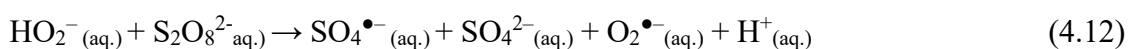
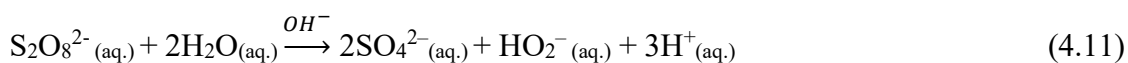


**Figure 4.4** – Influence of pH on the degradation efficiency of BP-3, FIP and PPB mixture by solar photo-Fenton using the (a) FeNTA and (b) FeCit complexes, ((c) and (d)) dissolved iron concentration, and ((e) and (f))  $S_2O_8^{2-}$  consumption. Initial conditions:  $[CEC]= 100 \mu\text{g L}^{-1}$  (for each compound),  $\text{Fe:L}= 1:1$  (FeNTA) and  $1:5$  (FeCit),  $[\text{Fe}^{3+}] = 100 \mu\text{mol L}^{-1}$  and  $[\text{S}_2\text{O}_8^{2-}]=2.94 \text{ mmol L}^{-1}$ .



pH also affects the speciation of radical species and matrix components of the tertiary sanitary effluent, directly impacting degradation efficiencies.  $\text{SO}_4^{\bullet-}$  is the predominant radical

under acidic conditions (equations 4.9 and 4.10 (SONG et al., 2019), which is conducive to higher degradation efficiencies of the target compounds in acidic medium. Both radicals ( $\text{SO}_4^{\bullet-}$  and  $\text{HO}^{\bullet}$ ) are present in a basic medium, with the  $\text{HO}^{\bullet}$  being the predominant species (LIANG; SU, 2009). As the pH increases, the conversion of  $\text{SO}_4^{\bullet-}$  to  $\text{HO}^{\bullet}$  becomes more and more evident (DOGLIOTTI; HAYON, 1967; NETA et al., 1977). Nevertheless, the standard reduction potential of  $\text{SO}_4^{\bullet-}$  and  $\text{HO}^{\bullet}$  is lower at  $\text{pH} > 7.0$  when compared to acidic medium and this also justifies the low degradation efficiencies obtained at  $\text{pH} 7.4$  (natural matrix) (Figures 4.3a-b). Added to this, in a basic medium, the dissociation of  $\text{S}_2\text{O}_8^{2-}$  is favoured, forming the hydroperoxyl ion ( $\text{HO}_2^-$ ) (Equation 4.11) (IKE et al., 2018) which is reduced by  $\text{S}_2\text{O}_8^{2-}$  to superoxide radicals ( $\text{O}_2^{\bullet-}$ ) (Equation 4.12) (IKE et al., 2018), a less oxidising species ( $E^\circ_{\text{O}_2^{\bullet-}} = +0,94 \text{ V}$ ) when compared to the  $\text{SO}_4^{\bullet-}$ .



Regarding the matrix components, it has already been reported in our previous study (AMILDON RICARDO et al., 2018b) that the reduction of pH of tertiary sanitary effluent from 7.7 to 6.0 resulted in increased degradation efficiency of chloramphenicol antibiotic by photo-Fenton process in the presence of ferrioxalate complex. This result was attributed to the partial removal of  $\text{HCO}_3^-$  and  $\text{CO}_3^-$ , which compete with the antibiotic for  $\text{HO}^{\bullet}$  (WACŁAWEK et al., 2017; YANG et al., 2019). Indeed, adjusting the natural pH (7.4) of the tertiary sanitary effluent to 5.5 resulted in partial removal of  $\text{HCO}_3^-$  (93% inorganic carbon (IC) removal (Table 4.3)). This corroborates to the lower degradation efficiencies of the mixture of BP-3, FIP and PPB obtained at  $\text{pH} 5.5$  when compared to those obtained at  $\text{pH} 4.0$  and  $2.5$  values (Figures 4.3a-b) in which the IC concentrations were below the respective LOQ ( $0.15 \text{ mg L}^{-1}$ ) (Table 4.3). The natural organic matter of the effluent, composed of humic and fulvic acids also competes for the radical species with the target compounds, decreasing the efficiency of degradation (RATHI; KUMAR; SHOW, 2021; WACŁAWEK et al., 2017). Although fulvic acids are soluble in a wide pH range, humic acids are insoluble in acid medium (CARDOSO, 2021). Therefore, acidification of the tertiary sanitary effluent resulted in 46% removal of humic acids (represented by total organic carbon (TOC)) (Table 4.3), which also justifies the higher

degradation efficiencies obtained in acid medium compared to those obtained at natural pH of the matrix.

**Tabela 4.3** – Variation of total carbon (TC), inorganic carbon (IC) and total organic carbon (TOC) of the tertiary sanitary effluent used in the experiments, as a function of pH.

pH	TC (mg L <sup>-1</sup> )	IC (mg L <sup>-1</sup> )	TOC (mg L <sup>-1</sup> )
2.5	18.28 ± 0.18	≤ 0.15	18.28 ± 0.18
4.0	15.43 ± 0.12	≤ 0.15	15.43 ± 0.12
5.5	21.64 ± 0.41	6.78 ± 0.11	14.86 ± 0.41
7.4	122.20 ± 1.18	92.25 ± 1.18	29.94 ± 1.18

Source: The Author, 2023.

Besides natural organic matter and bicarbonate and carbonate ions, other ions (chloride (Cl<sup>-</sup>), sulphate (SO<sub>4</sub><sup>2-</sup>), etc.) also affect the degradation efficiencies. Therefore, it is important to evaluate the isolated and/or combined influence of different inorganic ions present in the tertiary wastewater matrix on the degradation efficiency of the target compounds.

#### 4.5.4 Influence of Cl<sup>-</sup>, SO<sub>4</sub><sup>2-</sup> and HCO<sub>3</sub><sup>-</sup> on the degradation of the mixture of BP-3, FIP and PPB

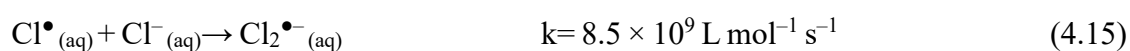
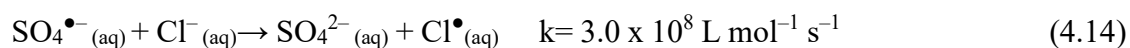
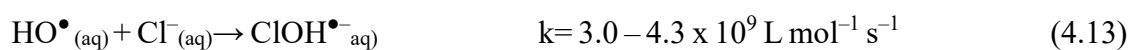
Table 4.4 shows the chemical characterization of the tertiary effluent after previous treatments performed.

**Tabela 4.4** – Characterization of the matrix after isolated and simultaneous removal of HCO<sub>3</sub><sup>-</sup>, Cl<sup>-</sup> and SO<sub>4</sub><sup>2-</sup>.

Parameter (mg L <sup>-1</sup> )	MWWTP Effluent	Cl <sup>-</sup> removal	HCO <sub>3</sub> <sup>-</sup> removal	SO <sub>4</sub> <sup>2-</sup> removal	Combined Removal
Total Carbon	122.2 ± 1.2	52.4 ± 0.6	41.5 ± 0.2	62.5 ± 0.6	30.4 ± 0.5
Inorganic Carbon	92.2 ± 4.2	50.9 ± 0.9	34.8 ± 0.6	59.1 ± 1.3	30.4 ± 0.5
Organic Carbon	29.9 ± 4.2	1.5 ± 0.9	6.8 ± 0.6	3.4 ± 1.3	0
Chloride	200	0	200	200	0
Sulphate	73.5	73.5	65	0	0

Source: The Author, 2023.

The acidification of the matrix resulted in 62% of  $\text{HCO}_3^-$  removal (decrease in the concentration of inorganic carbon, from  $92.2 \pm 4.2 \text{ mg L}^{-1}$  to  $34.8 \pm 0.6 \text{ mg L}^{-1}$  (Table 4.4)). In this matrix (after its neutralization) 53% of degradation of the mixture of the target compounds was obtained, against 35% obtained in the matrix *in natura* (Figure 4.5). These results are indicative that indeed the  $\text{HCO}_3^-$  present in the tertiary sanitary effluent interfere with the degradation efficiency of the target compounds by the modified photo-Fenton process in the presence of  $\text{S}_2\text{O}_8^{2-}$ , due to their competition with these compounds for  $\text{HO}^\bullet$  and  $\text{SO}_4^{\bullet-}$  (Equations 4.5-4.6) (RATHI; KUMAR; SHOW, 2021; WACŁAWEK et al., 2017). Although the removal of  $\text{HCO}_3^-$  resulted in a better degradation profile when compared to the degradation in the absence of  $\text{SO}_4^{2-}$ , similar efficiency (52%) was obtained after complete and isolated  $\text{SO}_4^{2-}$  removal (Table 4.4 and Figure 4.5) and these results are also consistent since  $\text{SO}_4^{2-}$  also exhibit inhibitory effect. One of the inhibitory effects of sulphates in photo-Fenton process is their ability to form stable complexes with ferric ions, such as  $\text{FeSO}_4^+$  and  $\text{Fe}(\text{SO}_4)_2^-$ , which are much less photoactive than  $\text{FeOH}^{2+}$  (SOARES et al., 2015). On the other hand, chloride removal resulted in effective degradation of the mixture of the target compounds, i.e., the concentrations were below LOQ ( $1.3 \text{ } \mu\text{g L}^{-1}$  for PPB and  $4.2 \text{ } \mu\text{g L}^{-1}$  for FIP and BP-3). This result is also within the expected range, since chloride ions also compete with target compounds for radical species at a higher rate when compared to  $\text{HCO}_3^-$  (Equations 4.13 e 4.14 (RATHI; KUMAR; SHOW, 2021; WACŁAWEK et al., 2017)). Furthermore, high chloride content generates soluble complexes with iron, such as  $\text{FeCl}^+$ ,  $\text{FeCl}^{2+}$  and  $\text{FeCl}_2^+$ , which are much less photoactive than  $\text{FeOH}^{2+}$  (MARSON et al., 2017; SOARES et al., 2015). These complexes are also generators of less oxidizing species such as  $\text{Cl}^\bullet$  and  $\text{Cl}_2^{\bullet-}$  when compared to  $\text{HO}^\bullet$  and  $\text{SO}_4^{\bullet-}$  (SOARES et al., 2015). In excess, chloride ions can also sequester  $\text{Cl}^\bullet$  by generating  $\text{Cl}_2^{\bullet-}$  (Eq. 4.15), a less reactive species than  $\text{SO}_4^{\bullet-}$  due to its lower standard reduction potential ( $E^0 = 2.09 \text{ V}$ ) (Eq. 4.16) (MARSON et al., 2017; XUE et al., 2022).



It is worth noting that the inhibitory effect of chloride ions is even greater in processes involving  $\text{S}_2\text{O}_8^{2-}$  when compared to that of  $\text{H}_2\text{O}_2$ , i.e, although the rate constant of the chloride

reaction with  $\text{HO}^\bullet$  is higher when compared to the reaction of this anion with  $\text{SO}_4^{\bullet-}$  (Equations 4.13 and 4.14), this reaction is reversible and significant only at low pH values. On the other hand, in the reaction of equation 4.14 there is direct generation of chlorine radicals ( $\text{Cl}^\bullet$ ), implying a greater reduction of  $\text{SO}_4^{\bullet-}$  in processes involving  $\text{S}_2\text{O}_8^{2-}$  (YANG et al., 2014).

Thus, the influence of ions on the degradation efficiency of the target compounds followed the descending order:  $\text{Cl}^- > \text{HCO}_3^- > \text{SO}_4^{2-}$ . This sequence is also consistent with the results obtained in previous work (FENG et al., 2017; GHANBARI; MORADI, 2017).

The inorganic ion removal processes were also accompanied by the partial removal of humic acids (reduction of organic carbon (Table 4.4)) which are also scavengers of radical species (IOANNIDI; FRONTISTIS; MANTZAVINOS, 2018; LEE; LEE; ZOH, 2021). This allows us to infer that the degradation efficiencies obtained (Figure 4.5) cannot be attributed solely to the removal of chloride, bicarbonate and sulphate ions. Indeed, the highest degradation efficiency (concentration below LOQ after 7.5 min of reaction (Figure 4.5)) was obtained after combined removal of inorganic ions (bicarbonate, sulphate and chloride) and this result is also attributed to the total removal of organic carbon and lower concentration of inorganic carbon (Table 4.4).

A decrease in pH was also observed in the processes involving matrices after removal of chloride and all anions (combined removal) and the drop was more significant in effluent after combined removal (7.4 to 2.5) (Figure 4.5b). These results suggest that the removal treatments of these ions (chloride and combined removal) also contributed to the breakdown of the matrix buffer and increased availability of soluble iron, resulting in an increase in the observed degradation efficiency of the target compounds.

Furthermore, the addition of excess  $\text{AgNO}_3$  in the chloride ion removal process must have resulted in silver ions ( $\text{Ag}^+$ ) in solution, which are also efficient for persulfate ion activation, resulting in additional sulfate radicals in the reaction medium (Eq. 4.17) (ANIPSITAKIS; DIONYSIOU, 2004b). Thus, the application of the process in the presence of  $\text{Ag}^+$  guaranteed higher rates of contaminant degradation due to the greater generation of sulfate radicals in the reaction medium.

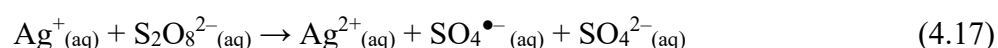
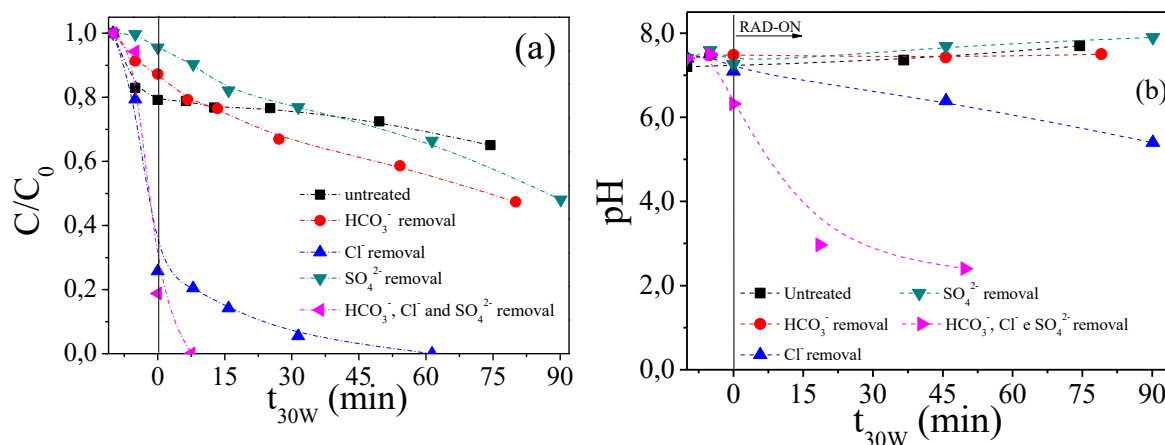


**Figure 4.5** – Effect of inorganic ion removal from tertiary wastewater on (a) degradation of BP-3, FIP and PPB mixture by solar photo-Fenton process using FeNTA and  $S_2O_8^{2-}$  and (b) pH variation. Initial conditions:  $[CEC]= 100 \mu\text{g L}^{-1}$  (for each compound),  $\text{Fe(III):NTA}= 1:1$ ,  $[\text{Fe}^{3+}] = 100 \mu\text{mol L}^{-1}$ ,  $[\text{S}_2\text{O}_8^{2-}] = 5.9 \text{ mmol L}^{-1}$  and  $\text{pH} = 7,4$  (natural da matriz).

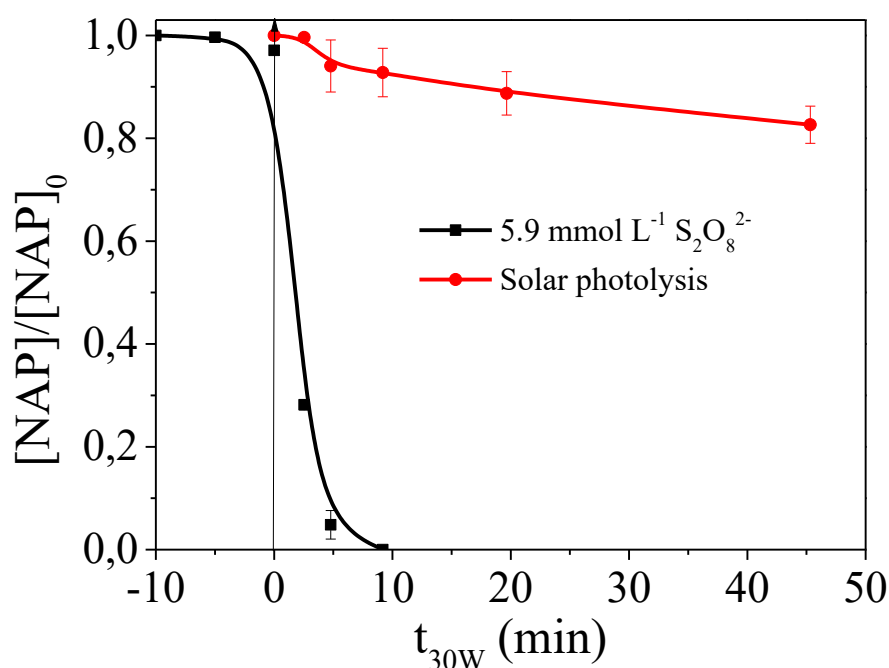


Better degradation efficiencies of contaminants of emerging concern (CEC) at near-neutral pH conditions have often been obtained by SR-AOPs when compared to those based on  $\text{HO}^\bullet$  alone (KANG; KIM; ZOH, 2018; SILVA et al., 2021). This was controversial in relation to the degradation results for the mixture of BP-3, IFP and PPB involving  $\text{S}_2\text{O}_8^{2-}$  (Figure 4.2) and, although it appears surprising, these results are consistent with results obtained in previous work. The strong competition of  $\text{HCO}_3^-$  and humic acids (constituents of the MWWTP effluent matrix) with the target compounds by  $\text{SO}_4^{\bullet-}$  negatively affected the degradation of  $200 \mu\text{g L}^{-1}$  of PPB by the UV-A/ $\text{S}_2\text{O}_8^{2-}$  process (IOANNIDI; FRONTISTIS; MANTZAVINOS, 2018). On the other hand, a strong inhibition in the degradation of BP-3 by different  $\text{S}_2\text{O}_8^{2-}$  activation methods at pH 7.0 was also reported (LEE; LEE; ZOH, 2021; PAN et al., 2018). Moreover, the presence of several carbonyl and hydroxyl groups in the structure of humic acids favours the reaction with  $\text{SO}_4^{\bullet-}$  by electron transfer. Therefore, considering that  $\text{SO}_4^{\bullet-}$  is highly reactive and more selective and that it reacts preferentially by electron transfer (GHANBARI; MORADI, 2017; XUE et al., 2022), the results with  $\text{S}_2\text{O}_8^{2-}$  (Figures 4.2) suggest that BP-3, FIP and PPB are compounds with low affinity for electron transfer reactions. To confirm this hypothesis, experiments involving the degradation of NAP (a compound that reacts preferentially by electron transfer (SILVA et al., 2021)) in the presence of  $5.9 \text{ mmol L}^{-1}$  of  $\text{S}_2\text{O}_8^{2-}$  using FeNTA were performed.

#### 4.5.5 Comparison of the efficiency of degradation of the target compounds with NAP

The NAP degradation results are presented in Figure 4.6. As observed (Figure 4.6), there was a synergism in NAP degradation when combining solar radiation with FeNTA and  $S_2O_8^{2-}$ . For the evaluated process, the concentration of NAP was below the LOQ ( $2.1 \mu\text{g L}^{-1}$ ) (Figure 4.6), compared to 21% degradation efficiency obtained for the mixture of BP-3, FIP and PPB under the same experimental conditions (Figure 4.2a). This difference between the degradation rate of NAP (Figure 4.6) and that of the mixture of the target compounds suggests that the degradation efficiency is also related to the structure of the target compound and radical species involved in the reaction medium. Since  $S_2O_8^{2-}$  activation in the presence of FeNTA generates  $SO_4^{\bullet-}$ , the degradation results of NAP (Figure 4.6) and the mixture (Figure 4.2a) suggest that the presence of  $SO_4^{\bullet-}$  in the reaction system favours NAP degradation and inverse role is played by  $HO^{\bullet}$ .

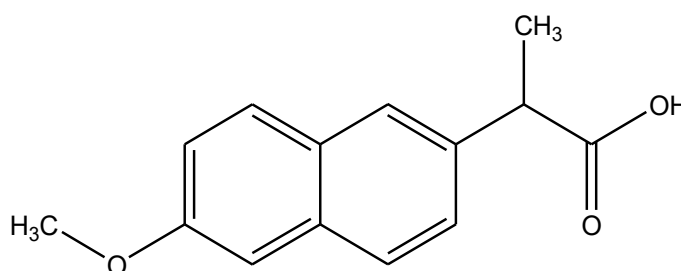
**Figure 4.6** – Degradation profile of NAP by solar photo-Fenton process using FeNTA complex in the presence of  $S_2O_8^{2-}$ . Initial conditions:  $[NAP]= 100 \mu\text{g L}^{-1}$ ,  $[Fe^{3+}]= 100 \mu\text{mol L}^{-1}$ , Fe:NTA = 1:1 and pH = 7.4 (natural of the matrix).



NAP (Figure 4.7) is a compound with two conjugated aromatic rings in its basic structure, possessing, however, sites of higher electronic density. This justifies the higher degradability observed for this compound (Figure 4.6), since the  $SO_4^{\bullet-}$  is an electrophilic

species, reacting preferentially with electron-rich organic contaminants, such as aromatic rings, derivatives of aromatic compounds with electron-donating substituent groups (-SH and -NH<sub>2</sub>), sulfur-containing compounds (thiophene) and nitrogen-containing compounds (amides, pyrrole, among others) (DUAN et al., 2022). In contrast, hydrogen abstraction (a mechanism characteristic of HO•) occurs in alkyl, hydroxyl, carboxyl and ether groups (DUAN et al., 2022) and these groups are present in the chemical structures of BP-3 and PPB. On the other hand, considering the presence of several electron withdrawing groups (CF<sub>3</sub>, chlorides and nitrile group) in the structure of FIP (Table 1.1) and the presence of conjugated aromatic rings and hydroxyl groups in the structures of humic acids (present in the tertiary sanitary effluent), it is expected that this insecticide suffers a strong competition with these acids for SO<sub>4</sub>•<sup>-</sup>.

**Figure 4.7** – Structural formula of NAP (C<sub>14</sub>H<sub>14</sub>O<sub>3</sub> – Molar weight = 230.3 g mol<sup>-1</sup>).



Source: The author, 2022.

Although further studies on mechanistic aspects are needed for a valid and complete inference, these results are indicative of the above mentioned hypothesis that the target compounds BP-3, FIP and PPB have a low affinity for electrode transfer reactions. Since HSO<sub>5</sub><sup>-</sup> can automatically adjust the pH of the solution with the production of protons, its use as a peroxide source in the evaluated AOPs proved to be disadvantageous due to the increased conductivity of the effluent and the need to adjust the pH after treatment in order to neutralize the treated solutions before disposal. Therefore, H<sub>2</sub>O<sub>2</sub> in the presence of FeNTA was the best source of peroxide for degradation of the mixture of the target compounds by the evaluated processes.

## 4.6 Conclusions

This study showed that SR-AOPs in the presence of organic iron complexes under solar radiation are not a good alternative for tertiary sanitary effluent treatment aiming at the degradation of the mixture of BP-3, FIP and PPB at near neutral pH. The choice of the best peroxide source strongly depends on matrix composition, pH and the structure of the target compound (compound with low or high electron density). Although concentration of the mixture of BP-3, FIP and PPB below LOQ ( $1.3 \mu\text{g L}^{-1}$  for PPB and  $4.2 \mu\text{g L}^{-1}$  for FIP and BP-3) was obtained in the presence of  $5.9 \text{ mmol L}^{-1}$  of  $\text{HSO}_5^-$  at initial pH 7.4 (natural matrix), for this same concentration of  $\text{S}_2\text{O}_8^{2-}$  and target compounds, low and high degradation rates (concentrations below LOQ) were respectively obtained at natural and acidic pH, highlighting the effect of  $\text{HSO}_5^-$  on the acidification of the reaction medium and the influence of pH on the performance of the peroxide source. Furthermore, adjustment of matrix pH to values below 7.0 and removal of inorganic ions and organic carbon resulted in higher degradation efficiencies (concentrations below LOQ), again highlighting the effect of pH and matrix composition on  $\text{S}_2\text{O}_8^{2-}$  performance. The best degradation efficiency obtained for NAP in the presence of  $\text{S}_2\text{O}_8^{2-}$  at natural pH of the matrix showed that the choice of the best peroxide source also strongly depends on the structure of the target compound (compound with low or high electron density). Finally, considering the complexity of MWWTP effluent composition, these results demonstrate the need for further studies evaluating the simultaneous degradation of organic compounds with high and low electronic density using different peroxide sources.

## 5 CHAPTER V: GENERAL CONCLUSIONS

This chapter contains all the conclusions drawn from this research. Overall, although several studies have reported satisfactory performance and novel findings for the application of AOPs for the removal of BP-3, FIP and PPB, low degradation efficiencies ( $\leq 60\%$ ) were achieved in real matrices, reinforcing the need for studies with this type of matrix aiming at the removal of the above-mentioned compounds. The proposed AOPs in the presence of  $\text{H}_2\text{O}_2$  were efficient in degrading the target compounds and removing acute toxicity to *D. melanogaster* flies of the Canton S strain. However, the best operating conditions for each system were different, with a lower Fe/L molar ratio being required for FeNTA due to the high value of its stability constant when compared to FeCit. On the other hand, a lower concentration of  $\text{H}_2\text{O}_2$  was sufficient for the efficiency of the FeCit system when compared to FeNTA due to the additional hydroxyl radical production resulting from the *in situ* generation of  $\text{H}_2\text{O}_2$  at pH 7.4. The FeNTA system has the advantage of adding less organic load and the treatment cost is 1.5-fold lower when compared to the FeCit system. Finally, this study showed that solar SR-AOPs in the presence of FeNTA and FeCit are inefficient for the degradation of the mixture of the target compounds at near neutral pH. The use of  $\text{HSO}_5^-$  reduces the pH of the matrix due to the presence of bisulphuric acid in the Oxone<sup>®</sup>, worsening the quality of the effluent as a consequence of increasing its conductivity, for example, at concentrations up to  $5.9 \text{ mmol L}^{-1}$  the pH will start to reduce. The natural pH of the matrix (7.4), the matrix components (inorganic ions and natural organic matter) and the structure of the target compounds negatively affected the degradation efficiency in processes involving  $\text{S}_2\text{O}_8^{2-}$  and, among the peroxide sources evaluated,  $\text{H}_2\text{O}_2$  was the best.

## 6 CHAPTER VI: FUTURE RECOMMENDATIONS

Several conclusions can be drawn from the recent literature reports extensively analysed in detail through a review article presented in this Ph.D. Thesis, as well as from the combination of experimental and theoretical approaches, with emphasis on organic iron complexes combined with different peroxide sources as powerful strategies for treatment of environmental aqueous matrices aimed at degradation of contaminants of emerging concern at near neutral pH. After an extensive literature review on the performance of AOPs on the degradation of BP-3, FIP and PPB and evaluation of the modified photo-Fenton process for the same purpose, it was possible to conclude that there is a need for studies with real matrices to better understand the influence of the matrix composition and the chemical structure of the target compounds aiming at the application of AOPs as tertiary treatment in wastewater treatment plants. This Ph.D. Thesis presented a practical example as a scheme to select the most suitable iron complex and peroxide source for the effective degradation of contaminants of emerging concern. However, some additional analysis could be carried out to elucidate some topics related to the results obtained here after the application of the evaluated processes, such as:

- Since hydroxyl radicals can be formed simultaneously with sulfate radicals during SR-AOPs, tests with radical species scavengers would clarify which radicals contribute to the degradation of the target compound in processes involving persulfate and monopersulfate ions.
- The identification of transformation products formed during oxidation of BP-3, FIP and PPB should be further investigated in order to clarify the acute toxicity results for *D. melanogaster*.
- Chemometric tools could be applied using the different iron and hydrogen peroxide concentrations evaluated in order to optimize the processes and evaluate the possibility of obtaining better results with a lower concentration of reagents at neutral pH.
- Toxicity testing should be carried out for other test organisms responsive to BP-3 and PPB, not just *D. Melanogaster*.
- The application of hydrogen peroxide and persulfate simultaneously could be evaluated in order to circumvent the effect of the structure of the target compounds on their degradation efficiency;
- Solar energy storage technologies should be developed to allow the application of the photo-Fenton process even on sunless days.

## 7 REFERENCES

- ABBAS, S. et al. Metabolism of Parabens (4-Hydroxybenzoic Acid Esters) by Hepatic Esterases and UDP-Glucuronosyltransferases in Man. **Drug Metabolism and Pharmacokinetics**, v. 25, n. 6, p. 568–577, 1 jan. 2010. <https://doi.org/10.2133/dmpk.DMPK-10-RG-013>
- ABIDA, O. et al. Impact of iron-complex (Fe(III)–NTA) on photoinduced degradation of 4-chlorophenol in aqueous solution. **Photochemical and Photobiological Sciences**, v. 5, n. 4, p. 395–402, 2006. <https://doi.org/10.1039/b518211e>
- ABIDI, J. et al. A boron-doped diamond anode for the electrochemical removal of parabens in low-conductive solution: From a conventional flow cell to a solid polymer electrolyte system. **Journal of Pest Science**, v. 92, n. 3, p. 314–319, 2019. <https://doi.org/10.1002/cefc.201901909>
- ADAMS, L. K.; LYON, D. Y.; ALVAREZ, P. J. J. Comparative eco-toxicity of nanoscale TiO<sub>2</sub>, SiO<sub>2</sub>, and ZnO water suspensions. **Water Research**, v. 40, n. 19, p. 3527–3532, 2006. <https://doi.org/10.1016/j.watres.2006.08.004>
- AHILE, U. J. et al. A review on the use of chelating agents as an alternative to promote photo-Fenton at neutral pH: Current trends, knowledge gap and future studies. **Science of the Total Environment**, v. 710, p. 134872, 25 mar. 2020. <https://doi.org/10.1016/j.scitotenv.2019.134872>
- AJIBOYE, T. O.; OYEWO, O. A.; ONWUDIWE, D. C. Photocatalytic removal of parabens and halogenated products in wastewater : a review. **Environmental Chemistry Letters**, v. 19, n. 5, p. 3789–3819, 2021. <https://doi.org/10.1007/s10311-021-01263-2>
- AMILDON RICARDO, I. et al. Degradation and initial mechanism pathway of chloramphenicol by photo-Fenton process at circumneutral pH. **Chemical Engineering Journal**, v. 339, n. February, p. 531–538, 2018a. <https://doi.org/10.1016/j.cej.2018.01.144>
- AMILDON RICARDO, I. et al. Chloramphenicol photo-Fenton degradation and toxicity changes in both surface water and a tertiary effluent from a municipal wastewater treatment plant at near-neutral conditions. **Chemical Engineering Journal**, v. 347, n. April, p. 763–770, 2018b. <https://doi.org/10.1016/j.cej.2018.04.169>
- AN, J. et al. Oxidation of propyl paraben by ferrate(VI): Kinetics, products, and toxicity assessment. **Journal of Environmental Science and Health - Part A Toxic/Hazardous Substances and Environmental Engineering**, v. 53, n. 10, p. 873–882, 2018. <https://doi.org/10.1080/10934529.2018.1459074>
- ANDERSEN, F. A. Final amended report on the safety assessment of Methylparaben, Ethylparaben, Propylparaben, Isopropylparaben, Butylparaben, Isobutylparaben, and Benzylparaben as used in cosmetic products. **International Journal of Toxicology**, v. 27, n. 4, p. 1–82, 2008. <https://doi.org/10.1177/109158180802704s01>
- ANIPSITAKIS, G. P.; DIONYSIOU, D. D. Transition metal/UV-based advanced oxidation technologies for water decontamination. **Applied Catalysis B: Environmental**, v. 54, n. 3, p. 155–163, 2004a. <https://doi.org/10.1016/j.apcatb.2004.05.025>

ANIPSITAKIS, G. P.; DIONYSIOU, D. D. Radical generation by the interaction of transition metals with common oxidants. **Environmental Science and Technology**, v. 38, n. 13, p. 3705–3712, 2004b. <https://doi.org/10.1021/es035121o>

ASIF, M. B. et al. Elucidating the performance of an integrated laccase- and persulfate-assisted process for degradation of trace organic contaminants (TrOCs). **Environmental Science: Water Research and Technology**, v. 6, n. 4, p. 1069–1082, 2020. <https://doi.org/10.1039/C9EW01022J>

AZALOK, K. A.; OLADIPO, A. A.; GAZI, M. Hybrid MnFe-LDO–biochar nanopowders for degradation of metronidazole via UV-light-driven photocatalysis: Characterization and mechanism studies. **Chemosphere**, v. 268, p. 128844, 2021a. <https://doi.org/10.1016/j.chemosphere.2020.128844>

AZALOK, K. A.; OLADIPO, A. A.; GAZI, M. UV-light-induced photocatalytic performance of reusable MnFe-LDO–biochar for tetracycline removal in water. **Journal of Photochemistry and Photobiology A: Chemistry**, v. 405, n. October 2020, p. 112976, 2021b. <https://doi.org/10.1016/j.jphotochem.2020.112976>

BABU, D. S. et al. Detoxification of water and wastewater by advanced oxidation processes. **Science of The Total Environment**, v. 696, p. 133961, 15 dez. 2019. <https://doi.org/10.1016/j.scitotenv.2019.133961>

BABUPONNUSAMI, A.; MUTHUKUMAR, K. A review on Fenton and improvements to the Fenton process for wastewater treatment. **Journal of Environmental Chemical Engineering**, v. 2, n. 1, p. 557–572, 2014. <https://doi.org/10.1016/j.jece.2013.10.011>

BASIN, V. et al. Residue levels and discharge loads of antibiotics in wastewater treatment plants (WWTPs), hospital lagoons, and rivers within Lake Victoria Basin, Kenya. **Environmental Monitoring and Assessment**, v. 188, p. 532, 2016. <https://doi.org/10.1007/s10661-016-5534-6>

BAZIN, I. et al. Hydroxy Benzoate Preservatives ( Parabens ) in the Environment : Data for Environmental Toxicity Assessment. v. 16, 2010. [https://doi.org/10.1007/978-90-481-3509-7\\_14](https://doi.org/10.1007/978-90-481-3509-7_14)

BEHRMAN, E. J.; DEAN, D. H. Sodium peroxydisulfate is a stable and cheap substitute for ammonium peroxydisulfate (persulfate) in polyacrylamide gel electrophoresis. **Journal of Chromatography B: Biomedical Sciences and Applications**, v. 723, n. 1–2, p. 325–326, 19 fev. 1999. [https://doi.org/10.1016/S0378-4347\(98\)00525-8](https://doi.org/10.1016/S0378-4347(98)00525-8)

BEKRIS, L. et al. Graphene: A new activator of sodium persulfate for the advanced oxidation of parabens in water. **Water Research**, v. 126, p. 111–121, 2017. <https://doi.org/10.1016/j.watres.2017.09.020>

BERNAL-ROMERO DEL HOMBRE BUENO, M. DE LOS Á.; BOLUDA-BOTELLA, N.; PRATS RICO, D. Removal of emerging pollutants in water treatment plants: adsorption of methyl and propylparaben onto powdered activated carbon. **Adsorption**, v. 25, n. 5, p. 983–999, 2019. <https://doi.org/10.1007/s10450-019-00120-7>

BHARDWAJ, U. et al. Ecotoxicology and Environmental Safety Persistence of fipronil and its risk assessment on cabbage , Brassica oleracea. **Ecotoxicology and Environmental Safety**, v.

79, p. 301–308, 2012. <https://doi.org/10.1016/j.ecoenv.2012.01.016>

BHARGAV, D. et al. Toxic potential of municipal solid waste leachates in transgenic *Drosophila melanogaster* (hsp70-lacZ): hsp70 as a marker of cellular damage. **Ecotoxicology and Environmental Safety**, v. 69, n. 2, p. 233–245, 1 fev. 2008. <https://doi.org/10.1016/j.ecoenv.2006.12.014>

BIELSKÁ, L.; HALE, S. E.; ŠKULCOVÁ, L. A review on the stereospecific fate and effects of chiral conazole fungicides. **Science of the Total Environment**, v. 750, 2021. <https://doi.org/10.1016/j.scitotenv.2020.141600>

BOBERG, J. et al. Possible endocrine disrupting effects of parabens and their metabolites. **Reproductive Toxicology**, v. 30, n. 2, p. 301–312, 2010. <https://doi.org/10.1016/j.reprotox.2010.03.011>

BOCZKAJ, G.; FERNANDES, A. **Wastewater treatment by means of advanced oxidation processes at basic pH conditions: A review** *Chemical Engineering Journal* Elsevier B.V., , 15 jul. 2017. [https://doi.org/10.1007/978-3-319-58421-8\\_53](https://doi.org/10.1007/978-3-319-58421-8_53)

BÖGER, B. et al. Occurrence of antibiotics and antibiotic resistant bacteria in subtropical urban rivers in Brazil. **Journal of Hazardous Materials**, v. 402, n. July 2020, p. 123448, 2021. <https://doi.org/10.1016/j.jhazmat.2020.123448>

BOLUJOKO, N. B. et al. Toxicity and removal of parabens from water : A critical review. **Science of the Total Environment**, v. 792, p. 148092, 2021. <https://doi.org/10.1016/j.scitotenv.2021.148092>

BUDD, R. et al. Monitoring Fipronil and Degradates in California Surface Waters, 2008–2013. **Journal of Environmental Quality**, v. 44, p. 1233–1240, 2015. <https://doi.org/10.2134/jeq2015.01.0018>

BUXTON, G. V. et al. Critical Review of rate constants for reactions of hydrated electrons, hydrogen atoms and hydroxyl radicals ( $\cdot\text{OH}/\cdot\text{O}^-$  in Aqueous Solution. **Journal of Physical and Chemical Reference Data**, v. 17, n. 2, p. 513–886, 1988. <https://doi.org/10.1063/1.555805>

BUXTON, G. V; MALONE, T. N.; SALMON, G. A. Reaction of  $\text{SO}_4^{\cdot-}$  with  $\text{Fe}^{2+}$ ,  $\text{Mn}^{2+}$  and  $\text{Cu}^{2+}$  in aqueous solution. **Journal of the Chemical Society - Faraday Transactions**, v. 93, n. 16, p. 2893–2897, 1997. <https://doi.org/10.1039/a701472d>

CAMPOS, D. et al. Toxicity of organic UV-filters to the aquatic midge *Chironomus riparius*. **Ecotoxicology and Environmental Safety**, v. 143, p. 210–216, 1 set. 2017. <https://doi.org/10.1016/j.ecoenv.2017.05.005>

CAMPOS, D. et al. Two-generational effects of Benzophenone-3 on the aquatic midge *Chironomus riparius*. **Science of the Total Environment**, v. 669, p. 983–990, 15 jun. 2019. <https://doi.org/10.1016/j.scitotenv.2019.03.023>

CANOSA, P. et al. Optimisation of a solid-phase microextraction method for the determination of parabens in water samples at the low ng per litre level. **Journal of Chromatography A**, v. 1124, n. 1–2, p. 3–10, 2006. <https://doi.org/10.1016/j.chroma.2006.03.045>

CARDOSO, T. S. **Estudo de caracterização dos ácidos húmicos e fúlvicos em perfil sedimentar e suas interações com metais pesados**. [s.l.] Universidade Federal do Sul da Bahia, 2021.

CELEIRO, M. et al. Assessment of advanced oxidation processes for the degradation of three UV filters from swimming pool water. **Journal of Photochemistry and Photobiology A: Chemistry**, v. 351, p. 95–107, 2018. <https://doi.org/10.1016/j.jphotochem.2017.10.023>

CELEIRO, M. et al. Photodegradation behaviour of multiclass ultraviolet filters in the aquatic environment: Removal strategies and photoproduct identification by liquid chromatography–high resolution mass spectrometry. **Journal of Chromatography A**, v. 1596, p. 8–19, 2019. <https://doi.org/10.1016/j.chroma.2019.02.065>

CHEN, D.; LI, F.; RAY, A. K. External and internal mass transfer effect on photocatalytic degradation. **Catalysis Today**, v. 66, n. 2–4, p. 475–485, 30 mar. 2001. [https://doi.org/10.1016/S0920-5861\(01\)00256-5](https://doi.org/10.1016/S0920-5861(01)00256-5)

CHEN, Y. et al. Photodegradation of propranolol by Fe(III)-citrate complexes: Kinetics, mechanism and effect of environmental media. **Journal of Hazardous Materials**, v. 194, n. 3, p. 202–208, 2011. <https://doi.org/10.1016/j.jhazmat.2011.07.081>

CHIIHA, M. et al. Modeling of ultrasonic degradation of non-volatile organic compounds by Langmuir-type kinetics. **Ultrasonics Sonochemistry**, v. 17, n. 5, p. 773–782, 1 jun. 2010. <https://doi.org/10.1016/j.ultsonch.2010.03.007>

CHIIHA, M. et al. Sonolytic degradation of endocrine disrupting chemical 4-cumylphenol in water. **Ultrasonics Sonochemistry**, v. 18, n. 5, p. 943–950, 1 set. 2011. <https://doi.org/10.1016/j.ultsonch.2010.12.014>

CIAMBELLI, P. et al. A step forwards in ethanol selective photo-oxidation. **Photochemical & Photobiological Sciences**, v. 8, p. 699–704, 2009. <https://doi.org/10.1039/b818053a>

CLARIZIA, L. et al. Applied Catalysis B: Environmental Homogeneous photo-Fenton processes at near neutral pH: A review. “**Applied Catalysis B, Environmental**”, v. 209, p. 358–371, 2017. <https://doi.org/10.1016/j.apcatb.2017.03.011>

CONNELL, D. W. **Bioaccumulation of Xenobiotic Compounds**. Boca Raton, Florida: CRC Press, 2000.

CUERDA-CORREA, E. M. et al. Degradation of Parabens in Different Aqueous Matrices by Several O<sub>3</sub>-Derived Advanced Oxidation Processes. **Industrial and Engineering Chemistry Research**, v. 55, n. 18, p. 5161–5172, 2016a. <https://doi.org/10.1021/acs.iecr.6b00740>

CUERDA-CORREA, E. M. et al. Ultraviolet-Photoassisted Advanced Oxidation of Parabens Catalyzed by Hydrogen Peroxide and Titanium Dioxide. Improving the System. **Industrial and Engineering Chemistry Research**, v. 55, n. 18, p. 5152–5160, 11 maio 2016b. <https://doi.org/10.1021/acs.iecr.5b04560>

CUERDA-CORREA, E. M.; ALEXANDRE-FRANCO, M. F.; FERNÁNDEZ-GONZÁLES, C. Advanced Oxidation Processes for the Removal of Antibiotics from Water. An Overview. **Water**, v. 12, n. 1, p. 102, 2020. <https://doi.org/10.3390/w12010102>

DA COSTA FILHO, B. M. et al. Coupling coagulation, flocculation and decantation with photo-Fenton process for treatment of industrial wastewater containing fipronil: Biodegradability and toxicity assessment. **Journal of Environmental Management**, v. 174, p. 71–78, 2016. <https://doi.org/10.1016/j.jenvman.2016.03.019>

DANOVARO, R. et al. Sunscreens cause coral bleaching by promoting viral infections. **Environmental Health Perspectives**, v. 116, n. 4, p. 441–447, 2008. <https://doi.org/10.1289/ehp.10966>

DAOUD-MAHAMMED, S. et al. Efficient Loading and Controlled Release of Benzophenone-3 Entrapped into Self-Assembling Nanogels. **Current Nanoscience**, v. 6, n. 6, p. 654–665, 2010. <https://doi.org/10.2174/157341310793348678>

DARBRE, P. D. et al. Concentrations of Parabens in Human Breast Tumours. **JOURNAL OF APPLIED TOXICOLOGY**, v. 24, n. 1, p. 5–13, 2004. <https://doi.org/10.1002/jat.958>

DE LUCA, A.; DANTAS, R. F.; ESPLUGAS, S. Assessment of iron chelates efficiency for photo-Fenton at neutral pH. **Water Research**, v. 61, p. 232–242, 2014. <https://doi.org/10.1016/j.watres.2014.05.033>

DE LUCA, A.; DANTAS, R. F.; ESPLUGAS, S. Study of Fe(III)-NTA chelates stability for applicability in photo-Fenton at neutral pH. **Applied Catalysis B: Environmental**, v. 179, p. 372–379, 2015. <https://doi.org/10.1016/j.apcatb.2015.05.025>

DE WITTE, B. et al. Ozonation and advanced oxidation by the peroxone process of ciprofloxacin in water. **Journal of Hazardous Materials**, v. 161, n. 2–3, p. 701–708, 30 jan. 2009. <https://doi.org/10.1016/j.jhazmat.2008.04.021>

DEBORDE, M.; VON GUNTEN, U. Reactions of chlorine with inorganic and organic compounds during water treatment-Kinetics and mechanisms: A critical review. **Water Research**, v. 42, n. 1–2, p. 13–51, 2008. <https://doi.org/10.1016/j.watres.2007.07.025>

DELGADO-VARGAS, C. A. et al. An efficient simultaneous degradation of sulfamethoxazole and trimethoprim by photoelectro - Fenton process under non - modified pH using a natural citric acid source: study of biodegradability , ecotoxicity , and antibacterial activity. **Environmental Science and Pollution Research**, n. 0123456789, 2021. <https://doi.org/10.21203/rs.3.rs-575639/v1>

DEWIL, R. et al. New perspectives for Advanced Oxidation Processes. **Journal of Environmental Management**, v. 195, p. 93–99, 2017. <https://doi.org/10.1016/j.jenvman.2017.04.010>

DOGLIOTTI, L.; HAYON, E. Flash photolysis of per[oxydi]sulfate ions in aqueous solutions. The sulfate and ozonide radical anions. **The Journal of Physical Chemistry**, v. 71, n. 8, p. 2511–2516, 1967. <https://doi.org/10.1021/j100867a019>

DOROTA, B.; GROMADZIŃSKA, J.; WOJCIECH, W. Parabens . From environmental studies to human health. **Environment International**, v. 67, p. 27–42, 2014. <https://doi.org/10.1016/j.envint.2014.02.007>

DU, E. et al. Insight into the degradation of two benzophenone-type UV filters by the UV/H<sub>2</sub>O<sub>2</sub>

advanced oxidation process. **Water (Switzerland)**, v. 10, n. 9, 2018. <https://doi.org/10.3390/w10091238>

DUAN, X. et al. Comparison of sulfate radical with other reactive species. **Current Opinion in Chemical Engineering**, v. 38, p. 100867, 2022. <https://doi.org/10.1016/j.coche.2022.100867>

EATON, A. D. et al. (EDS.). **Standard Methods for Examination of Water & Wastewater**. 21. ed. Washington DC: [s.n.].

ESPLUGAS, S. et al. Comparison of different advanced oxidation processes for phenol degradation. **Water Research**, v. 36, p. 1034–1042, 2002. [https://doi.org/10.1016/S0043-1354\(01\)00301-3](https://doi.org/10.1016/S0043-1354(01)00301-3)

FANG, H. et al. Advanced oxidation kinetics and mechanism of preservative propylparaben degradation in aqueous suspension of TiO<sub>2</sub> and risk assessment of its degradation products. **Environmental Science and Technology**, v. 47, n. 6, p. 2704–2712, 2013. <https://doi.org/10.1021/es304898r>

FANG, W. et al. A critical review of synthetic chemicals in surface waters of the US, the EU and China. **Environment International**, v. 131, n. June, p. 104994, 2019. <https://doi.org/10.1016/j.envint.2019.104994>

FENG, Y. et al. Degradation of ketoprofen by sulfate radical-based advanced oxidation processes: Kinetics, mechanisms, and effects of natural water matrices. **Chemosphere**, v. 189, p. 643–651, 2017. <https://doi.org/10.1016/j.chemosphere.2017.09.109>

FENOLL, J. et al. Fipronil decomposition in aqueous semiconductor suspensions using UV light and solar energy. **Journal of the Taiwan Institute of Chemical Engineers**, v. 45, n. 3, p. 981–988, 1 maio 2014. <https://doi.org/10.1016/j.jtice.2013.09.015>

FERNÁNDEZ-IBÁÑEZ, P. et al. Application of the colloidal stability of TiO<sub>2</sub> particles for recovery and reuse in solar photocatalysis. **Water Research**, v. 37, n. 13, p. 3180–3188, 2003. [https://doi.org/10.1016/S0043-1354\(03\)00157-X](https://doi.org/10.1016/S0043-1354(03)00157-X)

FERREIRA, T. P. et al. Determination of Fipronil and Fipronil - Sulfone in Surface Waters of the Guandu River Basin by High - Performance Liquid Chromatography with Mass Spectrometry. **Bulletin of Environmental Contamination and Toxicology**, v. 108, n. 2, p. 225–233, 2022. <https://doi.org/10.1007/s00128-021-03369-3>

FURMAN, O. S.; TEEL, A. L.; WATTS, R. J. Mechanism of base activation of persulfate. **Environmental Science and Technology**, v. 44, n. 16, p. 6423–6428, 2010. <https://doi.org/10.1021/es1013714>

GAO, L. et al. Effect of ethylparaben on the growth and development of *Drosophila melanogaster* on preadult. v. 80, n. August, p. 1–7, 2020. <https://doi.org/10.1016/j.etap.2020.103495>

GAO, Y. Q. et al. Factors affecting sonolytic degradation of sulfamethazine in water. **Ultrasonics Sonochemistry**, v. 20, n. 6, p. 1401–1407, 1 nov. 2013. <https://doi.org/10.1016/j.ultsonch.2013.04.007>

GARCIA, H. A. et al. Laccase-catalyzed oxidation of oxybenzone in municipal wastewater primary effluent. **Water Research**, v. 45, n. 5, p. 1921–1932, 2011. <https://doi.org/10.1016/j.watres.2010.12.027>

GHANBARI, F.; MORADI, M. Application of peroxymonosulfate and its activation methods for degradation of environmental organic pollutants: Review. **Chemical Engineering Journal**, v. 310, p. 41–62, 2017. <https://doi.org/10.1016/j.cej.2016.10.064>

GHAZIPURA, M. et al. Exposure to benzophenone-3 and reproductive toxicity: A systematic review of human and animal studies. **Reproductive Toxicology**, v. 73, p. 175–183, 2017. <https://doi.org/10.1016/j.reprotox.2017.08.015>

GMUREK, M. et al. Photodegradation of single and mixture of parabens - Kinetic, by-products identification and cost-efficiency analysis. **Chemical Engineering Journal**, v. 276, p. 303–314, 5 set. 2015. <https://doi.org/10.1016/j.cej.2015.04.093>

GOGATE, P. R.; PANDIT, A. B. A review of imperative technologies for wastewater treatment I: Oxidation technologies at ambient conditions. **Advances in Environmental Research**, v. 8, n. 3–4, p. 501–551, 2004. [https://doi.org/10.1016/S1093-0191\(03\)00032-7](https://doi.org/10.1016/S1093-0191(03)00032-7)

GOMES JÚNIOR, O. et al. Optimization of fipronil degradation by heterogeneous photocatalysis: Identification of transformation products and toxicity assessment. **Water Research**, v. 110, p. 133–140, 2017. <https://doi.org/10.1016/j.watres.2016.12.017>

GOMES JÚNIOR, O. et al. Degradation mechanism of fipronil and its transformation products, matrix effects and toxicity during the solar/photo-Fenton process using ferric citrate complex. **Journal of Environmental Management**, v. 269, n. April, p. 110756, 1 set. 2020. <https://doi.org/10.1016/j.jenvman.2020.110756>

GONÇALVES, B. R. et al. Reducing toxicity and antimicrobial activity of a pesticide mixture via photo-Fenton in different aqueous matrices using iron complexes. **Science of the Total Environment**, v. 740, p. 140152, 20 out. 2020. <https://doi.org/10.1016/j.scitotenv.2020.140152>

GONÇALVES, B. R. et al. Influence of water matrix components and peroxide sources on the transformation products and toxicity of tebuthiuron under UVC-based advanced oxidation processes. **Science of the Total Environment**, v. 859, n. October 2022, 2023. <https://doi.org/10.1016/j.scitotenv.2022.160120>

GUNASEKARA, A. S. et al. Environmental fate and toxicology of fipronil. **Journal of Pesticide Science**, v. 32, n. 3, p. 189–199, 2007. <https://doi.org/10.1584/jpestics.R07-02>

GUO, Y.; KANNAN, K. A survey of phthalates and parabens in personal care products from the United States and its implications for human exposure. **Environmental Science and Technology**, v. 47, n. 24, p. 14442–14449, 2013. <https://doi.org/10.1021/es4042034>

H.J.H. FENTON, M. A. Oxidation of tartaric acid in presence of iron. **Journal of the Chemical Society, Transactions**, v. 65, p. 899–910, 1894. <https://doi.org/10.1039/CT8946500899>

HABER, F.; WEISS, J. The catalytic decomposition of hydrogen peroxide by iron salts. **Proceedings of the royal society A**, v. 147, n. 861, p. 332–351, 1934. <https://doi.org/10.1098/rspa.1934.0221>

HAMAN, C.; DAUCHY, X.; ROSIN, C. Occurrence, fate and behavior of parabens in aquatic environments: A review. **Water Research**, v. 8, p. 1–11, 2014. <https://doi.org/10.1016/j.watres.2014.09.030>

HANEKAMP, J. C.; BAST, A. Antibiotics exposure and health risks: **Environmental Toxicology and Pharmacology**, v. 39, n. 1, p. 213–220, 2014. <https://doi.org/10.1016/j.etap.2014.11.016>

HAO, D. et al. A reusable, separation-free and biodegradable calcium alginate/g-C<sub>3</sub>N<sub>4</sub> microsphere for sustainable photocatalytic wastewater treatment. **Journal of Cleaner Production**, v. 314, n. March, p. 128033, 2021. <https://doi.org/10.1016/j.jclepro.2021.128033>

HARVEY, P. W.; EVERETT, D. J. Significance of the detection of esters of p-hydroxybenzoic acid (parabens) in human breast tumours. **Journal of Applied Toxicology**, v. 24, n. 1, p. 1–4, 2004. <https://doi.org/10.1002/jat.957>

HE, G. et al. Chloramines in a pilot-scale water distribution system: Transformation of 17 $\beta$ -estradiol and formation of disinfection byproducts. **Water Research**, v. 106, p. 41–50, 1 dez. 2016. <https://doi.org/10.1016/j.watres.2016.09.047>

HEIDT, L. J. The photolysis of persulfate. **The Journal of Chemical Physics**, v. 10, n. 5, p. 297–302, 1942. <https://doi.org/10.1063/1.1723724>

HENGLEIN, A. Sonochemistry: Historical developments and modern aspects. **Ultrasonics**, v. 25, n. 1, p. 6–16, 1 jan. 1987. [https://doi.org/10.1016/0041-624X\(87\)90003-5](https://doi.org/10.1016/0041-624X(87)90003-5)

HOFFMANN, M. R.; HUA, I.; HÖCHEMER, R. Application of ultrasonic irradiation for the degradation of chemical contaminants in water. **Ultrasonics Sonochemistry**, v. 3, n. 3, p. S163–S172, 1 nov. 1996. [https://doi.org/10.1016/S1350-4177\(96\)00022-3](https://doi.org/10.1016/S1350-4177(96)00022-3)

HOIGNÉ, J.; BADER, H. Rate constants of reactions of ozone with organic and inorganic compounds in water-I. Non-dissociating organic compounds. **Water Research**, v. 17, n. 2, p. 173–183, 1 jan. 1983. [https://doi.org/10.1016/0043-1354\(83\)90098-2](https://doi.org/10.1016/0043-1354(83)90098-2)

HOPKINS, Z. R.; BLANEY, L. An aggregate analysis of personal care products in the environment: Identifying the distribution of environmentally-relevant concentrations. **Environment International**, v. 92–93, p. 301–316, 2016. <https://doi.org/10.1016/j.envint.2016.04.026>

HOUSE, D. A. Kinetics and mechanism of oxidations by peroxydisulfate. **Chemical Reviews**, v. 62, n. 3, p. 185–203, 1962. <https://doi.org/10.1021/cr60217a001>

HOWSAWKENG, J. et al. Evidence for simultaneous abiotic-biotic oxidations in a microbial-Fenton's system. **Environmental Science and Technology**, v. 35, n. 14, p. 2961–2966, 2001. <https://doi.org/10.1021/es001802x>

IBHADON, A. O.; FITZPATRICK, P. Heterogeneous photocatalysis: Recent advances and applications. **Catalysts**, v. 3, n. 1, p. 189–218, 2013. <https://doi.org/10.3390/catal3010189>

IGHALO, J. O. et al. A review of methods for the removal of penicillins from water. **Journal**

of **Water Process Engineering**, v. 39, n. September 2020, p. 101886, 2021. <https://doi.org/10.1016/j.jwpe.2020.101886>

IKE, I. A. et al. Critical review of the science and sustainability of persulphate advanced oxidation processes. **Chemical Engineering Journal**, v. 338, p. 651–669, 15 abr. 2018. <https://doi.org/10.1016/j.cej.2018.01.034>

INMETRO, I. N. DE M. Q. E T. **Orientação sobre validação de métodos analíticos DOQ-CGCRE-008, revisão 08**, 2020.

INTICHER, J. J. et al. Advanced treatment of water contaminated with atrazine, difenoconazole and fipronil mixture, its by-products and bio-toxicity levels. **Journal of Environmental Chemical Engineering**, v. 9, n. 5, p. 105883, 1 out. 2021. <https://doi.org/10.1016/j.jece.2021.105883>

IOANNIDI, A.; FRONTISTIS, Z.; MANTZAVINOS, D. Destruction of propyl paraben by persulfate activated with UV-A light emitting diodes. **Journal of Environmental Chemical Engineering**, v. 6, n. 2, p. 2992–2997, 2018. <https://doi.org/10.1016/j.jece.2018.04.049>

JL, G.; ZHANG, B.; WU, Y. Combined ultrasound/ozone degradation of carbazole in APG 1214 surfactant solution. **Journal of Hazardous Materials**, v. 225–226, p. 1–7, 30 jul. 2012. <https://doi.org/10.1016/j.jhazmat.2012.02.044>

JOSÉ, S. F. et al. Fipronil decomposition in aqueous semiconductor suspensions using UV light and solar energy. **Journal of the Taiwan Institute of Chemical Engineers**, v. 45, p. 981–988, 2014. <https://doi.org/10.1016/j.jtice.2013.09.015>

JUNG, C. et al. Chemical oxidation for mitigation of UV-quenching substances (UVQS) from municipal landfill leachate: Fenton process versus ozonation. **Water Research**, v. 108, p. 260–270, 1 jan. 2017. <https://doi.org/10.1016/j.watres.2016.11.005>

KAGAYA, S. et al. Separation of titanium dioxide photocatalyst in its aqueous suspensions by coagulation with basic aluminium chloride. **Water Research**, v. 33, n. 7, p. 1753–1755, 1999. [https://doi.org/10.1016/S0043-1354\(99\)00004-4](https://doi.org/10.1016/S0043-1354(99)00004-4)

KANG, Y. M.; KIM, M. K.; ZOH, K. D. Effect of nitrate, carbonate/bicarbonate, humic acid, and H<sub>2</sub>O<sub>2</sub> on the kinetics and degradation mechanism of Bisphenol-A during UV photolysis. **Chemosphere**, v. 204, p. 148–155, 1 ago. 2018. <https://doi.org/10.1016/j.chemosphere.2018.04.015>

KHAKI, M. R. D. et al. Application of doped photocatalysts for organic pollutant degradation - A review. **Journal of Environmental Management**, v. 198, p. 78–94, 2017. <https://doi.org/10.1016/j.jenvman.2017.04.099>

KHAN, A. et al. Titanium Dioxide-Mediated Photocatalysed Degradation of Two Herbicide Derivatives Chloridazon and Metribuzin in Aqueous Suspensions. **International Journal of Chemical Engineering**, v. 2012, n. 1, p. 8, 2012. <https://doi.org/10.1155/2012/850468>

KIM, S.; CHOI, K. Occurrences, toxicities, and ecological risks of benzophenone-3, a common component of organic sunscreen products: A mini-review. **Environment International**, v. 70, p. 143–157, 2014. <https://doi.org/10.1016/j.envint.2014.05.015>

KISHIMOTO, N.; NISHIMURA, H. Effect of pH and molar ratio of pollutant to oxidant on a photochemical advanced oxidation process using hypochlorite. **Environmental Technology (United Kingdom)**, v. 36, n. 19, p. 2436–2442, 2015. <https://doi.org/10.1080/09593330.2015.1034187>

KOLTHOFF, I. M.; MILLER, I. K. The Chemistry of Persulfate. I. The Kinetics and Mechanism of the Decomposition of the Persulfate Ion in Aqueous Medium. **Journal of the American Chemical Society**, v. 73, n. 7, p. 3055–3059, 1951. <https://doi.org/10.1021/ja01151a024>

KRZEMINSKI, P. et al. Performance of secondary wastewater treatment methods for the removal of contaminants of emerging concern implicated in crop uptake and antibiotic resistance spread: A review. **Science of the Total Environment**, v. 648, p. 1052–1081, 2019. <https://doi.org/10.1016/j.scitotenv.2018.08.130>

LAPERTOT, M. et al. Photo-Fenton and biological integrated process for degradation of a mixture of pesticides. **Journal of Photochemistry and Photobiology A: Chemistry**, v. 186, n. 1, p. 34–40, 2007. <https://doi.org/10.1016/j.jphotochem.2006.07.009>

LEE, H. B.; PEART, T. E.; SVOBODA, M. L. Determination of endocrine-disrupting phenols, acidic pharmaceuticals, and personal-care products in sewage by solid-phase extraction and gas chromatography-mass spectrometry. **Journal of Chromatography A**, v. 1094, n. 1–2, p. 122–129, 2005. <https://doi.org/10.1016/j.chroma.2005.07.070>

LEE, Y. M. et al. Kinetics and degradation mechanism of Benzophenone-3 in chlorination and UV/chlorination reactions. **Chemical Engineering Journal**, v. 393, n. November 2019, p. 124780, 2020. <https://doi.org/10.1016/j.cej.2020.124780>

LEE, Y. M.; LEE, G.; ZOH, K. D. Benzophenone-3 degradation via UV/H<sub>2</sub>O<sub>2</sub> and UV/persulfate reactions. **Journal of Hazardous Materials**, v. 403, n. August 2020, p. 123591, 2021. <https://doi.org/10.1016/j.jhazmat.2020.123591>

LEYVA, E. et al. A Review on Chemical Advanced Oxidation Processes for Pharmaceuticals with Paracetamol as a Model Compound. Reaction Conditions, Intermediates and Total Mechanism. **Current Organic Chemistry**, v. 22, n. 1, p. 2–17, 2017. <https://doi.org/10.2174/1385272821666171019145520>

LI, M. et al. VUV/UV/Chlorine as an Enhanced Advanced Oxidation Process for Organic Pollutant Removal from Water: Assessment with a Novel Mini-Fluidic VUV/UV Photoreaction System (MVPS). **Environmental Science and Technology**, v. 50, n. 11, p. 5849–5856, 2016a. <https://doi.org/10.1021/acs.est.6b00133>

LI, W. et al. Occurrence, fate and risk assessment of parabens and their chlorinated derivatives in an advanced wastewater treatment plant. **Journal of Hazardous Materials**, v. 300, p. 29–38, 2015a. <https://doi.org/10.1016/j.jhazmat.2015.06.060>

LI, Y. et al. Effects of propylparaben on fecundity and lifespan in *Drosophila melanogaster*. **Toxicological & Environmental Chemistry**, v. 96, n. 7, p. 1064–1074, 2015. <https://doi.org/10.1080/02772248.2015.1005091>

LI, Y. et al. Photochemical transformation of sunscreen agent benzophenone-3 and its

metabolite in surface freshwater and seawater. **Chemosphere**, v. 153, p. 494–499, 2016b. <https://doi.org/10.1016/j.chemosphere.2016.03.080>

LIANG, C. et al. A rapid spectrophotometric determination of persulfate anion in ISCO. **Chemosphere**, v. 73, n. 9, p. 1540–1543, 2008. <https://doi.org/10.1016/j.chemosphere.2008.08.043>

LIANG, C.; SU, H. W. Identification of sulfate and hydroxyl radicals in thermally activated persulfate. **Industrial and Engineering Chemistry Research**, v. 48, n. 11, p. 5558–5562, 2009. <https://doi.org/10.1021/ie9002848>

LIU, J.; LI, X.; WANG, X. Toxicological effects of ciprofl oxacin exposure to *Drosophila*. **Chemosphere**, v. 237, 2019. <https://doi.org/10.1016/j.chemosphere.2019.124542>

LLORENTE-GARCÍA, B. E. et al. First insights into photocatalytic degradation of HDPE and LDPE microplastics by a mesoporous N-TiO<sub>2</sub> coating: Effect of size and shape of microplastics. **Coatings**, v. 10, n. 7, 2020. <https://doi.org/10.3390/coatings10070658>

LÓPEZ-GARCÍA, E. et al. Drugs of abuse and their metabolites in river sediments: Analysis, occurrence in four Spanish river basins and environmental risk assessment. **Journal of Hazardous Materials**, v. 401, n. April 2020, p. 123312, 2021. <https://doi.org/10.1016/j.jhazmat.2020.123312>

LUCAS, M. S. et al. Ozonation kinetics of winery wastewater in a pilot-scale bubble column reactor. **Water Research**, v. 43, n. 6, p. 1523–1532, 1 abr. 2009. <https://doi.org/10.1016/j.watres.2008.12.036>

LUCAS, M. S.; PERES, J. A. Removal of Emerging Contaminants by Fenton and UV-Driven Advanced Oxidation Processes. **Water, Air, and Soil Pollution**, v. 226, n. 8, 2015. <https://doi.org/10.1007/s11270-015-2534-z>

LUO, J. et al. The individual and Co-exposure degradation of benzophenone derivatives by UV/H<sub>2</sub>O<sub>2</sub> and UV/PDS in different water matrices. **Water Research**, v. 159, p. 102–110, 2019. <https://doi.org/10.1016/j.watres.2019.05.019>

LUTTERBECK, C. A. et al. Removal of the anti-cancer drug methotrexate from water by advanced oxidation processes: Aerobic biodegradation and toxicity studies after treatment. **Chemosphere**, v. 141, p. 290–296, 1 dez. 2015. <https://doi.org/10.1016/j.chemosphere.2015.07.069>

MA, N. et al. In situ synthesis of a cadmium sulfide/reduced graphene oxide/bismuth Z-scheme oxyiodide system for enhanced photocatalytic performance in chlorinated paraben degradation. **Chemical Engineering Journal**, v. 359, n. November 2018, p. 530–541, 2019. <https://doi.org/10.1016/j.cej.2018.11.181>

MACHULEK, A. et al. Fundamental Mechanistic Studies of the Photo-Fenton Reaction for the Degradation of Organic Pollutants. **Organic Pollutants Ten Years After the Stockholm Convention - Environmental and Analytical Update**, 2012. <https://doi.org/10.5772/30995>

MANENTI, D. R. et al. Insights into solar photo-Fenton process using iron(III)-organic ligand complexes applied to real textile wastewater treatment. **Chemical Engineering Journal**, v.

266, p. 203–212, 2015. <https://doi.org/10.1016/j.cej.2014.12.077>

MANIAKOVA, G. et al. Comparison between heterogeneous and homogeneous solar driven advanced oxidation processes for urban wastewater treatment: Pharmaceuticals removal and toxicity. **Separation and Purification Technology**, v. 236, n. October 2019, 2020. <https://doi.org/10.1016/j.seppur.2019.116249>

MAO, F.; HE, Y.; GIN, K. Y. H. Occurrence and fate of benzophenone-type UV filters in aquatic environments: A review. **Environmental Science: Water Research and Technology**, v. 5, n. 2, p. 209–223, 2019. <https://doi.org/10.1039/C8EW00539G>

MARCELINO, R. B. P.; QUEIROZ, M. T. A.; AMORIM, C. C. Solar energy for wastewater treatment : review of international technologies and their applicability in Brazil. **Environ Sci Pollut Res**, v. 22, n. 6627, p. 762–773, 2015. <https://doi.org/10.1007/s11356-014-3033-2>

MARSON, E. O. et al. Degradation of Direct Red 81 mediated by Fenton reactions : multivariate optimization , effect of chloride and sulfate , and acute ecotoxicity assessment. **Environmental Science and Pollution Research**, v. 24, p. 6176–6186, 2017. <https://doi.org/10.1007/s11356-016-6977-6>

MARSON, E. O. et al. A review toward contaminants of emerging concern in Brazil: Occurrence, impact and their degradation by advanced oxidation process in aquatic matrices. **Science of the Total Environment**, v. 836, n. April, p. 155605, 2022a. <https://doi.org/10.1016/j.scitotenv.2022.155605>

MARSON, E. O. et al. Effect of Iron Complex Source on MWWTP Effluent Treatment by Solar Photo-Fenton: Micropollutant Degradation, Toxicity Removal and Operating Costs. **Molecules**, v. 27, n. 17, p. 5521, 2022b. <https://doi.org/10.3390/molecules27175521>

MARTÍNEZ-HUITLE, C. A.; BRILLAS, E. Decontamination of wastewaters containing synthetic organic dyes by electrochemical methods: A general review. **Applied Catalysis B: Environmental** Elsevier, , 7 abr. 2009. <https://doi.org/10.1016/j.apcatb.2008.09.017>

MATAFONOVA, G.; BATOEV, V. Recent advances in application of UV light-emitting diodes for degrading organic pollutants in water through advanced oxidation processes : A review. **Water Research**, v. 132, p. 177–189, 2018. <https://doi.org/10.1016/j.watres.2017.12.079>

MATTHAIYOU, V. et al. Utilization of raw red mud as a source of iron activating the persulfate oxidation of paraben. **Process Safety and Environmental Protection**, v. 119, p. 311–319, 2018. <https://doi.org/10.1016/j.psep.2018.08.020>

MATTHAIYOU, V. et al. Valorization of steel slag towards a Fenton-like catalyst for the degradation of paraben by activated persulfate. **Chemical Engineering Journal**, v. 360, n. May 2018, p. 728–739, 2019. <https://doi.org/10.1016/j.cej.2018.11.198>

MATZAPETAKIS, M. et al. Synthesis , Spectroscopic and Structural Characterization of the First Mononuclear , Water Soluble Iron - Citrate Complex ,. **J. Am. Chem. Soc.**, v. 120, n. 10, p. 13266–13267, 1998. <https://doi.org/10.1021/ja9807035>

MAZIVILA, S. J. et al. A review on advanced oxidation processes: From classical to new perspectives coupled to two- and multi-way calibration strategies to monitor degradation of contaminants in environmental samples. **Trends in Environmental Analytical Chemistry**, v.

24, p. 1–10, 2019. <https://doi.org/10.1016/j.teac.2019.e00072>

MCMAHEN, R. L. et al. Comparison of fipronil sources in North Carolina surface water and identification of a novel fipronil transformation product in recycled wastewater. **Science of the Total Environment**, v. 569–570, p. 880–887, 1 nov. 2016. <https://doi.org/10.1016/j.scitotenv.2016.05.085>

MEANS, J. L.; KUCAK, T.; CRERAR, D. A. Relative degradation rates of NTA, EDTA and DTPA and environmental implications. **Environmental Pollution. Series B, Chemical and Physical**, v. 1, n. 1, p. 45–60, 1980. [https://doi.org/10.1016/0143-148X\(80\)90020-8](https://doi.org/10.1016/0143-148X(80)90020-8)

MEJRI, A. et al. Effect of liquid depth on microcontaminant removal by solar photo-Fenton with Fe(III):EDDS at neutral pH in high salinity wastewater. **Environmental Science and Pollution Research**, v. 26, n. 27, p. 28071–28079, 2019. <https://doi.org/10.1007/s11356-019-06042-9>

MELO, S. A. S. et al. Degradação de fármacos residuais por processos oxidativos avançados. **Química Nova**, v. 32, n. 1, p. 188–197, 2009. <https://doi.org/10.1590/S0100-40422009000100034>

MIRALLES-CUEVAS, S. et al. Removal of pharmaceuticals from MWTP effluent by nanofiltration and solar photo-Fenton using two different iron complexes at neutral pH. **Water Research**, v. 64, p. 23–31, 1 nov. 2014. <https://doi.org/10.1016/j.watres.2014.06.032>

MIRALLES-CUEVAS, S. et al. EDDS as complexing agent for enhancing solar advanced oxidation processes in natural water: Effect of iron species and different oxidants. **Journal of Hazardous Materials**, v. 372, n. March 2018, p. 129–136, 2019. <https://doi.org/10.1016/j.jhazmat.2018.03.018>

MONDAL, S. K.; SAHA, A. K.; SINHA, A. Removal of ciprofloxacin using modified advanced oxidation processes: Kinetics, pathways and process optimization. **Journal of Cleaner Production**, v. 171, p. 1203–1214, 2018. <https://doi.org/10.1016/j.jclepro.2017.10.091>

MONTAGNER, C. C.; VIDAL, C.; ACAYABA, R. D. Emerging contaminants in aquatic matrices from Brazil: Current scenario and analytical, ecotoxicological and legislative aspects. **Química Nova**, v. 40, n. 9, p. 1094–1110, 2017.

MUSTAFA, F. S.; OLADIPO, A. A. Photocatalytic degradation of metronidazole and bacteria disinfection activity of Ag-doped Ni<sub>0.5</sub>Zn<sub>0.5</sub>Fe<sub>2</sub>O<sub>4</sub>. **Journal of Water Process Engineering**, v. 42, n. March, p. 102132, 2021. <https://doi.org/10.1016/j.jwpe.2021.102132>

NETA, P. et al. Rate constants and mechanism of reaction of sulfate radical anion with aromatic compounds. **Journal of the American Chemical Society**, v. 99, n. 1, p. 163–164, 1977. <https://doi.org/10.1021/ja00443a030>

NEZAR, S.; LAOUFI, N. A. Electron acceptors effect on photocatalytic degradation of metformin under sunlight irradiation. **Solar Energy**, v. 164, n. March, p. 267–275, 2018. <https://doi.org/10.1016/j.solener.2018.02.065>

NGIGI, E. M.; NOMNGONGO, P. N.; NGILA, J. C. Recent methods used in degradation of parabens in aqueous solutions : a review. **International Journal of Environmental Science**

**and Technology**, v. 1, n. 0123456789, 2021. <https://doi.org/10.1007/s13762-021-03228-y>

NGUYEN, V. et al. The degradation of paraben preservatives : Recent progress and sustainable approaches toward photocatalysis. **Chemosphere**, v. 276, p. 130163, 2021. <https://doi.org/10.1016/j.chemosphere.2021.130163>

NIHEMAITI, M. et al. Removal of trace organic chemicals in wastewater effluent by UV/H<sub>2</sub>O<sub>2</sub> and UV/PDS. **Water Research**, v. 145, p. 487–497, 2018. <https://doi.org/10.1016/j.watres.2018.08.052>

NOGUEIRA, R. F. P. et al. Fundamentals and environmental applications of Fenton and photo-Fenton processes. **Quimica Nova**, v. 30, n. 2, p. 400–408, 2007. <https://doi.org/10.1590/S0100-40422007000200030>

NOSAKA, Y.; NOSAKA, A. Y. Generation and Detection of Reactive Oxygen Species in Photocatalysis. **Chemical Reviews**, v. 117, n. 17, p. 11302–11336, 2017. <https://doi.org/10.1021/acs.chemrev.7b00161>

O'SHEA, K. E.; PERNAS, E.; SAIERS, J. Influence of mineralization products on the coagulation of TiO<sub>2</sub> photocatalyst. **Langmuir**, v. 15, n. 6, p. 2071–2076, 1999. <https://doi.org/10.1021/la9806808>

PALHARIM, P. H.; GRAÇA, C. A. L.; TEIXEIRA, A. C. S. C. Comparison between UVA- and zero-valent iron-activated persulfate processes for degrading propylparaben. **Environmental Science and Pollution Research**, v. 27, p. 22214–22224, 2020. <https://doi.org/10.1007/s11356-020-08141-4>

PAN, X. et al. Degradation of the UV-filter benzophenone-3 in aqueous solution using persulfate activated by heat, metal ions and light. **Chemosphere**, v. 196, p. 95–104, 2018. <https://doi.org/10.1016/j.chemosphere.2017.12.152>

PANIAGUA, C. E. S. et al. Matrix Effects on the Degradation of Gemfibrozil, Hydrochlorothiazide, and Naproxen by Heterogeneous Photocatalysis. **J. Braz. Chem. Soc.**, v. 31, n. 6, p. 1161–1169, 2020. <https://doi.org/10.21577/0103-5053.20200002>

PÉREZ, J. A. S. et al. Neutral or acidic pH for the removal of contaminants of emerging concern in wastewater by solar photo-Fenton? A techno-economic assessment of continuous raceway pond reactors. **Science of the Total Environment**, v. 736, p. 139681, 2020. <https://doi.org/10.1016/j.scitotenv.2020.139681>

PÉTRIER, C.; COMBET, E.; MASON, T. Oxygen-induced concurrent ultrasonic degradation of volatile and non-volatile aromatic compounds. **Ultrasonics Sonochemistry**, v. 14, n. 2, p. 117–121, 1 fev. 2007. <https://doi.org/10.1016/j.ultsonch.2006.04.007>

PIRKANNIEMI, K.; SILLANPÄÄ, M.; SOROKIN, A. Degradative hydrogen peroxide oxidation of chelates catalysed by metallophthalocyanines. **Science of the Total Environment**, v. 307, n. 1–3, p. 11–18, 2003. [https://doi.org/10.1016/S0048-9697\(02\)00499-0](https://doi.org/10.1016/S0048-9697(02)00499-0)

PLGNATELLO, J. J. Dark and Photoassisted Fe<sup>3+</sup>-Catalyzed Degradation of Chlorophenoxy Herbicides by Hydrogen Peroxide. **Environmental Science and Technology**, v. 26, n. 5, p. 944–951, 1992. <https://doi.org/10.1021/es00029a012>

QIN, L. et al. Kinetic models and pathways of ronidazole degradation by chlorination, UV irradiation and UV/chlorine processes. **Water Research**, v. 65, p. 271–281, 2014. <https://doi.org/10.1016/j.watres.2014.07.041>

RAHIM POURAN, S.; ABDUL AZIZ, A. R.; WAN DAUD, W. M. A. Review on the main advances in photo-Fenton oxidation system for recalcitrant wastewaters. **Journal of Industrial and Engineering Chemistry**, v. 21, p. 53–69, 2015. <https://doi.org/10.1016/j.jiec.2014.05.005>

RAJAK, P. et al. Exploring hazards of acute exposure of Acephate in *Drosophila melanogaster* and search for L-ascorbic acid mediated defense in it. **Journal of Hazardous Materials**, v. 321, p. 690–702, 2017. <https://doi.org/10.1016/j.jhazmat.2016.09.067>

RAMOS, S. et al. Science of the Total Environment Advances in analytical methods and occurrence of organic UV- filters in the environment — A review. **Science of the Total Environment**, The, v. 526, p. 278–311, 2015. <https://doi.org/10.1016/j.scitotenv.2015.04.055>

RASHID, M. M.; TAVČER, P. F.; BRIGITA, T. Influence of Titanium Dioxide Nanoparticles on Human Health and the Environment. **Nanomaterials**, v. 11, n. 9, p. 2354, 2021. <https://doi.org/10.3390/nano11092354>

RASTOGI, A.; AL-ABED, S. R.; DIONYSIOU, D. D. Effect of inorganic, synthetic and naturally occurring chelating agents on Fe(II) mediated advanced oxidation of chlorophenols. **Water Research**, v. 43, n. 3, p. 684–694, 2009. <https://doi.org/10.1016/j.watres.2008.10.045>

RATHI, B. S.; KUMAR, P. S.; SHOW, P. L. A review on effective removal of emerging contaminants from aquatic systems: Current trends and scope for further research. **Journal of Hazardous Materials**, v. 409, n. September 2020, p. 124413, 2021. <https://doi.org/10.1016/j.jhazmat.2020.124413>

RAYAROTH, M. P. et al. Advanced oxidation processes (AOPs) based wastewater treatment - unexpected nitration side reactions - a serious environmental issue: A review. **Chemical Engineering Journal**, v. 430, p. 133002, 15 fev. 2022. <https://doi.org/10.1016/j.cej.2021.133002>

RICARDO, I. A. et al. A critical review of trends in advanced oxidation processes for the removal of benzophenone-3, fipronil, and propylparaben from aqueous matrices: pathways and toxicity changes. **Journal of Water Process Engineering**, v. 49, p. 102973, 2022. <https://doi.org/10.1016/j.jwpe.2022.102973>

RUALES-LONFAT, C. et al. Bacterial inactivation with iron citrate complex: A new source of dissolved iron in solar photo-Fenton process at near-neutral and alkaline pH. **Applied Catalysis B: Environmental**, v. 180, p. 379–390, 2016. <https://doi.org/10.1016/j.apcatb.2015.06.030>

SADARIA, A. M. et al. Retrospective nationwide occurrence of fipronil and its degradates in U . S . wastewater and sewage sludge from 2001 - 2016. **Water Research**, v. 155, p. 465–473, 2019. <https://doi.org/10.1016/j.watres.2019.02.045>

SEMONES, M. C. et al. Photodegradation of UV filters oxybenzone and sulisobenzene in wastewater effluent and by dissolved organic matter. **Applied Geochemistry**, v. 83, p. 150–157, 2017. <https://doi.org/10.1016/j.apgeochem.2017.02.008>

SHAH, A. D. et al. Trade-offs in disinfection byproduct formation associated with precursor

preoxidation for control of N -nitrosodimethylamine formation. **Environmental Science and Technology**, v. 46, n. 9, p. 4809–4818, 2012. <https://doi.org/10.1021/es204717j>

SHUKLA, P. et al. Adsorption and heterogeneous advanced oxidation of phenolic contaminants using Fe loaded mesoporous SBA-15 and H<sub>2</sub>O<sub>2</sub>. **Chemical Engineering Journal**, v. 164, n. 1, p. 255–260, 2010. <https://doi.org/10.1016/j.cej.2010.08.061>

SILLANPÄÄ, M.; PIRKANNIEMI, K.; DHONDUP, P. The acute toxicity of gluconic acid,  $\beta$ -alaninediacetic acid, diethylenetriaminepentakismethylenephosphonic acid, and nitrilotriacetic acid determined by *Daphnia magna*, *Raphidocelis subcapitata*, and *Photobacterium phosphoreum*. **Archives of Environmental Contamination and Toxicology**, v. 44, n. 3, p. 332–335, 2003. <https://doi.org/10.1007/s00244-002-1220-5>

SILVA, A. M. N. et al. Iron(iii) citrate speciation in aqueous solution. **Dalton Transactions**, n. 40, p. 8616–8625, 2009. <https://doi.org/10.1039/b910970f>

SILVA, A. M. N.; KONG, X.; HIDER, R. C. Determination of the pK<sub>a</sub> value of the hydroxyl group in the  $\alpha$ -hydroxycarboxylates citrate, malate and lactate by <sup>13</sup>C NMR: implications for metal coordination in biological systems. **Biometals**, v. 22, p. 771–778, 2009. <https://doi.org/10.1007/s10534-009-9224-5>

SILVA, G. D. et al. Contrasting the performance of photo-Fenton at neutral pH in the presence of different organic iron-complexes using hydrogen peroxide or persulfate as oxidants for naproxen degradation and removal of antimicrobial activity. **Process Safety and Environmental Protection**, v. 147, p. 798–807, 1 mar. 2021. <https://doi.org/10.1016/j.psep.2021.01.005>

SINGH, H. K.; MUNEER, M.; BAHNEMANN, D. Photocatalysed degradation of a herbicide derivative, bromacil, in aqueous suspensions of titanium dioxide. **Photochemical & Photobiological Sciences**, v. 2, p. 151–156, 2003. <https://doi.org/10.1039/b206918k>

SINGH, N. S. et al. A comprehensive review of environmental fate and degradation of fipronil and its toxic metabolites. **Environmental Research**, v. 199, n. November 2020, p. 111316, 2021. <https://doi.org/10.1016/j.envres.2021.111316>

SIVARAMAN, L. et al. Safety assessment of propylparaben in juvenile rats. **Regulatory Toxicology and Pharmacology**, v. 92, p. 370–381, 1 fev. 2018. <https://doi.org/10.1016/j.yrtph.2017.12.009>

SOARES, P. A. et al. Enhancement of a solar photo-Fenton reaction with ferric-organic ligands for the treatment of acrylic-textile dyeing wastewater. **Journal of Environmental Management**, v. 152, p. 120–131, 2015. <https://doi.org/10.1016/j.jenvman.2015.01.032>

SOLTERMANN, F. et al. ScienceDirect Photolysis of inorganic chloramines and efficiency of trichloramine abatement by UV treatment of swimming pool water. **Water Research**, v. 56, p. 280–291, 2014. <https://doi.org/10.1016/j.watres.2014.02.034>

SONG, Q. et al. Degradation of the flame retardant triphenyl phosphate by ferrous ion-activated hydrogen peroxide and persulfate : Kinetics, pathways, and mechanisms. **Chemical Engineering Journal**, v. 361, n. December 2018, p. 929–936, 2019. <https://doi.org/10.1016/j.cej.2018.12.140>

SONI, M. G.; CARABIN, I. G.; BURDOCK, G. A. Safety assessment of esters of p-hydroxybenzoic acid (parabens). **Food and Chemical Toxicology**, v. 43, n. 7, p. 985–1015, 1 jul. 2005. <https://doi.org/10.1016/j.fct.2005.01.020>

SORIANO-MOLINA, P. et al. Effect of volumetric rate of photon absorption on the kinetics of micropollutant removal by solar photo-Fenton with Fe<sup>3+</sup>-EDDS at neutral pH. **Chemical Engineering Journal**, v. 331, p. 84–92, jan. 2018. <https://doi.org/10.1016/j.cej.2017.08.096>

SORIANO-MOLINA, P. et al. Assessment of different iron sources for continuous flow solar photo-Fenton at neutral pH for sulfamethoxazole removal in actual MWWTP effluents. **Journal of Water Process Engineering**, v. 42, n. February, p. 102109, 2021. <https://doi.org/10.1016/j.jwpe.2021.102109>

STARLING, M. C. V. M.; AMORIM, C. C.; LEÃO, M. M. D. Occurrence, control and fate of contaminants of emerging concern in environmental compartments in Brazil. **Journal of Hazardous Materials**, v. 372, n. April 2018, p. 17–36, 2019. <https://doi.org/10.1016/j.jhazmat.2018.04.043>

STONE, W. W.; GILLIOM, R. J.; RYBERG, K. R. Pesticides in U.S. Streams and Rivers: Occurrence and Trends during 1992 – 2011. **Environ. Sci. Technol.**, v. 48, n. 19, p. 11025–11030, 2014. <https://doi.org/10.1021/es5025367>

SURYAMAN, D.; HASEGAWA, K. Biological and photocatalytic treatment integrated with separation and reuse of titanium dioxide on the removal of chlorophenols in tap water. **Journal of Hazardous Materials**, v. 183, n. 1–3, p. 490–496, 2010. <https://doi.org/10.1016/j.jhazmat.2010.07.050>

SVENSON, A.; KAJ, L.; BJÖRNDAL, H. Aqueous photolysis of the iron (III) complexes of NTA, EDTA and DTPA. **Chemosphere**, v. 18, n. 9–10, p. 1805–1808, 1989. [https://doi.org/10.1016/0045-6535\(89\)90464-5](https://doi.org/10.1016/0045-6535(89)90464-5)

SWOBODA, F.; SOLAR, S. Comparative study on the radiolytic degradation of 4-hydroxybenzoate and 4-hydroxybenzoic ethyl ester. **Radiation Physics and Chemistry**, v. 56, n. 3, p. 291–301, 1999. [https://doi.org/10.1016/S0969-806X\(98\)00350-8](https://doi.org/10.1016/S0969-806X(98)00350-8)

TAHIR, M. B. et al. Advances in photo - catalysis approach for the removal of toxic personal care product in aqueous environment. **Environment, Development and Sustainability**, v. 22, n. 7, p. 6029–6052, 2020. <https://doi.org/10.1007/s10668-019-00495-1>

TAY, K. S.; RAHMAN, N. A.; ABAS, M. R. BIN. Ozonation of parabens in aqueous solution: Kinetics and mechanism of degradation. **Chemosphere**, v. 81, n. 11, p. 1446–1453, 1 dez. 2010. <https://doi.org/10.1016/j.chemosphere.2010.09.004>

THANGAMANI, R. et al. Advance electrochemical oxidation of fipronil contaminated wastewater by graphite anodes and sorbent nano hydroxyapatite. **Energy Sources, Part A: Recovery, Utilization and Environmental Effects**, v. 41, n. 7, p. 866–880, 2019. <https://doi.org/10.1080/15567036.2018.1520365>

TINGLE, C. C. D. et al. Fipronil: environmental fate, ecotoxicology, and human health concerns. In: WARE, G. W. (Ed.). **Reviews of Environmental Contamination and Toxicology**. New York: Springer, 2003. v. 176p. 1–66. <https://doi.org/10.1007/978-1-4899-7283->

[5 1](#)

TOVAR-SÁNCHEZ, A. et al. Sunscreen Products as Emerging Pollutants to Coastal Waters. **PLoS ONE**, v. 8, n. 6, 2013. <https://doi.org/10.1371/journal.pone.0065451>

TROVÓ, A. G. et al. Degradation of the antibiotic chloramphenicol by photo-Fenton process at lab-scale and solar pilot plant: Kinetic, toxicity and inactivation assessment. **Solar Energy**, v. 97, p. 596–604, 1 nov. 2013. <https://doi.org/10.1016/j.solener.2013.09.017>

TSUI, M. M. P. et al. Occurrence, Distribution, and Fate of Organic UV Filters in Coral Communities. **Environmental Science and Technology**, v. 51, n. 8, p. 4182–4190, 2017. <https://doi.org/10.1021/acs.est.6b05211>

USP TECHNOLOGIES. **Titanium Oxalate (Spectrophotometric)**. <https://www.h2o2.com/technical-library/analytical-methods/default.aspx?pid=71&name=Titanium-Oxalate-Spectrophotometric>. Accessed 22 June 2020, 2015.

VANDEBRIEL, R. J.; DE JONG, W. H. A review of mammalian toxicity of ZnO nanoparticles. **Nanotechnology, Science and Applications**, v. 5, n. 1, p. 61–71, 2012. <https://doi.org/10.2147/NSA.S23932>

VANDENBERG, L. N.; BUGOS, J. Assessing the Public Health Implications of the Food Preservative Propylparaben: Has This Chemical Been Safely Used for Decades. **Current Environmental Health Reports**, v. 8, n. 1, p. 54–70, 2021. <https://doi.org/10.1007/s40572-020-00300-6>

VEGA, L. P.; PEÑUELA, G. A. High Frequency Sonochemical Degradation of Benzophenone-3 in Water. **Journal of Environmental Engineering**, v. 144, n. 8, p. 04018058, 2018. [https://doi.org/10.1061/\(ASCE\)EE.1943-7870.0001406](https://doi.org/10.1061/(ASCE)EE.1943-7870.0001406)

VIONE, D. et al. Phototransformation of the sunlight filter benzophenone-3 (2-hydroxy-4-methoxybenzophenone) under conditions relevant to surface waters. **Science of the Total Environment**, v. 463–464, p. 243–251, 1 out. 2013. <https://doi.org/10.1016/j.scitotenv.2013.05.090>

WACŁAWEK, S. et al. Chemistry of persulfates in water and wastewater treatment: A review. **Chemical Engineering Journal**, v. 330, n. July, p. 44–62, 2017. <https://doi.org/10.1016/j.cej.2017.07.132>

WACŁAWEK, S.; GRÜBEL, K.; ČERNÍK, M. Simple spectrophotometric determination of monopersulfate. **Spectrochimica Acta - Part A: Molecular and Biomolecular Spectroscopy**, v. 149, p. 928–933, 2015. <https://doi.org/10.1016/j.saa.2015.05.029>

WANG, Y. R.; CHU, W. Degradation of a xanthene dye by Fe(II)-mediated activation of Oxone process. **Journal of Hazardous Materials**, v. 186, n. 2–3, p. 1455–1461, 28 fev. 2011. <https://doi.org/10.1016/j.jhazmat.2010.12.033>

WANG, Z. et al. Pilot-scale study on photodegradation of benzophenone-3 and benzophenone-8 ultraviolet filters enriched synthetic effluent. **Journal of Water Process Engineering**, v. 44, n. July, 2021. <https://doi.org/10.1016/j.jwpe.2021.102327>

WESTON, D. P.; LYDY, M. J. Toxicity of the insecticide fipronil and its degradates to benthic macroinvertebrates of urban streams. **Environmental Science and Technology**, v. 48, n. 2, p. 1290–1297, 2014. <https://doi.org/10.1021/es4045874>

WNUK, A. et al. Prenatal exposure to benzophenone-3 (BP-3) induces apoptosis, disrupts estrogen receptor expression and alters the epigenetic status of mouse neurons. **Journal of Steroid Biochemistry and Molecular Biology**, v. 182, n. February, p. 106–118, 2018. <https://doi.org/10.1016/j.jsbmb.2018.04.016>

XI, W.; GEISSEN, S. U. Separation of titanium dioxide from photocatalytically treated water by cross-flow microfiltration. **Water Research**, v. 35, n. 5, p. 1256–1262, 2001. [https://doi.org/10.1016/S0043-1354\(00\)00378-X](https://doi.org/10.1016/S0043-1354(00)00378-X)

XUE, Y. et al. Role of halide ions on organic pollutants degradation by peroxygens-based advanced oxidation processes: A critical review. **Chemical Engineering Journal**, v. 433, n. P1, p. 134546, 2022. <https://doi.org/10.1016/j.cej.2022.134546>

YANG, Q. et al. Recent advances in photo-activated sulfate radical-advanced oxidation process (SR-AOP) for refractory organic pollutants removal in water. **Chemical Engineering Journal**, v. 378, n. June, p. 122149, 2019. <https://doi.org/10.1016/j.cej.2019.122149>

YANG, Y. et al. Comparison of halide impacts on the efficiency of contaminant degradation by sulfate and hydroxyl radical-based advanced oxidation processes (AOPs). **Environmental Science and Technology**, v. 48, n. 4, p. 2344–2351, 2014. <https://doi.org/10.1021/es404118q>

YANG, Y. et al. Degradation of sulfamethoxazole by UV, UV/H<sub>2</sub>O<sub>2</sub> and UV/persulfate (PDS): Formation of oxidation products and effect of bicarbonate. **Water Research**, v. 118, p. 196–207, 2017. <https://doi.org/10.1016/j.watres.2017.03.054>

YE, Z. et al. Photoelectro-Fenton as post-treatment for electrocoagulated benzophenone-3-loaded synthetic and urban wastewater. **Journal of Cleaner Production**, v. 208, p. 1393–1402, 2019. <https://doi.org/10.1016/j.jclepro.2018.10.181>

YING, G. G.; KOOKANA, R. S. Sorption of fipronil and its metabolites on soils from South Australia. **Journal of Environmental Science and Health - Part B Pesticides, Food Contaminants, and Agricultural Wastes**, v. 36, n. 5, p. 545–558, 2001. <https://doi.org/10.1081/PFC-100106184>

ZHANG, Q. et al. Evaluation of ecotoxicological effects of benzophenone UV filters: Luminescent bacteria toxicity, genotoxicity and hormonal activity. **Ecotoxicology and Environmental Safety**, v. 142, p. 338–347, 1 ago. 2017. <https://doi.org/10.1016/j.ecoenv.2017.04.027>

ZHANG, Y. et al. Kinetic and mechanistic investigation of azathioprine degradation in water by UV, UV/H<sub>2</sub>O<sub>2</sub> and UV/persulfate. **Chemical Engineering Journal**, v. 302, p. 526–534, 2016. <https://doi.org/10.1016/j.cej.2016.05.085>

ZHANG, Y.; ZHOU, M. A critical review of the application of chelating agents to enable Fenton and Fenton-like reactions at high pH values. **Journal of Hazardous Materials**, v. 362, n. March 2018, p. 436–450, 2019. <https://doi.org/10.1016/j.jhazmat.2018.09.035>

ZHONG, L.; HAGHIGHAT, F.; LEE, C. Ultraviolet photocatalytic oxidation for indoor environment applications : Experimental validation of the model. **Building and Environment**, v. 62, p. 155–166, 2013. <https://doi.org/10.1016/j.buildenv.2013.01.009>

ZÚÑIGA-BENÍTEZ, H.; ARISTIZÁBAL-CIRO, C.; PEÑUELA, G. A. Photodegradation of the endocrine-disrupting chemicals benzophenone-and methylparaben using Fenton reagent: Optimization of factors and mineralization/biodegradability studies. **Journal of the Taiwan Institute of Chemical Engineers**, v. 59, p. 380–388, 2016. <https://doi.org/10.1016/j.jtice.2015.09.004>

ZÚÑIGA-BENÍTEZ, H.; SOLTAN, J.; PEÑUELA, G. A. Application of ultrasound for degradation of benzophenone-3 in aqueous solutions. **International Journal of Environmental Science and Technology**, v. 13, n. 1, p. 77–86, 2016. <https://doi.org/10.1007/s13762-015-0842-x>